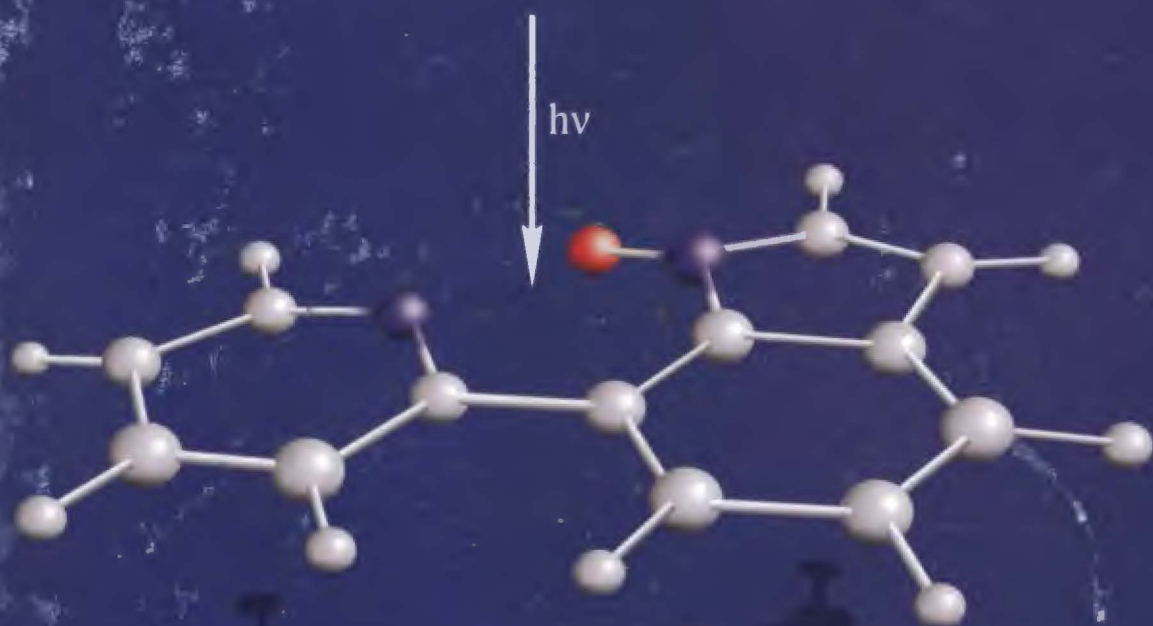Gabriela Wiosna-Sałyga

Phototautomerization
in heteroazaaromatic systems

hv

Phototautomerization in

heteroazaaromatic systems

Institute of Physical Chemistry, Polish Academy of Sciences
Kasprzaka 44/52, 01-224 Warsaw

Gabriela Wiosna-Sałyga

Phototautomerization in heteroazaaromatic systems

A - 71 - 15
K - g - 180

Ph.D. dissertation written under the supervision of
prof. dr. hab. Jacek Waluk

This dissertation has been completed in the framework of the
International Ph.D. Studies at the Institute of Physical Chemistry
of the Polish Academy of Sciences

Warsaw 2009

ACKNOWLEDGMENTS

I would like to thank cordially dissertation supervisor prof. dr. hab. Jacek Waluk for his guidance and support.

My special thanks to dr. Yevgeniy Nosenko for his significant contribution to the part of work related to supersonic molecular beam experiments and dr. Irina Petkova for performing picosecond time-resolved fluorescence and femtosecond transient absorption measurements.

I would like to thank:
- prof. Randolph P. Thummel (the University of Houston) and his group for synthesis of studied objects;
- prof. Bernd Brutschy for offering the opportunity to visit his group at the Frankfurt University to perform supersonic molecular beam experiments,
- prof. Wybren Jan Buma for offering the opportunity to perform femtosecond transient absorption experiments at the University of Amsterdam.

I would like to thank all, present and future, co-authors of papers describing the results presented in this dissertation, especially:
- dr. hab. Jacek Dobkowski (transient absorption and fluorescence experiments);
- Michał Kijak (theoretical calculations).

I am grateful for support and goodwill of all colleagues at the Photochemistry and Spectroscopy Department of IChF PAN.

Finally, I would like to thank my family for
being my support, especially Mariusz and Zuzia, my inspiration and motivation.

Napotkał Nobla kumpel raz,
I tak mu rzekł - Alfredzie,
Powiedzieć to najwyższy czas,
Że marnie ci się wiedzie.

Choć do doświadczeń wciąż cię gna,
Choć starasz się od świtu,
Ty prochu nie wymyślisz, a
Tym bardziej dynamitu!

A Nobel spłonił się jak rak,
Po cichu zaś pomyślał, jak?:

Róbmy swoje,
Pewne jest to jedno, że
Róbmy swoje,
Póki jeszcze ciut się chce,
W myśleniu sens, w działaniu racja,
Próbujmy więc, a nuż ..
Może to coś da? Kto wie?...

Wojciech Młynarski

Moim najbliższym, dzięki którym mogłam robić swoje najlepiej jak
potrafię...

Table of contents

10

CHAPTER I. Introduction

I.1. Foreword

After over more than ninety years of studying the complex nature of H-bonding interaction in various molecular systems, it is well established today that the hydrogen bonds play crucial role in numerous areas of physical, chemical, and biological phenomena. Their presence explains many of the unique properties of water, they are involved in the mechanism of enzyme catalysis via so-called low-barrier hydrogen bond (LBHB),[1,2] and they are partly responsible for the secondary, tertiary, and quaternary structures of proteins and nucleic acids,[3,4] thereby serving an important function in determining the nature of all living things. Thus, the research on the role of HB, in particular the changes in photophysical properties caused by HB formation have been actively pursued for many decades.[5-24]

According to the IUPAC definition,[25] hydrogen bond is "a form of association between an electronegative atom and a hydrogen atom attached to a second, relatively electronegative atom. It is best considered as an electrostatic interaction, heightened by the small size of hydrogen, which permits proximity of the interacting dipoles or charges." However, the question on "what is the fundamental nature of hydrogen bond?" has not one simple answer because the hydrogen bonds are surprisingly complex. They reveal contributions from electrostatic interaction, polarization effects, van der Waals interaction and covalency. There are many ways of classifying the hydrogen bonds. They may be classified as intermolecular (a proton donor and an acceptor belong to different molecules) or intramolecular (when a molecule possesses simultaneously a donor and an acceptor group). The second criterion of classification may be the H-bond strength, which depends on the local geometry (distance and angle between the hydrogen bond donor and acceptor groups). For strong, moderate and weak H-bonds this value varies from 15-40, 4-15, to 1-4 kcal/mol, respectively.

The importance of H-bondings in molecular clusters, molecular solvation, and biomolecules comes from their limited strength and, as a result, the possibility of easy making and breaking of bonds, which is essential for many photobiological and photochemical processes, as well as the fundamental processes of life. These processes include the hydrogen atom or proton transfer along pre-existing hydrogen bonds. The proton transfer (in the electronic ground and in the excited state) is one of the most

intensively studied reactions in various branches of science. A great number of experimental techniques and theoretical methods have been applied to understand this reaction.[26] However, the problem is as important as complicated and far from the solution and completion.

This chapter gives a brief overview of experimental and theoretical studies of (i) photoinduced intramolecular proton transfer (ESIPT) between two groups of the same molecule (I.3). In choosing the examples for ESIPT, the idea was to present an interesting aspect of photostability, using results of investigations of several most representative and most intensely studied systems; (ii) intermolecular processes where the reaction occurs between two molecules (I.4). Beside the solvent-assisted excited states proton transfer, other possible phenomena induced by intermolecular hydrogen bonds have been discussed. The fifth section of this chapter (I.5) is devoted to the problem of how the solvent can interfere with intramolecular excited state proton transfer. The idea of this chapter is to present the main issues related to the author's field of investigation.

I.2. Excited state proton transfer. Intra and intermolecular cases

One of the most important reaction being a cornerstone of many processes in chemistry and biology lies in a transfer of a hydrogen atom or a proton from one group (named a donor) to another (named an acceptor):

$$A–H...B \rightarrow A...H–B$$
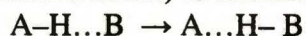
Such processes can take place in the electronic ground state or, after the photon absorption, in a higher electronic state. In this work the focus is mainly limited to the subjects related to the excited state proton transfer (ESPT). Even though the phenomenon of the photoinduced proton transfer was first observed nearly half a century ago,[27] it still attracts attention. The long-lasting efforts to understand the nature of this process have provided a lot of information and, simultaneously, have demonstrated the complexity of this problem.

A vast number of investigations have been published relating to various types of such kind of reaction in the gas phase under isolated conditions (molecular beam and matrices) or in condensed environments.[26,28] Depending on the system, the reaction can be intramolecular or intermolecular and may occur as a barrierless process or through a barrier. Kasha[29] proposed to divide the proton transfer reactions

12

into four mechanistic classes: (i) intrinsic intramolecular proton transfer involving the H-bond between the H atom of the donor and the acceptor group; (ii) concerted biprotonic transfer where the proton is far away from the acceptor and requires a mediator; (iii) processes exhibiting static (the case of cyclic H-bonded complexes) and dynamic (when rearrangement, upon excitation, to the cyclic doubly H-bonded structure is required) catalysis; and (iv) proton-relay tautomerization, where the proton transfers are coupled through the inductive electronic effect in the cyclic complex.

The rates of proton transfer have been shown to cover a wide time range, starting from times as short as femtoseconds. The reaction can proceed as fast as nuclear motions or take much longer, when a barrier is characteristic for the potential energy surface (PES). In order to understand the kinetics of the reaction it is necessary to define a proper coordinate of the proton transfer reaction and to find the rate-determining step. Sometimes it is quite a big challenge. Recent experimental and theoretical developments demonstrate that not in all cases the reaction can be described in terms of a localized coordinate along the hydrogen bond, but rather more complex motions of molecular skeleton are involved in the reactive pathway.[30] To get a more proper description of proton transfer one should consider several factors. One of them is the probability of quantum mechanical tunneling resulting from the small mass of hydrogen compared to all other atoms. It is important whether the reaction can occur along the existing hydrogen bond or if reaction partners have to overcome diffusion limitations to encounter each other. In many systems, the problem is even more complicated because of the existence of at least two rotameric forms, of which only one is able to form intramolecular hydrogen bond and, as a result, the interconversion between the rotamers may play the crucial role in the proton transfer process. Finally, a role of vibrations, which are able either to promote or suppress ESPT should not be neglected.[31]

I.3. Intramolecular excited state proton transfer (ESIPT) from the point of view of photostability

A large number of observations allow to state that intramolecular hydrogen bonds in π systems can act as molecular photostabilizers by rapid tautomerisation in the excited state, followed by rapid internal conversion. As a consequence, most of the absorbed energy is thermally dissipated in the singlet system of the chelates and a molecule returns to the ground state via a nondestructive deactivation path. This phenomenon is used to protect

polymers from photodegradation, for example by copolymerization of another molecule, a so-called photostabilizer, into the polymer chain.[32-34] The embedded chromophores can directly absorb the UV photons and simply act as UV screens for polymer units. Sometimes, instead of direct absorption, energy migration mechanism occurs. In this case, electronic excitation initially localized on the chromophore of the polymer is transferred to the chromophore of the photostabilizer and "trapped" there. The best photostabilizers may absorb nearly a million of photons without undergoing destructive photochemical reactions.

Excited state proton transfer along intramolecular hydrogen bond plays an important role in the stabilizing efficiency of such UV absorbers as *methyl salicylate* (MS), *2-(2'-hydroxy-5'-methylphenyl)benzotriazole* (TIN), *2-(2'-hydroxyphenyl)benzothiazole* (BHT) and *[2,2'-bipyridyl]-3,3'-diol* (BP(OH)$_2$). Since these UV stabilizers are widely applied to diminish the photodegradation of polymers or used in specialized applications such as intraocular and contact lenses, considerable effort has been given to the elucidation of their photophysical deactivation mechanism and, therefore, they seem to be good examples to illustrate the problems related to ESIPT.

Otterstedt[35] explains the photostability phenomenon in terms of the energy gap between the first excited state and the ground state, which is smaller in the keto form than in the enol one. Assuming that in cyclic aromatics the rate of radiationless processes decreases exponentially with this energy difference, in the keto form internal conversion proceeds much faster and the probability of photodegradation via a chemical reaction in the excited state is reduced drastically. The paths of returning to the ground state are complicated and different type of mechanisms may contribute. Figure I.1 presents a model of deactivation path proposed by Otterstedt for benzotriazole-type molecules.
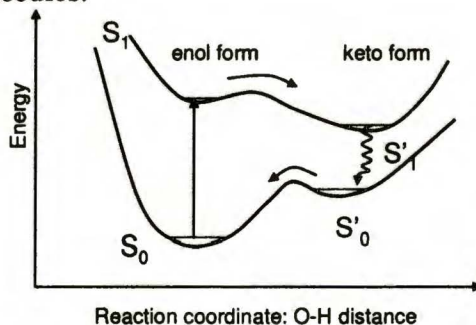
Figure I.1. Deactivation scheme for bezotriazole-type molecules proposed by Otterstedt.[35]

Historically, the first example of phototautomerization was found by Weller for *salicylic acid* (**SA**) and *methyl salicylate* (**MS**).[36] Marsh observed that the fluorescence in a polar solvent occurred at very low frequencies. In hydrocarbon solvents salicylic acid exhibited two fluorescence bands and the one at the low frequency was similar to that observed in polar media.[37] Weller proposed that the red-shifted fluorescence was due to a zwitterion formed as a result of phototautomerism in the lowest excited singlet state. The pioneering work of Weller on **SA** and **MS** initiated extensive studies of such systems.[38-56] Further studies allowed to verify Weller's postulate of a proton motion along a double well potential (Figure I.2)
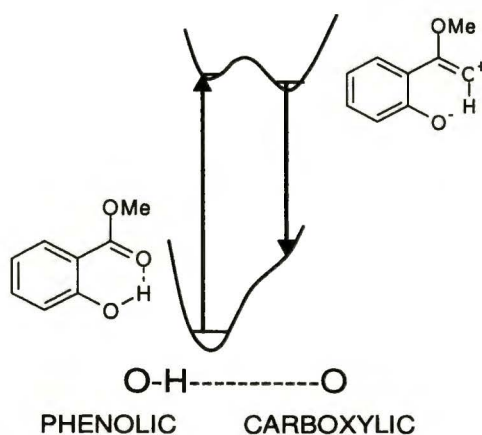
Figure I.2. The schematic potential energy curves for the proton transfer in **MS** suggested by Weller.[36]

The finding that the excitation spectra of the two emissions are not identical and the observed changes in the relative intensity of the two bands as a function of excitation wavelength,[51,52] temperature and solvent nature suggested the presence of two different ground state forms. It is now well known that in the gas phase,[57] as well as in liquid solution at room temperature[51,52,58] and supersonic jet conditions,[40,43,59] in both ground and excited states, two conformers of **MS** coexist (Figure I.3). A similar observation has been made for durene crystals (4.2 K).[41]

15
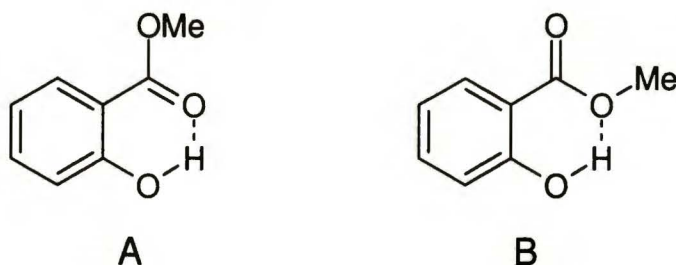
Figure I.3. The rotameric forms of methyl salicylate.

The structures of the two rotamers A and B have been studied by Catalán *et al.*,[38,49,50,60] and Pimentel and co-workers.[53] Heimbrook at al. have obtained high resolution spectra of both different internally hydrogen-bonded rotamers in a molecular beam.[40,59] The ratio of ground state populations of the form A to the form B was estimated to be 70/1. The more abundant species (more stable by 10.5 kJ/mol) is responsible for the blue fluorescence which has been assigned to a $\pi\pi^*$ transition. After excitation of this form the phenolic proton is significantly displaced toward the carbonyl oxygen (Figure I.4). The UV emission is related to form B, where the internal hydrogen bond is between the phenol and methoxy groups. In this case very little movement of proton is observed as a result of the excitation and the excited state is most likely of $n\pi^*$ character. The tautomer decays by a nonradiative process with an activation energy of 1300 cm^{-1}. This nonradiative process has been attributed to various effects: the torsion of the –COOMe group, crossing of the $\pi\pi^*$ and $n\pi^*$ surfaces, breaking of the hydrogen bond, and a decay analogous to the channel three process in benzene[40,42,43,59,61]. A basic question for **MS** is whether the excited state surface has two local minima, as in Figure I.2, or simply one minimum. Theoretical studies indicated either a low barrier[62,63] or no barrier at all.[64-67] Goodman and Brus[47] have studied **MS** and deuterated **MS** in Ne matrices at 4.2 K, where only the red-shifted emission was observed. They have shown that in such environment MS does not appear to have a barrier to tautomerization. Similar conclusions have been drawn by Felker *et al.*[43] Picosecond time-resolved studies of jet-cooled **MS** have shown that ESIPT occurs on a time scale less than 10 ps, suggesting barrierless character of the process. These beam experiments are also consistent with the lower limit on the rate of hydrogen transfer deduced in the solution phase.[68] In order to answer the questions concerning the real-time dynamics of tautomerization and the mechanism of the reaction Herek at al. have employed femtosecond fluorescence depletion spectroscopy in the jet. The studies led to the

16

conclusion that the transfer occurs within 60 fs and showed that the PES for the internal hydrogen motion in the excited state along the reaction coordinate is asymmetric and with a single minimum corresponding to the formed keto tautomer (as discussed previously by Catalán and Nagaoka).[62,64,67] The experimental and theoretical results support a single minimum (Figure I.4), rather than a double minimum originally proposed by Weller (Figure I.2). Interestingly, spectroscopy and dynamics of **MS** seem to be mainly described by the motion of heavy nuclei and the reaction path may not be necessarily related to proton movement.[39]
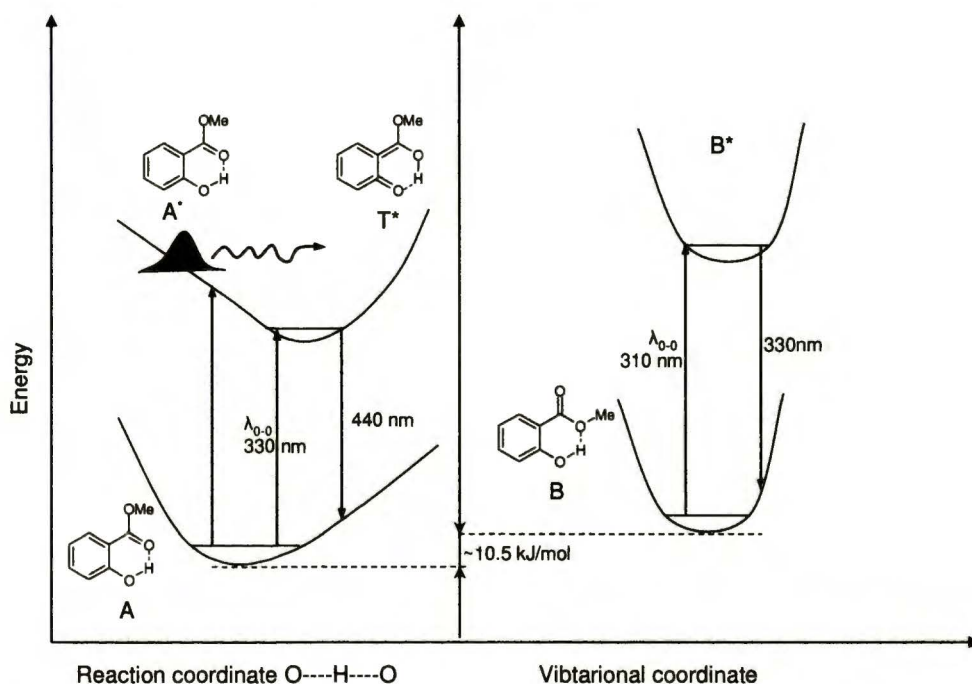
Figure I.4. A schematic for the potential for A and B rotamers of **MS**.

Another molecule with a nonsymetric H-bonded chelate ring as part of the electronic system and strongly asymmetric potential energy surface with only one stable geometry is *2-(2'-hydroxy-5'-methylphenyl)benzotriazole* (**TIN**) (Figure I.5). This compound has received increasing attention after the pioneering work of Heller and Blattmann,[69] because of its particularly high efficiency as an UV photostabilizer of polymers. The spectroscopy of **TIN** have been investigated extensively in room-temperature solutions, in a variety of low-temperature glasses, and in crystals.

In intramolecularly hydrogen-bonded organic molecules, the acidity/basicity of the intramolecular donor/acceptor group increases upon excitation. These changes, measured using Förster's theory,[70] promote an intramolecular proton-transfer process which is the origin of the large Stokes shift in the fluorescence spectrum. The **TIN** performs a closed fully reversible reaction cycle (Figure I.5) as has been deduced from a number of the pump-probe studies.[30,71-73]
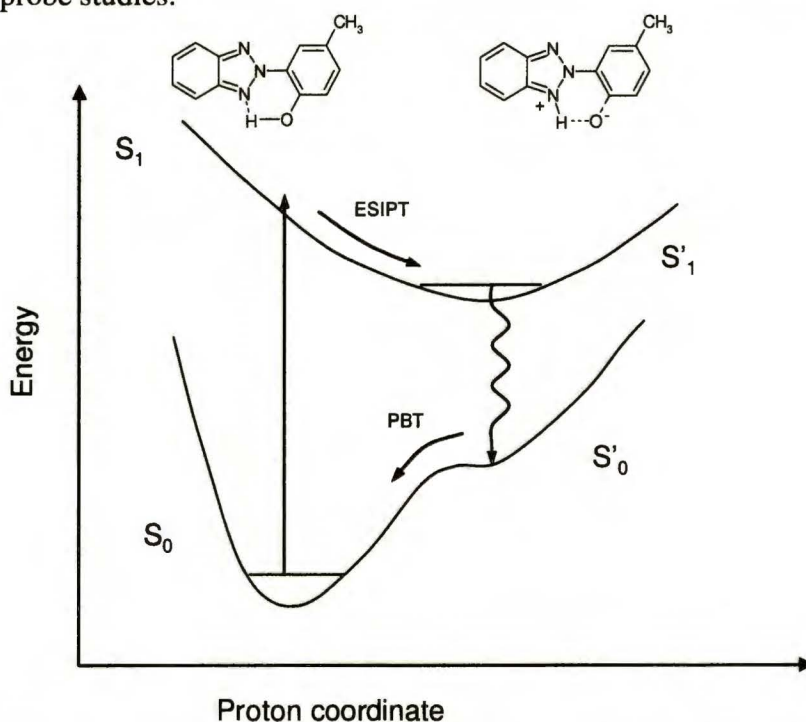
Figure I.5. Proton transfer reaction path in **TIN**. Abbreviations: ESIPT- excited state intramolecular proton transfer, PBT – proton back-transfer.

After excitation, the enol form is transformed into a keto structure as a result of ultrafast (60-80 fs) ESIPT. The product of this reaction undergoes radiationless deactivation with a time constant of about 150 fs. The next step of the cycle is a proton back-transfer to the ground enol form with a time constant of 600 fs. The dynamics of proton transfer is independent on the amount of vibronic excess energy in the initial excitation,[30] suggesting barierless character of the reaction. However, the possibility of phototautomerization process may be related with the planar or non-planar geometric structure of molecule. The change from a planar to a twisted conformation leads to the breaking of the intramolecular hydrogen bond and

18

the recovery of the normal fluorescence.[74] To elucidate the mechanism of the proton transfer the question which modes constitute the reaction coordinate have to be answered. The information about it may be derived from ultrafast absorption spectroscopy studies. Choudoba at al.,[75] using an optical pump-probe method with 20 fs resolution, have found that the highly anharmonic in-plane deformation mode (470 cm^{-1}), characterized on the basis of the infrared and resonance Raman studies,[76,77] plays an important role in the reaction by modulating and moving the reactive wave packet along a barrierless pathway along the potential energy surface. Such motions involve the strongest modulation of the separation between the hydrogen donor and acceptor groups among all vibrational modes of **TIN**.[78] It should be stressed that the OH stretching mode is not part of the wavepacket. That was the first time when the oscillatory signal contributions associated with the ESIPT were observed. This pioneering work encouraged scientists to study the ESIPT molecules with the time resolution sufficient to temporally resolve the nuclear motions during the transfer. One of the most extensively analyzed object is *2-(2'-hydroxyphenyl)benzothiazole* (**HBT**). The internal conversion in this molecule is much slower than in the case of **TIN** and does not mask the ESIPT dynamics. In the electronic ground state the enol form with the proton bound to the hydroxyl substituent of the phenyl ring is stable (Figure I.6). In the electronically excited molecule ultrafast structural changes take place, which are manifested by a large Stokes shift between the electronic absorption bands of the initial structure and the emission spectra of the excited reaction product.[79,80]
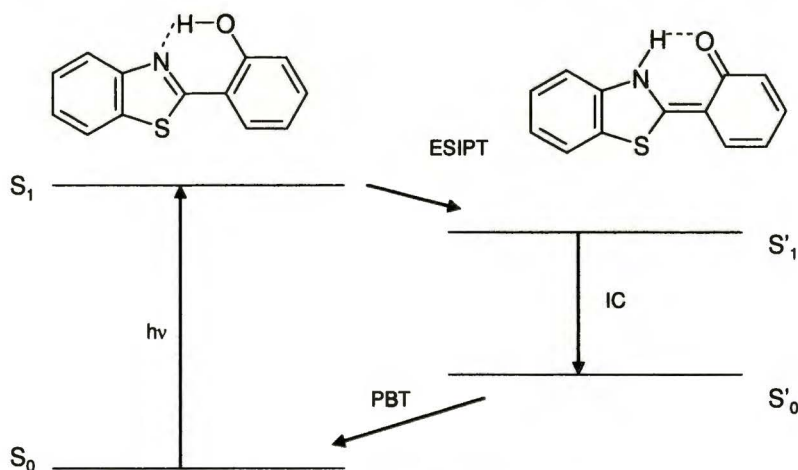

Figure I.6. Ultrafast reaction cycle of **HBT**.

Time-resolved infrared spectroscopy provided direct evidence for ESIPT. The N-H and C=O stretching vibrations of the keto tautomer, which is formed after excitation, have been detected.[81,82] The time scale of the excited state proton transfer in this molecule was found to be 170 fs, as was reported by Laermer *et al.*,[79] the authors of the first femtosecond investigation concentrated on the probing of the rise of product emission on the $S_1^{'} - S_0^{'}$ transition after pumping into the S_0-S_1 transition. Femtosecond IR spectroscopy has also been reported on the intramolecular proton transfer enol-keto reaction in **HBT**.[83] These experiments have shown that after excitation the C=O stretch vibration appears on a time scale of 30-50 fs. Similar results were obtained from absorption spectroscopy with the time resolution of 30 fs.[80] The authors found that the emission signal appears after about 60 fs. This short time is too long for a barrierless motion of only the proton and suggests a strong coupling between proton transfer dynamics and the molecular vibrations. The comparison of experimental vibrational patterns for several molecules with a similar proton transfer unit and the high level ab initio calculations[84] allow to find a common mechanism.[85] After optical excitation with an ultrashort pulse, the created wavepacket propagates in a ballistic fashion along the adiabatic PES of the S_1 state. This propagation is accompanied by skeletal deformations related with bending or contraction of the whole molecule. This initial motion changes the distance between the donor and acceptor groups. Interesting is that the proton itself plays a rather passive role staying at its local potential minimum that is shifted by the skeletal motions.

A similar proton behavior during the ESIPT was observed in *[2,2'-bipyridyl]-3,3'-diol* (**BP(OH)₂**), a molecule containing two intramolecular hydrogen bonds. For such system parallel and branching reaction channels are possible: single or double proton transfer. In early investigations, the double proton transfer reaction was found to take place in the S_1 singlet state of **BP(OH)₂**.[86,87] Femtosecond fluorescence upconversion experiments have shown that two mechanisms: concerted (one step) and consecutive (two step) double proton transfer occur concurrently.[88,89] The ratio of the reaction yields of the monoketo and diketo tautomeric products varies strongly with the excess energy. If **BP(OH)₂** is excited at 350 nm the single proton transfer is more effective than when the excitation wavelength is larger.

Lochbrunner *et al.* applied time-resolved absorption spectroscopy with time resolution of 30 fs in order to answer the question if coherent wavepacket dynamics can be observed for systems with parallel reactions and, if so, whether it may be used to obtain any information about the

mechanisms of each of them. They have found that the simultaneous transfer of both protons takes place within 50 fs. In a 'step by step' scenario, the first proton is transferred in about 50 fs, forming the intermediate mono-keto isomer which is transformed with the time constant of 10 ps to the final diketo geometry.[90,91] The comparison of the most dominant oscillatory signal contributions (Figure I.7) with *ab initio* calculation allowed to identify two dominant modes playing a crucial role in excited state dynamics.
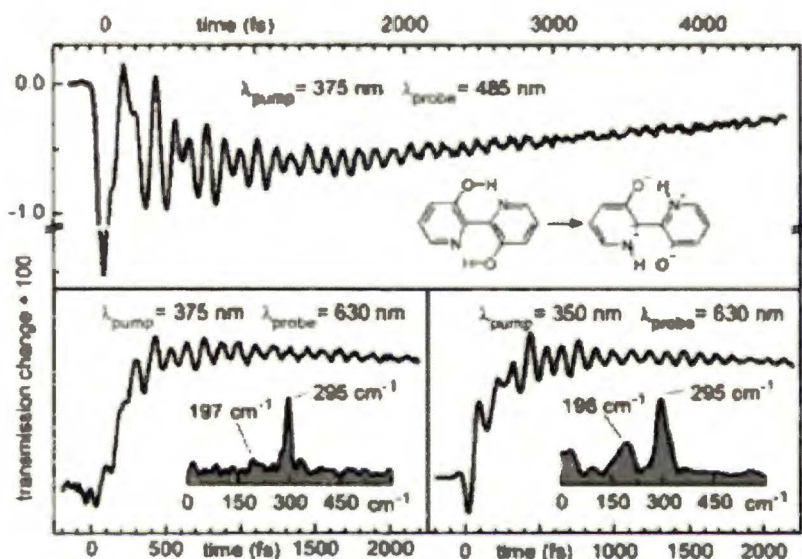
Figure I.7. Transient absorption of **BP(OH)₂** at different excitation wavelengths probed at 485 nm (upper) and 630 nm (lower part of the figure). The Fourier transformation of the oscillatory contributions detected at 630 nm for different excitation wavelengths are presented as insets.[90]

The low frequency mode of 196 cm^{-1} is an antisymmetric in-plane bending vibration which compresses the donor-acceptor distance in only one of the two H-chelate rings and is related to a single proton transfer. The other mode at 295 cm^{-1} is a symmetric stretch vibration reducing simultaneously donor–acceptor distances in both H-chelate rings and is thus promoting a double proton transfer (Figure I.8).

This assignment was confirmed by the excitation energy dependence of the intensity of these modes. If **BP(OH)₂** is excited at 375 nm the mode at 196 cm^{-1} is much weaker (Figure I.7), corresponding to a less effective

generation of the monoketo tautomer.[89] This experiment clearly shows that a characteristic coherent wavepacket behavior can be observed for different reactions. Changing the excitation wavelength gives the possibility to distinguish these wavepackes dynamics from each other and to learn more about mechanisms responsible for studied reactions.
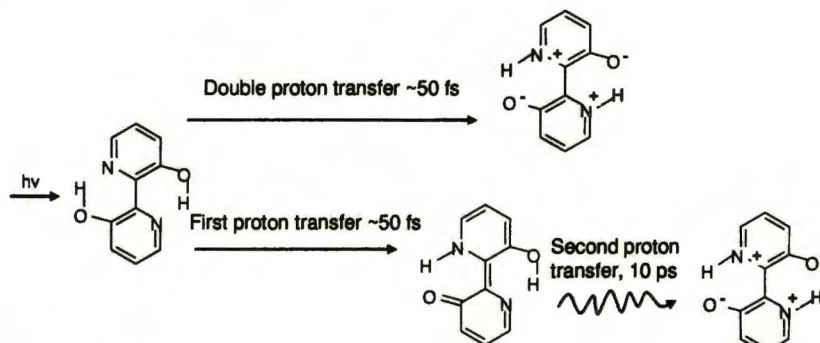
Figure I.8. Concerted double proton transfer involving symmetric in plane-bending of the hydroxy groups vibration (295 cm^{-1}) and sequential double proton transfer assisted by antisymmetric overall bending mode of **BP(OH)₂** (196 cm^{-1}).

The results presented above point to a prominent role of low frequency skeletal modes in hydrogen transfer. Such modes are part of the initially created multidimensional vibrational wavepacket and determine the time scale of hydrogen transfer which occurs along a practically barrierless reaction path. Therefore, models which treat tautomerization as one-dimensional H atom transfer may not have sufficient complexity to describe spectroscopic and kinetic observations for this class of molecules. In general, the proton transfer reaction is not as simple as it was commonly assumed.

I.4. The phenomena induced by intermolecular hydrogen bond

One of the most interesting question in science is: how can nature protect the genetic code from damage by harmful UV radiation? It is well known that UV photons are one of the most effective and toxic agents threatening DNA stability. They can break covalent bonds and thus initiate a complex chain of events that culminates in photodamage. In DNA, four nucleic acid bases encode the genetic information of all living things and it seems amazing that being under continuous photochemical attack this

"material of life" is exceptionally stable. This phenomenon must be related to remarkably rapid decay pathways quickly converting dangerous electronic excitation into less-dangerous vibrational energy that subsequently becomes dissipated rapidly in solution. The fundamental components of DNA form complementary pairs: adenine-thymine and cytosine-guanine (Watson-Crick base pairs)[92] bonded by hydrogen bonds. The DNA photostability mechanism is connected with the radiationless ultrafast excited state deactivation of these hydrogen bonded base pairs.

It is generally known that formation of intermolecular hydrogen bonding influences the photophysical behavior of many heteroaromatic systems.[8,14,21,22,24,93-96] Until now, numerous experimental and theoretical tools have been used to investigate intermolecular hydrogen bonds and several mechanisms of altering the photophysical properties by HB formation have been proposed. For instance, different energy shifts of close-lying $\pi\pi^*$ and $n\pi^*$ states upon hydrogen bonding may cause the reversal of the ordering of these states or lead to large changes in the strength of vibronic or spin-orbit coupling.[21] This is related with so-called proximity effects. If the vibrational coupling is large, the Franck-Condon factor associated with the radiationless transition is large, leading to a rapid conversion to the ground-state. The hydrogen bonding shifts the $n\pi^*$ states to the blue whereas $\pi\pi^*$ states are red-shifted (Figure I.9).
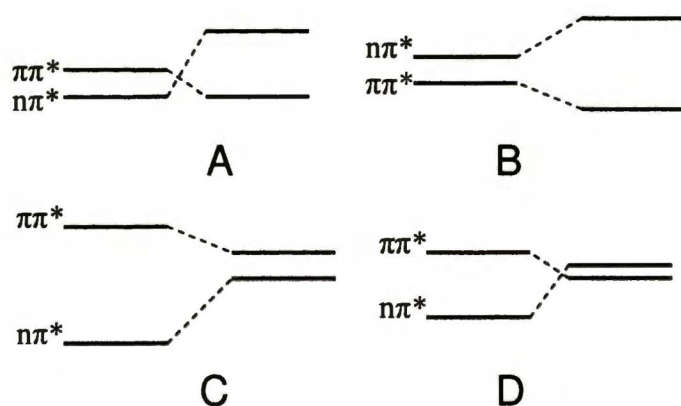

Figure I.9. Effect of intermolecular hydrogen bond formation on the energy level disposition of $\pi\pi^*$ and $n\pi^*$ states. Left, non-bonded; right, H-bonded molecules.

Depending on disposition of these states in molecules in the gas phase the presence of intermolecular hydrogen bonds may enhance the emission quantum yield or make radiationless channels more effective. For example,

when the situation A or B from Figure I.9 takes place the energy gap between the mentioned states may increase considerably in going from aprotic to protic solvent, which should diminish the $n\pi^*$- $\pi\pi^*$ vibronic coupling and, as a result, intensify the emissive properties of molecule. The opposite situation is observed when the $n\pi^*$ state is much lower in energy than the lowest energy $\pi\pi^*$ state in the gas phase (C, D). In this case the intensity of luminescence decreases in a protic solvent because of lowering of the $n\pi^*$-$\pi\pi^*$ energy gap and increasing the efficiency of radiationless transition. Such situation was observed for 9,10-diazaphenantrene, where the fluorescence yield is smaller in alcoholic solvents than in aprotic ones.[97] The explanation was that the hydrogen bonding decreases the $S_2(\pi\pi^*)$-$S_1(n\pi^*)$ energy gap and enhances the proximity effect. Contrary, the examples of fluorescence activation by protic solvents are provided by photophysics of many molecules, among them isoquinoline or acridine.[98]

Another possible deactivation mechanism may operate when the strength of hydrogen bonding is changing upon excitation. Because of different shapes and minima position in the potential energy hypersurfaces of the two states fast internal conversion channel from S_1 may be activated. *1-azacarbazole* (**1AC**) is one of the molecules where

1-azacarbazole (1AC)

strong intermolecular interaction in excited state leads to a significant change in the S_1 deactivation pathway. Waluk *et al.* [99] determining the triplet efficiency for **1AC** in nonpolar solvents and alcohols have found that contrary to former case where monomeric **1AC** is depopulated via intersystem crossing, another fast deactivation channel is switched on in alcohols. This process was attributed to internal conversion enhanced by hydrogen bonding interaction with two different **1AC** nitrogen atoms. Similar behavior has been observed for many hydrogen bonded systems (indoloquinoxalines,[100,101] 2-(2'-hydroxy-5-methylphenyl)benzotriazole,[102] 3-hydroxyflavone,[103] and others. The results of many experiments allow to state that the increase of nonradiative deactivation is typical for bifunctional molecules which are able to form cyclic complexes involving more than one hydrogen bond.[14,104,105] It was found that both HB centers play an active role in quenching, and therefore the NH group replacement by methyl group in 2-phenylindole or in 2-(2'-pyridyl)indoles leads to the lack of efficient internal conversion process.[106] It should be noted that such cyclic structures can take part in double or triple excited state proton transfer. However, in 1:2 complexes this process seems to be improbable because it requires a correlated shift of three protons. In this case, instead of proton transfer, only
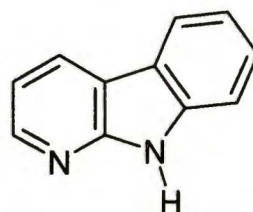
partial movement from the donor to the acceptor occurs and excited state energy is dissipated. Such process may be interpreted as "unsuccessful chemical reaction mechanism".[107] The deactivation process involves a photochemical reaction which is aborted at the conical intersection between the excited and ground state potential energy surfaces of the reacting system. The assumption that the cyclic 1:2 complexes play a crucial role in nonradiative excited state decay seems to be confirmed by the photophysics of isomeric 2-(pyridyl)indoles.[108]

syn anti
2-(2'-pyridyl)indole   2-(3'-pyridyl)indole 2-(4'-pyridyl)indole
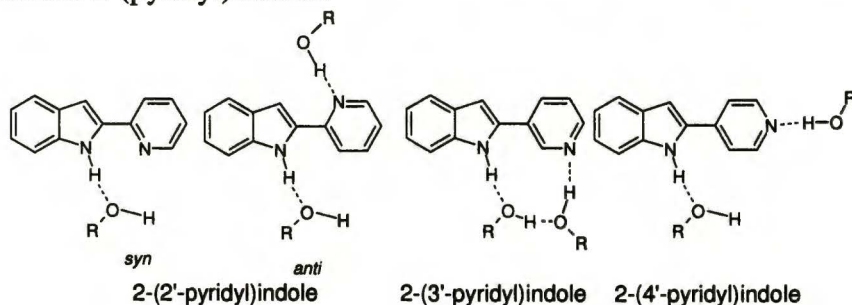
Figure I.10. The isomers of 2-pyridylindoles and possible complexes with alcohols or water.

The fluorescence of 2-(3'-pyridyl)indole is quenched in alcohols by formation of complexes. In this molecule the two hydrogen bonding centers are far from each other and the steric factors make 1:2 cyclic complexes the most probable: indeed the titration has shown that most of the complexes have 1:2 stoichiometry. However no tautomeric fluorescence was detected. Contrary, alcohols do not quench fluorescence in 2-(4'-pyridyl)indole. The lack of fluorescence quenching in alcohol solutions may be interpreted as due to the geometry of molecule which is inappropriate for the formation of cyclic complexes with alcohols.

  Hydrogen bonding can also work in concert with charge-transfer interactions to produce a radiationless decay mechanism. A scheme based on electron transfer has been proposed to be responsible for fluorescence quenching in many systems consisting of two conjugate π-electronic units directly combined by hydrogen-bonding interaction.[93,109-113] HB makes photoinduced electron transfer possible by lowering the ionization potential of the donor and by enhancing the electron affinity of the acceptor. From Mataga's studies, it is well established that the quenching of fluorescence in pyridine (P) complexes with such molecules as: **_carbazole, carbazole derivatives_** and **_1-aminopyrene_** (**AP**), is due to the formation of a nonfluorescent charge transfer state from the excited singlet state of the

25

hydrogen- bonded complex. It was also found that the charge transfer occurs only when the two partners are hydrogen-bonded to each other. The factors governing the charge transfer process are the changes of ionization potential and the structure of the complexes. Mataga and co-workers suggested that the former is related to the changing of the hydrogen-bonding interaction strength in the excited state,

1-aminopyrene AP   aniline   phenol

dibenzocarbazole   1-pyrenol
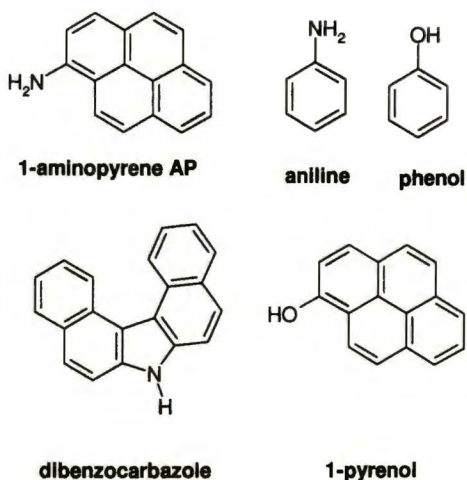
accompanied by very slight movement of the proton toward the acceptor. This results in the stronger CT interaction and, as a consequence, the proton of the donor may be further shifted toward the acceptor. A similar scenario was predicted by calculations for aniline and phenol-pyridine complexes.[114] The results show that the barrier for the charge transfer coupled with the proton movement toward the acceptor is low. The shift of the proton toward pyridine in the charge-transfer state, however, causes a large destabilization of the ground state according to the results of the calculations. Consequently, the energy gap between the charge-transfer state and the ground state becomes small, making the nonradiative deactivation feasible. One can envisage that in the extreme case, neutral radical formation due to the mechanism of charge transfer followed by large proton shift may occur. Nevertheless, only the ion pair formation due to ET with moderate amount of proton shift takes place and the (LE ↔ CT) equilibrium with a fairly long lifetime of hundreds of picoseconds to nanoseconds is established in **AP-P** or **dibenzocarbazole-P**. Contrary, the **pyrenol-P** CT state, (D^+-H--A^-), produced from the LE state, $(D^*- H--A)$, undergoes much faster nonradiative degradation to the ground state than its formation process and therefore it was not possible to detect the CT state in the transient absorption spectra. Herbich and co-workers, on the basis of photohysical studies for the series of over twenty azaaromatic compounds based on pyrrole, indole and carbazole, have shown that the rate-limiting step of the quenching via electron transfer depends on the strength of intermolecular hydrogen bond between two partners of the complex.[113] The excited state LE→CT conversion is faster for molecules with the larger equilibrium constant for the ground state complex formation, and thus with stronger hydrogen bonds. While low-lying CT states were predicted by calculations, transient

26

picosecond studies for pyridine solution have shown the lack of any transient band in the visible region which could be assigned to a CT state. This suggests that the back-electron-transfer rate is larger than the rate of CT formation. Figure I.11 presents the proposed scheme of fluorescence quenching based on the above-mentioned results.

(LE) D$^\cdot$—H····A $\xrightarrow{\quad ET \quad}$ D$^+$—H····A$^-$ (CT)

hv

BET

D—H····A
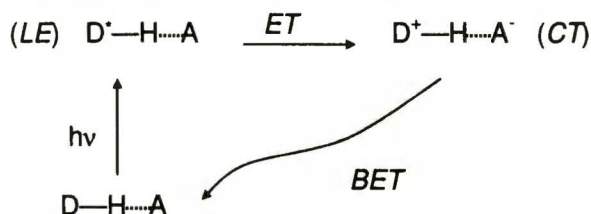
Figure I.11. The mechanism of fluorescence quenching by electron transfer. Abbreviations: LE, locally excited state; ET, electron transfer; CT, charge-transfer state; BET, back electron transfer.

A similar deactivation pathway was found to be responsible for the photostability of DNA base pairs. The calculation of the potential energy functions of GC and AT have revealed that electron-driven proton transfer process between the bases plays the crucial role in their photophysics.[115,116] According to this mechanism electron transfer initiates movement of proton from the donor atom towards the acceptor, and then at the second conical intersection between S_1 (CT) and S_0 along the proton transfer coordinate the back electron transfer takes place. The proton follows the electron and finally is driven back to its original location (Figure I.12). In this way, the dangerous energy of the UV photon is converted into vibrational energy before the system can be destroyed by a photochemical reaction.
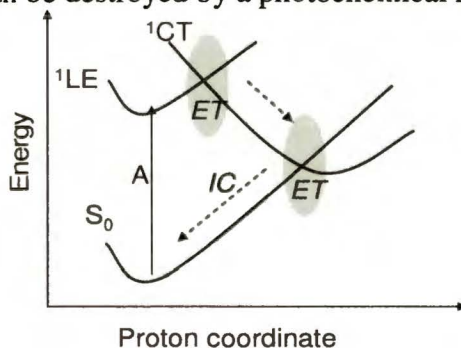
Figure I.12. Schematic view of the excited state electron-driven proton transfer process in intermolecularly hydrogen-bonded systems. Abbreviations: LE, locally excited state; CT, charge-transfer state; ET, electron transfer; IC, internal conversion.

This result takes us naturally to the one of the most dramatic examples of a hydrogen bonding effect in aromatic photophysics: the excited-state intermolecular proton transfer in the lowest excited singlet state. Studies carried out over the years on many factors (e.g., solvent polarity, acidity, viscosity) that can determine the dynamics of intermolecular phototautomerization have shown that various mechanisms of this reaction may be proposed. Recent important progress in the development of femtosecond spectroscopy, supersonic jet techniques and new theoretical methods gives the possibilities for a deeper look into the nature of this phenomenon. Excited state proton transfer reactions are usually initiated by changes in the electronic distribution occurring upon excitation. In heteroazaaromatic molecules containing both hydrogen bonding donor and acceptor group this redistribution leads to an increase in the excited state pK_a of the basic group and the decrease in the excited state pK_a of the acidic group. If the position of both groups is appropriate and the hydrogen bonding partner is also bifunctional it is possible to form HB bridges linking the donor and acceptor and, consequently, protons can be transferred via the bridges connecting the molecules, allowing either tautomerization or the reverse process. In this case the role of solvent is critical because the solvent is responsible for transporting proton to and from prototropic sites in the molecule.

The literature is abundant in this kind of examples; the most representative is *7-azaindole* (**7AI**) and its dimers and complexes with water and alcohols. The mechanism of the excited state double proton transfer (ESDPT) in **7AI** has been a controversial issue in the literature in old and more recent times. Owing to the fact that **7AI** dimers may be treated as a unique model for photoinduced double proton transfer processes in biological systems, they continue to be a subject of intense research. The direct evidence for the phototautomerization in excited state is the additional low-energy fluorescence band. The observation of Stokes-shifted emission in the **7AI** dimer (**7AI₂**) is a sign of occurrence of ESDPT.[117-119] Two mechanisms (presented in Figure I.13) of this reaction have been widely discussed. The *concerted mechanism* was proposed by Kasha and co-workers, who were the first to observe the ESDPT in **7AI₂** in solution.[117] They consider the geometry of **7AI₂** in the lowest excited state as C_{2h} since the two monomer units are equivalent. In their opinion, protons should move simultaneously on the double minimum excited state potential energy surface. This mechanism was supported by temperature studies on the value of the F_2/F_1 intensity ratio and by deuteration effect.[119] The reaction is not stopped even at 4 K, which suggested that proton tunneling plays an important role, at least at low temperatures.
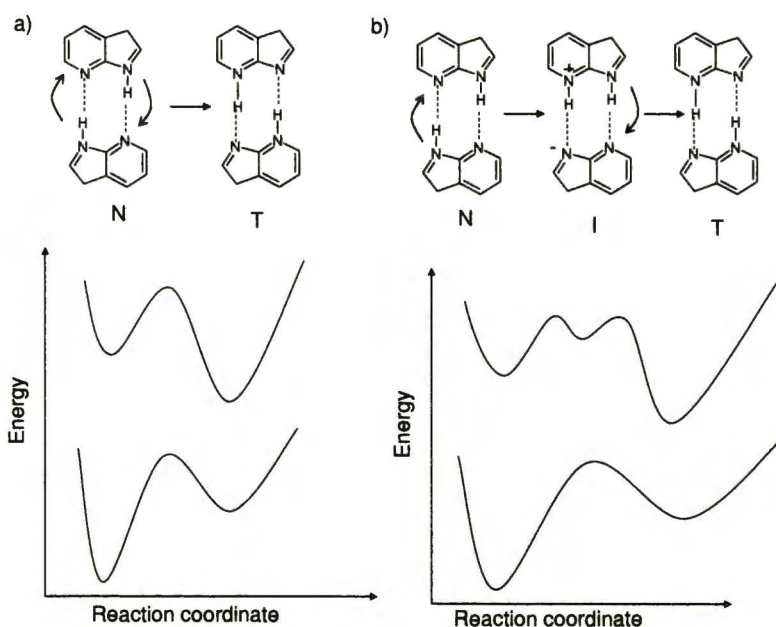
Figure I.13. Two mechanisms of ESDPT in **7AI₂**: concerted (a), sequential (b) and related schematic drawing of one-dimensional potential energy curves.

The *concerted mechanism* in condensed phase was supported by Hetherington *et al.*,[120] who found that the transfer takes place on a time scale shorter than 5 ps. They suggested two possible tautomerization pathways: thermally activated crossing of the barrier and a direct process from nonequilibrated dimers. In solutions, studies of **7AI** with femtosecond resolution were carried out by Takeuchi's[121-123] and Zewail's groups.[124] Using the femtosecond fluorescence upconversion technique Takeuchi observed that fluorescence decay profiles depend on the excitation energy. For shorter wavelengths of laser pulses the decay is biexponential (τ_1=200 fs, τ_2=1.1 ps), but when the system is excited at the red edge of the absorption spectrum the decay has monoexponential character. The single exponential decay was ascribed to the *concerted mechanism*. Zewail and coworkers obtained similar time constants to those of Takeuchi. While the long component of the decay was readily interpreted as formation of tautomer by both groups, the interpretation of the short time is totally different. Takeuchi assigned it to S_2-S_1 electronic relaxation,[122] whereas Zewail and coworkers explained it as the single proton transfer occurring within 250 fs from the normal dimer to an intermediate state.[124] A lot of studies were also carried out in supersonic jet expansion. Fuke *et al.* have shown that under jet conditions two dimeric structures are possible, of

which only one was able to undergo the proton transfer reaction.[125] The results of femtosecond time-resolved mass spectrometry supplied evidence for *sequential mechanism* tautomerization with the time constant of 650 fs for the first proton transfer and 3.3 ps for the formation of tautomer from a zwitterionc state.[10] These findings were confirmed by Castleman and coworkers who, using Coulomb explosion technique, arrested the intermediate state of $7AI_2$ and found the time scales for its building (660 fs) and its decay (5 ps).[126] It was a beautiful suggestion that the proton transfer reaction should be described by a triple-minimum potential energy surface. The calculation performed by Douhal *et al.*[127-129] support the idea of *a stepwise scenario* (Figure I.13b). In contrast to Catalán at al.,[130,131] they obtained a potential minimum that corresponds to the reaction intermediate. Efforts devoted to clarify the mechanism of ESDPT in $7AI_2$ have been summarized by Sekiya and Sakota.[132]. They tried to settle the controversy of the stepwise versus concerted mechanism. Armed with previous results and on the basis of findings from picosecond time-resolved experiments and the kinetic isotope effect on the ESDPT measured by vibronic-state selective dispersed fluorescence, they have concluded that the ESDPT reaction occurs via *the concerted mechanism*. They have shown that the ESDPT rate in the 7AI dimer depends on the excited vibronic state, which was not taken into account in the discussion of the femtosecond results. The comparison of the femtosecond and picosecond experiments have revealed that the biexponential decay previously observed is due to simultaneous excitation of the origin and an intermolecular stretching fundamental mode states, which decay with different lifetimes (Figure I.14). The decay profile obtained by excitation of a single vibronic state was monoexponential, which precluded a stepwise mechanism. This behavior is similar to that observed for the dimer of structurally related *1-azacarbazole* (1AC) studied by Fuke *et al.*[133,134] For this compound no evidence of any intermediates in ESDPT has been reported and the rate of this reaction seemed much slower than in $7AI_2$, as suggested by the bandwidth in the fluorescence excitation spectrum. Additionally, Sekiya and Sakota have found prominent nonlinear kinetic isotope effects. The reaction rate for $7AI_2$-*dd* was nearly three orders of magnitude smaller than for $7AI_2$-*hh*. This observation was interpreted as due to the occurrence of *a dynamic cooperative effect* related to the coupling of the proton motion and electronic reorganization. They stressed that the complexity of the ESDPT in $7AI_2$ is due to the presence of two quantum effects: exciton resonance interaction (the lowest excited state of $7AI_2$ was classified as corresponding to the weak coupling case of the exciton theory) and proton tunneling.
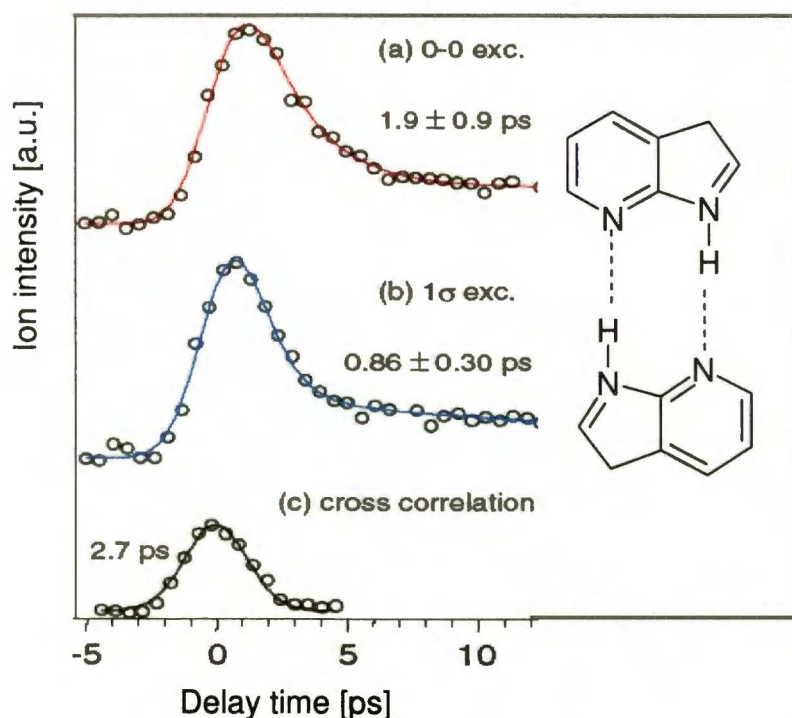
Figure I.14. Decay profiles of **7AI₂-*hh*** pumped at (a) the origin and (b) the intermolecular stretching band, respectively. The wavelength of the probe laser was fixed at 620 nm in (a) and (b). The open circles are experimental data, while the solid curves are best-fitted curves obtained by biexponential functions. The cross correlation trace is also indicated in (c). The instrumental time resolution given by the fwhm of the cross-correlation trace is 2.7 ps. Adapted from ref. 132.

One question that should be answered is: what is the origin of discrepancies between the Sekiya experiment and that of the Castelman's group? The computational results suggest that the Coulomb explosion experiment should be interpreted with caution.[135] The presence of protonated **7AI** fragments (mass-119 species) in the Coulomb-explosion time-of-flight mass spectra may be related with electron detachment predicted by calculation as the initial step of a fast single proton transfer. Since the single-proton transfer in $(7AI)_2^{\bullet+}$ is expected to occur in the period of a vibration (10^{-13}–10^{-14} sec), the second ionisation laser used in the pump–probe Coulomb-explosion experiment may disturb the reaction process to be probed.

Very recently, Sekiya and Sakota published a new article reviewing the results and discussion related to ESDPT mechanism in $7AI_2$.[136] They

31

have shown that many groups reinvestigated their results,[137,138] the new theoretical studies were done,[139-141] and the stepwise and concerted mechanism controversy is still topical.

In addition to investigations of proton transfer in the **7AI** dimer, many studies have focused on the hydrated complexes of this molecule. The monomeric species of **7AI** is also capable of excited-state proton transfer (ESPT) in the condensed phase when assisted by solvent molecules, and also in this case could not do it without controversy. In particular, the two step model presented in Figure I.15 has been discussed widely.
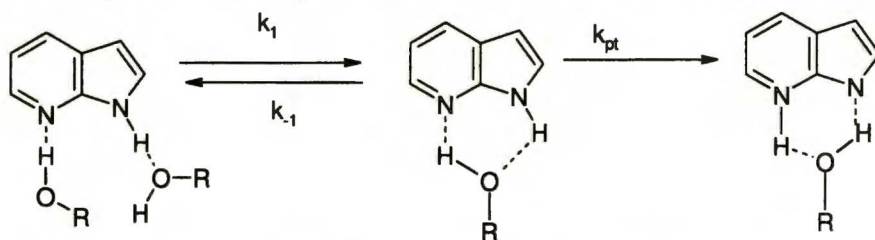
Figure I.15. The mechanism of solvent–catalyzed ESPT in 7AI complexes with alcohol molecules.

The mechanism involves first, the excited state solvent rearrangement toward a favorable structure and second, intrinsic proton transfer. It has been suggested that **7AI** molecules in bulk alcohols form a wide range of hydrogen bonded-structures. It is generally known that only a selected part of the equilibrium population, with appropriately hydrogen-bonded structure is able to undergo direct and rapid tautomerization. There is no doubt that this precursor for the ESDPT corresponds to a 1:1 cyclic double hydrogen bonded complex with an alcohol molecule. However, the subject of the long dispute is the rate-limiting step of the mechanism. Differences among the interpretations arise mainly from whether static or dynamic aspects of the first step control the reaction. The observation of the correlation between the activation energy of tautomerization and the energy of viscous flow in alcohol suggested that the rate-controlling step may involve large-amplitude solvent motions in order to obtain a favorable proton transfer geometry (in such case, the rate of proton transfer $\approx k_1$).[142-145] However, when the equilibrium between solvent reorganization and randomization is rapid relative to k_{pt}, the rate constant is independent of solvent dynamics but is controlled by an equilibrium constant expressed as (k_1/k_{-1}).[146] On the other hand, some authors consider the proton transfer itself as the rate determining process.[147,148] Some workers also noted that the proton transfer rate was strongly correlated with the hydrogen-bonding strength or the acidity of the

alcohol solvents.[145,146] Maroncelli *et al.* proposed to express the observed reaction rate as $k = k_{pt}\exp(-\Delta G/kT)$ where k_{pt} is the intrinsic proton transfer rate in a proper configuration and ΔG is the equilibrium solvation free energy needed to achieve that cyclic complex.[149] The situation in water solution is even more complicated. In this case only one emission band assigned to "normal" fluorescence is observed. However, it was shown that the reaction, impossible in pure water, may occur in ethyl ether or *p*-dioxane solution saturated with water.[150] The time-resolved studies of **7AI** have revealed biexponential decays and growths. Chou and collaborators shared the viewpoint that these emission features reflect the inability to tautomerize as a result of different solvation structure in water compared with that in alcohol solvents. Petrich and coworkers suggested that only a small fraction of correctly solvated **7AI** reacts quickly (~20% at ~70 ps, measured in emission and transient absorption experiments) [147]. On the other hand, Chapman and Maroncelli have argued that the tautomerization is slower (~830 ps in water), and that the nonradiative decay rate of the tautomer formed is much faster (5×10^9 s^{-1}) than in alcohols, but the mechanisms in both solvent are much the same.[151] Similar observation can be made with respect to **1AC** in water. However, both experimental and theoretical studies indicate that a crucial structure for ESDPT in **7AI** and **1AC** can only be achieved after excitation. The required solvent rearrangement makes the reaction slower; moreover it can be stopped by increasing solvent viscosity.[144] This is not the case of other bifunctional structurally related molecules. It was shown that in *1H-pyrrolo[2,3-h]quinoline* (**PQ**) and *dipyrido[2,3-a:3',2'-i]carbazole* (**DPC**) the excited state proton transfer is related with the 1:1 cyclic complexes with alcohol, however, such cyclic precursors for the ESDPT are formed already on the ground state level.[152] The decay of the primary fluorescence and the rise time of tautomeric emission were found not to be monoexponential, but consisting of two components with the time constant between 0.6-0.9 ps for the first and 6-11 ps for the second.[153] The presence of noncyclic complexes in the studied molecules was also observed,[152-155] but the excited state behavior of these species differs from that of **7AI** and **1AC**. In this case the excited noncyclic solvates

1H-pyrrolo[3,2-*h*]quinoline (PQ)

dipyrido[2,3-*a*:3',2'-*i*]carbazole (DPC)

undergo fast radiationless S_1-S_0 deactivation. The differences in the rate of
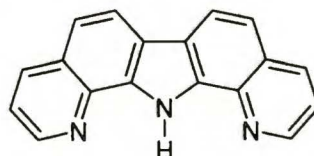
excited state proton transfer in the mentioned molecules result from the fact that in **7AI** and **1AC** solvent rearrangement around the excited chromophore is required prior to ESDPT, whereas in **PQ** and **DPC** correctly solvated structures are present already before the excitation. According to molecular dynamics simulations of adding minute traces of alcohol to nonpolar solutions, the relative equilibrium fractions of cyclic 1:1 complexes of **7AI** and **PQ** are 13-37% and 69-88%, respectively. The situation changes for simulations of bulk alcohol and water. In this case no cyclic 1:1 solvates for **7AI** are present, whereas for **PQ** this form remains dominant (70%).[156] The Monte Carlo simulations in bulk methanol for **DPC**[149] have shown that **DPC** solute behaves similarly to **PQ**, which is in perfect agreement with experimental observations.[152,155]

Since the structure of the complex is a clue for ESDPT, the scientists have spared no effort to clarify some questions concerning this issue. The supersonic jet experiments have played a big part in this field. Such experiments provide a link between the gas phase and the bulk solvent. Making it possible to add solvent molecules to the species of the study, one by one, and to monitor the changes, this technique allows one to look at both static and dynamic aspects of solvation phenomena on a molecular level. In this way a variety of jet-cooled **7AI**,[157-160] **1AC**,[161] or **PQ**[162-164] clusters have been studied. The key parameters to characterize the structures of the clusters are the NH stretch vibration of the chromophore and the OH stretches of water or alcohol. Their frequencies sensitively reflect the hydrogen bonds properties in solvated clusters. These vibrations, as a rule, are observed by IR dip spectroscopy, which measures IR transitions of a specific cluster by the depletion of the S_1-S_0 resonance-enhanced multiphoton ionization signal. Owing to this technique, it is possible to select the molecular species not only by the mass, but also by the electronic transition. The analysis of IR depletion and rotationally-resolved laser induced fluorescence spectra revealed that the most stable isomer of **7-AI(H$_2$O)$_n$** up to $n = 3$ is the single ring structure constructed through hydrogen bonds.[157] However, other authors suggested that a cyclic structure is not achieved for **7AI** complexes with water and methanol.[159]

Laser spectroscopic techniques combined with the supersonic jet expansion are very powerful tools to investigate not only the structure of hydrogen-bonded clusters, but also the proton transfer dynamics of such species in relation to their structures at a molecular level. Folmer *et al.* observed very fast decays of the **7AI-(H$_2$O)$_n$** (n=2-4) with the femtosecond pump-probe experiment under jet-cooled conditions. The biexponential decay observed for **7AI-(H$_2$O)$_2$** and **7AI-(H$_2$O)$_3$** was interpreted as a manifestation of the stepwise proton transfer, whereas the monoexponential

decay in the transient of **7AI-(H₂O)₄** was attributed to the concerted proton transfer. However, very narrow bands (fwhm $\approx$ 0.02 cm^{-1}) in the fluorescence excitation spectra observed by Nakijama *et al.*[157] and the absence of the visible emission from the tautomer in the dispersed fluorescence spectra may suggest that the ESPT reaction competes with the radiative or nonradiative decay processes in the S$_1$ state of the normal forms.[165] Recently, Sakota *et. al*, using dispersed fluorescence spectroscopy, have shown the occurrence of the triple proton/hydrogen relay in **7AI(MeOH)₂** by the observation of tautomeric fluorescence.[166] The process was found to be enhanced by exciting an intermolecular stretching vibration involving the cooperative motion of the whole hydrogen-bonded network. However, an analysis of the resonance-enhanced multiphonon ionization spectra of isotopomers allowed the authors to determine the relative reaction rates for vibronic states in the S$_1$ excited state and to propose that the nature of the mechanism is dependent on the internal energy, changing from vibrational-mode specific in the low energy region to statistical fashion with increasing energy.[167]

Understanding the mechanism of solvent-assisted proton transfer reaction which involves cooperative migration of several protons very often requires the knowledge of possible intermediates and transition states along the reaction path. Therefore the *ab initio* or density functional calculations, in addition to experiment, may be helpful in understanding the kinetics of proton transfer in differently solvated species. Several groups calculated the excited state energies for the S$_1$ states of the normal and tautomer forms of **7AI-(H₂O)ₙ** n=1-4, suggesting that the latter is more stable. However, predictions related to ESDPT are very different for different groups and sometimes even contradict the experiments.

I.5. Solvent influence on the excited state proton transfer

As previously shown, very often solvent molecules play an important role of a mediator making possible proton transfer between the donor and the acceptor groups. This process is named solvent-assisted excited state proton transfer. However, there are several additional ways the solvent can interfere with excited state proton transfer (related with specific and nonspecific effects). One of them takes place when the molecule with an intramolecular hydrogen bond is dissolved in a protic solvent. Then the competition between intra- and intermolecular hydrogen bonds occurs. Very often the tendency to form the intermolecular hydrogen bonds with solvent molecules makes ESIPT less effective (when the intramolecular bond is

35

weakened) or even impossible, in the case when the intramolecular bond is broken.[51,52,168-173] The changes in the rate of ESIPT may depend on the structure of possible solvates. However, the solvent may also not influence the rate of ESIPT: such was the case of salicylidenaniline.[174] As was shown for many molecules, among them *2-(2'-hydroxyphenyl)imidazo[1,2-a]pyridine* (**HPIP**), instead of dual fluorescence (characteristic for normal and tautomeric form) occurring in non-hydrogen bonding solvents, only one emission of nontautomerizing species is observed in protic solvents. When **HPIP** is placed in β-cyclodextrin (β-CD) cavity, the tautomeric emission is recovered, which is a nice confirmation of the important role of the hydrogen-bonding nature of solvent.[168]
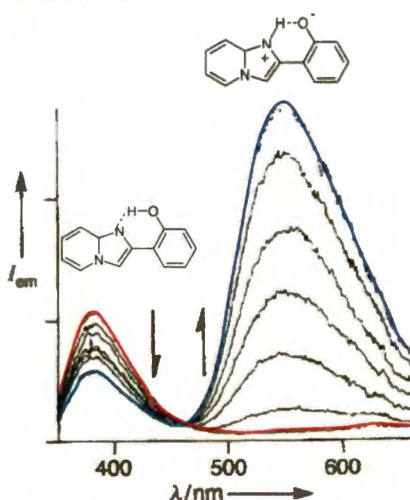
Figure I.16. Fluorescence spectra of **HPIP** in water upon addition of β-CD. Fluorescence spectrum of **HPIP** in water (red); water plus β-CD, [β-CD]=7.0x10^{-3} M (blue). This figure was prepared based on Ref. 168.

Sometimes adding trace amounts of water may change the emission drastically. In many cases, the absorption spectra of intermolecular forms resemble those of the intramolecular one to such extent that it is hard to distinguish between them and the absorption spectrum may not inform directly about the presence of both species. This sensitivity to hydrogen-bonding perturbations forces scientists into carefully interpreting the emission spectra. In the literature there are known examples of misreading of the origin of the emission bands caused by the presence of trace amounts of moisture in the sample. It was shown for **3- hydroxyflavone** that the

3-hydroxyflavone
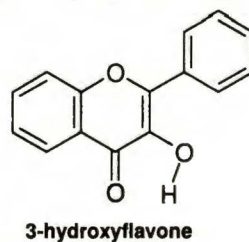
careful removal of protic impurities from nonpolar solvent caused disappearance of a short wavelength emission band, which should be assigned to the solvated species unable to undergo ESIPT, not to the primarily excited form, as was proposed previously.[172] A similar consideration was made about the fluorescence of **TIN** occurring about 400 nm. Finally, it was attributed to the 'inter' form in which the intramolecular hydrogen bond is disrupted by hydrogen bonding to the solvent molecules: as a result, intramolecular phototautomerization can not proceed. Very often, the interpretation is even more complicated by the fact that the hydroxylic solvent may be directly involved in proton transfer processes.[169]

At the end of this chapter it is worth to make some considerations about solvent-induced rotamerization. This phenomenon occurs in a class of compounds that consist of HB donor and acceptor moieties linked by single bond. The relative position of HB centers defines two possible rotamers: the *syn* (both hydrogen bonding groups on the same side of the molecule) and the *anti* (HB groups on the opposite side of molecule). For one of such compounds, **2-(2'-pyridyl)indole** the calculations predict *syn* and *anti* forms, with the former more stable by about 5 kcal/mol. In aprotic solvent, both polar and nonpolar, only the *syn* structure is detected. However, in alcohols a considerable fraction of the *anti* form was found.[108] Different excited state deactivation patterns for the *syn* and the *anti* forms allow distinguishing them using such parameters as lifetimes and quantum yields. Molecular dynamics simulation for *n*-hexane, chloroform and methanol suggest that in alcohol three per four molecules are in the *anti* form. The *syn-anti* rotamerization is induced by the formation of two independent hydrogen bonds with solvent molecules. Another factor which leads to stabilization of the *anti* form is solvent polarity, which makes the *anti* form more favorable due to its larger dipole moment than that of the *syn* rotamer. The rotamerization has important photophysical consequences, since in the *anti* form the two deactivation paths: ESDPT and S_1-S_0 internal conversion, characteristic for the *syn* structure, are no longer possible. It was shown that fast deactivation is related to cyclic complexes and the *anti* form is not able to form such structures. Another interesting case is that of ***2-(2'-pyridyl)pyrrole*** (**PP**) which, depending on the polarity and the protic ability of the solvent may exist as the *syn* or the *anti* rotamer. However, the most interesting is that **PP** (in the *syn* form) is able to undergo intramolecular excited state proton transfer as well as solvent-assisted excited state double proton transfer.[175]

syn   anti

2-(2'-pyridyl)pyrrole (PP)

37
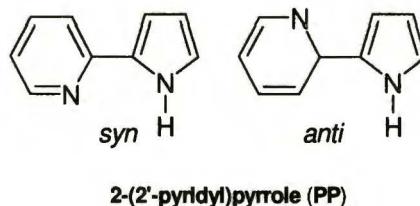
All the mentioned examples emphasize how important is the nature of solvent not only in determining the structure of ground-state species present in solution, but also for a proper description of the excited state deactivation mechanism of the solutes.

CHAPTER II. Goals

Although a large number of articles, reviews, and books have appeared over the last fifty years on the properties of H-bonds and the elementary reaction of proton transfer, we are still far from completely understanding these phenomena. One can safely predict that they will remain an important subject of research in the near future. In order to deepen our understanding of many mechanisms, e.g., those crucial for complex biological systems, it is worth to learn as much as possible about the nature of hydrogen bonds and the intra-and intermolecular proton transfer reactions (ESIPT), studying the photochemistry and photophysics of simple model molecules.

This work is devoted to ground and excited state processes induced by formation of intra- and intermolecular hydrogen bonds in a new class of heteroazaaromatic molecules represented by the series of three isomeric 7-(pyridyl)indoles (Figure II.1), bifunctional molecules possessing both a proton donor (indole NH group) and an acceptor (pyridine type nitrogen). The main aim is to explore the mechanisms, kinetics, and dynamics of the excited states deactivation processes. To attain this goal the experiments in the condensed phase as well as in supersonic jets have been performed using a number of spectroscopic techniques, as well as computational methods.

The choice of the objects to study was well-considered. These compounds differ in the relative position of the donor and the acceptor groups. As a consequence, they can form different type of hydrogen bonds. 7-(2'-pyridyl)indole (**1**) possesses a fairly strong intramolecular hydrogen bond and, therefore, occurrence of the proton transfer reaction in the excited state along this bond seemed to be very probable for this molecule. For 7-(3'-pyridyl)indole (**2**), where the pyridine nitrogen is moved one bond away from the NH group, the intramolecular ESPT is not possible. However, this molecule should be able to form cyclic, intermolecularly hydrogen-bonded complexes with protic solvent molecules, such as alcohols or water. For such a case, one can envisage a solvent-assisted excited state tautomerization, with solvent molecules bridging the proton donor and acceptor groups. In 7-(4'-pyridyl)indole (**3**), the last member of the series, with the acceptor group in the *para* position of the pyridyl ring, the distance between the hydrogen bond centers seemed to exclude a possibility of formation of cyclic solvates, favouring instead a formation of separate

hydrogen bonds between the solvent molecules and either the pyridine nitrogen or the NH group.

7-(2'-pyridyl)indole **1**   7-(3'-pyridyl)indole **2**   7-(4'-pyridyl)indole **3**

2,9-(di-2'-pyridyl)-4,7-di(*t*-butyl)carbazole **4**
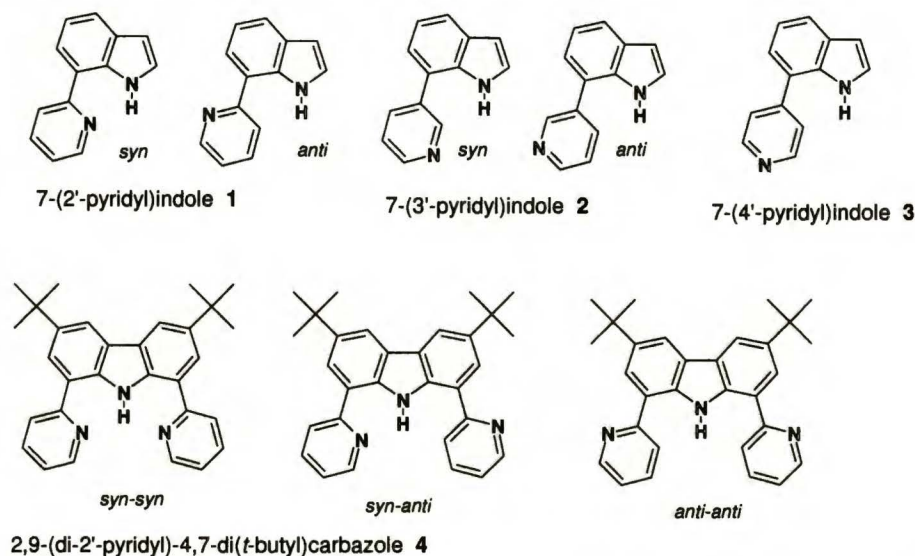
Figure II.1. The molecules investigated in this work and their possible rotameric forms.

In all the selected compounds the HB donor and acceptor groups are located in separate parts linked by single bonds, which implies a possibility of conformational changes caused by specific interaction with protic solvents. As was shown in the previous section, solvent induced *syn-anti* rotamerisation may have important photophysical consequences for the tautomerization process. Additionally, it enriches the photophysics of the studied molecules by increasing the number of possible types of hydrogen-bonded complexes.

To throw light on the problem of competition between the intra- and intermolecular hydrogen bonds, 2,9-(di-2'-pyridyl)-4,7-di(*t*-butyl)carbazole (**4**), a molecule structurally related to 7-(2'-pyridyl)indole has been studied. Both systems have the same proton donor (NH) and acceptor (pyridyl nitrogen), but the number of acceptor groups is doubled in the former. It should be stressed that *syn* → *anti* rotamerization in molecules with one donor and one acceptor group can stop the phototautomerization by breaking the intramolecular hydrogen bond. However, this need not be the case for 9-(di-2'-pyridyl)-4,7-di(*t*-butyl)carbazole, for which a rotameric form with one pyridyl in the *syn* and the other in the *anti* conformation is

possible. Such a conformational change may reinforce the intramolecular hydrogen bond, which may no longer be bifurcated. Thus, this molecule gives the opportunity to study the influnce of intra- and intermolecular hydrogen bond, both of them simultaneously, on excited states deactivation processes.

Besides the steady-state and time-resolved absorption (UV/VIS and IR) and emission spectroscopy, magnetic circular dichroism spectroscopy (MCD) and combination of various methods of laser-induced spectroscopy coupled with isolation in molecular beam were applied in order to answer the following questions:

a) What is the nature of the lowest electronic states?

b) What is the role the structure and geometry play in phototautomerization processes?

c) How can conformational changes influence the mechanisms of deactivation processes?

d) How do the photophysics and photochemistry of the studied systems depend on the nature (polarity, viscosity, and the ability to form hydrogen bonds with the solute) of the solvent/environment?

e) What is the proper definition of the proton transfer reaction path? Does tunneling and/or conformational changes contribute to it?

f) What is the structure and stoichiometry of solute-solvent complexes and how can it affect excited states depopulation processes?

g) How can an intermolecular hydrogen bond interfere with an existing intramolecular hydrogen bond, can such interference change the rate of the ESIPT?

The results of this work should help to understand the correlation between photoinduced electron density redistribution, the proton transfer reaction, and the large amplitude motions. It should be noted that none of the investigated compounds have been explored earlier with spectroscopic and theoretical methods, with one exception, discussion on **1** in ref.176, which actually was inspired by the results presented in this work. Finally, a practical goal was to check whether the photophysics of the investigated chromophores can make them good candidates for photostabilizers.

41

CHAPTER III. Experimental procedures

III.1. Reagents and preparations

All the studied compounds were synthesized and purified in the laboratory of Professor R. P. Thummel from the University of Huston, USA. A series of three isomeric 7-pyridylindoles were prepared by the Stille coupling of 7-bromoindole, synthesized by the Bartoli reaction, and the appropriate tri(*n*-butylstannyl)pyridine.[177] The 2,9-(di-2'-pyridyl)-4,7-di(*t*-butyl)carbazole have been prepared by means of Stille coupling from dibromo precursors, obtained following such methodologies as oxidative cyclization and Sandmeyer reaction.[178,179] The compounds were purified by vacuum sublimation.

All solvents used for studies: *n*-hexane, acetonitrile (Aldrich), methanol, propanol-1, buthanol-1, dimethyl sulfoxide (Merck) and ethanol (Chempur), 1-octanol (Fluka Chemika) were of spectral or HPLC grade and were examined for the presence of fluorescent impurities. Methylcycloxexane (Merck) and 3-methylpentane (Fluka Chemika) was dried by percolating them through a column with silica gel and alumina.

The polymer films were obtained as follows: PMMA (poly (methyl methacrylate)) was prepared by distilling out the inhibitor from MMA monomer solution. The powder sample was dissolved in MMA and the solution placed in a cylindrical cell immersed in an oil bath, slowly heating from 40 to 80^0 C for a few days in an oven. The glass form was removed simply by smashing. The polymeric samples were shaped into rectangular cells or cut into thin layers.

III.2. Steady-state investigations

Electronic absorption spectra were recorded on a Shimadzu UV 3100 spectrophotometer, equipped with a home-made temperature control system, allowing to vary the temperature between 88 and 333 K with the accuracy of ± 2K.

To record the **IR spectra** in KBr tablets and solutions a NICOLET SX 170 Fourier transform infrared spectrometer (FTIR) was used.

Steady-state emission and excitation spectra were measured either on an Edinburgh Analitycal Instruments FS 900 CDT or on a compact Jasny spectrofluorimeter.[180] The latter instrument was used for studies of

temperature dependence of luminescence, guaranteeing a temperature stability of $\pm$ 2 K. To obtain true emission spectra, the observed plots of luminescence intensity were divided by the spectral sensitivity curves of the instruments and multiplied by the factor λ^2 in order to convert counts per wavelength into counts per wavenumber. Quinine sulfate in 0.1 N H_2SO_4 (Φ_{fl} = 0.51)[181] served as a standard for the determination of the quantum yields. To determine these values, the solution of the standard and the investigated molecule were excited at the wavelength where the optical density was identical for both of them. For the measurements of fluorescence excitation spectra, optical density of the sample did not exceed the value of 0.1 at the maximum of the absorption spectrum.

Magnetic circular dichroism (MCD) curves were recorded using a dual beam OLIS DSM 17 CD spectropolarimeter, equipped with a permanent magnet (M) of about 1.1 kG (1.1 Tesla) magnetic field strength. The MCD setup is schematically shown in Figure III.1. To produce the required UV light, a 150-watt xenon arc lamp is used. The output wavelength is determined by a Cary 17 monochromator which provides a broad spectral range from 185 nm to 2600 nm. The monochromatic beam passes through a linear beam splitting polarizer (P) and a 50 kHz photoelastic modulator (PEM) which converts linearly polarized light to circularly polarized, and as a consequence, two beams of right (RCPL) and left (LCPL) polarization are produced. RCPL and LCPL beams pass simultaneously through the sample placed between magnet (M) poles. After detection by the photomultiplier tubes (R955 PMTs), the two 50 kHz components are normalized by dividing through their respective DC levels, and then digitally subtracted to give the CD signal. The spectrometer is completely interfaced to a PC for data collection and analysis. The advantages of using this instrument result from the fact that the absorption for right and left-handed polarized light is measured simultaneously. Thus, lamp noise is reduced and, in principle, no calibration against a photometric standard is required.

The direct data from the OLIS instrument, reported as ellipticity in millidegrees (mdeg), are corrected for concentration and expressed as magnetically induced molar elipticity per unit magnetic field $[\Theta]_M$ (in units of deg G^{-1} M^{-1} m^{-1}).

All the MCD experiments were performed at ambient temperature on solutions with an optical density of ca. 0.9 in a 1 cm cell. It was shown that the relationship between absorbance and signal to noise ratio is the best for A= 0.89.[182]
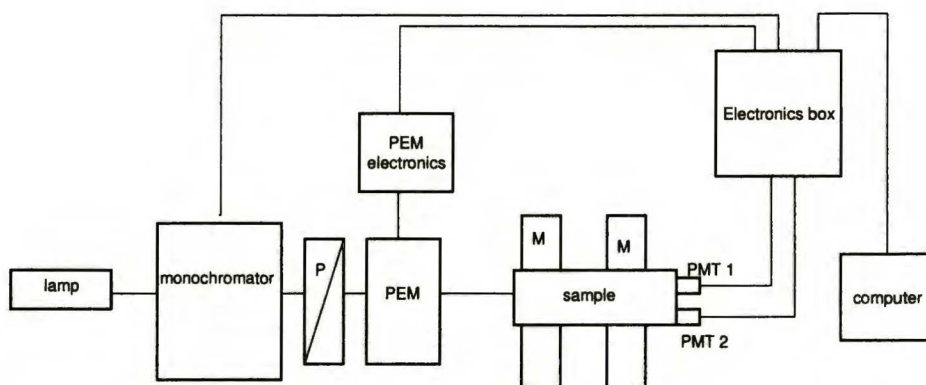
Figure III.1. A schematic of an Olis MCD instrument.

III.3. Time-resolved techniques

Fluorescence decays in the nanosecond range were recorded on an Edinburgh FL 900 CDT time-resolved fluorometer, with estimated time resolution of 500-300 ps, using time-correlated single-photon counting method.

The fluorescence lifetime investigations in the subnano- and picosecond ranges were performed applying time-correlated single-photon counting technique. Two different apparatuses were used to carry out these measurements.

In the Laboratory of Photochemistry and Spectroscopy of the Polish Academy of Sciences in Warsaw the fluorescence decays were studied using a time-correlated single-photon counting card (Time Harp 100 Picoquant) which can offer 39 ps time per channel. As an excitation source a picosecond blue laser diode (NanoLED-295 Horiba Jobin Yvon), controlled by a NanoLed pulsed diode controller (IBH) and working with the repetition frequency of 1 MHz was used. The fluorescence of the sample was directed onto a slit of a Digikröm CM122 1/8m Double Monochromator (Spectral Products) working in the subtractive mode, and then detected by a photomultiphier (PCM-100-4 Becker & Hickl GmbH). The instrument response function (IRF) was determined by the scattering method and was found to be ~850 ps. The time resolution was estimated to be ca. 200 ps. An unquestionable advantage of this instrument is the possibility of coupling it with a home-made temperature control system designed by Jasny.[183] This equipment allows studying the temperature dependence of fluorescence

lifetimes. For the analysis of fluorescence decay kinetics, Fluofit version 3.3 software provided by Picoquant was used. Fluofit implements an iterative reconvolution of the instrument response and the fluorescence decay with nonlinear error minimization based on the Levenberg- Marquardt and Simplex algorithms.[184]

Some decays with higher time resolution were recorded at the Van 't Hoff Institute for Molecular Sciences, University of Amsterdam, using a picosecond time-correlated single-photon counting setup described in detail before.[185] Excitation was provided by a mode-locked argon ion laser (Coherent 486 AS Mode Locker and Coherent Innova 200 laser), which synchronously pumped a dye laser (Coherent model 700) operating on DCM. The dye laser, frequency-doubled with a BBO crystal, yielded 310-320 nm pulses. A Hamamatsu microchannel plate photomultiplier (R3809) was used as the detector. The response function of the instrument had an fwhm of 17 ps.

Time-resolved fluorescence/absorption measurements in the picosecond range were also performed using a home-made transient absorption/emission spectrofluorimeter[186,187] upgraded with a new Light Conversion Nd:glass laser as the light source (Figure III.2). The mean pulse energy is stabilized by negative feedback control system. A single pulse ($\Delta t=1.3$ ps fwhm, $\lambda=1055$ nm, repetition rate 33 Hz) is selected by an opto-electronic pulse selector, amplified and separated into two parts. For fluorescence measurements the first beam is directed into the KDP crystals (3H) to generate the third harmonic ($\lambda=351$ nm) used as the excitation beam. The second beam is passed through the optical Kerr shutter (C), consisting of a cell with CS_2 or C_2Cl_4 placed between two crossed Glan polarizers (P). Fluorescence emitted by the sample is collected and transferred by two spherical off axis parabolic mirrors (PM) (Janos Technology Inc.). The Kerr shutter is opened by the fundamental pulse (1055 nm), therefore the fluorescence can be transmitted by the shutter only during the time window of ca.6 ps. An optical delay line (maximum delay 3000 ps, 0.1 ps/step) is used to delay the opening pulse with respect to the excitation pulse. Subsequently, fluorescence is transmitted by a quartz fiber to the detection system composed of a Acton SpectraPro 275 spectrograph, and a CCD detector (Princeton Instruments Inc.). The signal from the negative feedback unit of the Nd:glass laser is used for intensifier triggering. The temporal resolution of time-resolved fluorescence measurements was estimated to be ca. 6 ps. The setup allows also for transient absorption (TA) measurements with a pump-probe technique. To obtain a probing pulse in such experiments, the second beam of the fundamental frequency is focused

45

inside a long cell containing D_2O in order to generate pulses of spectral continuum extending between 430 and 800 nm. The probe beam is optically delayed with respect to the excitation pulse. After passing the sample, the portion of probing light absorbed due to excitation of the sample is detected (back-thinned CCD, 1024px/128px, S7031series, product of Hamamtsu) and analyzed. The temporal resolution of transient absorption measurements was approximately 2.5 ps.
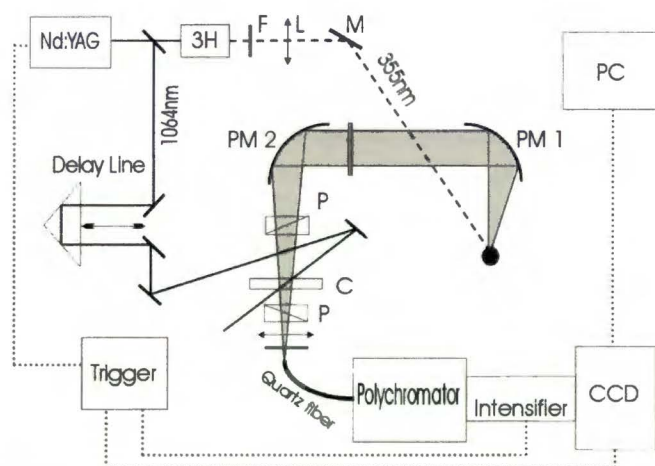
Figure III.2. Optical scheme of the picosecond spectrofluorimeter. 3H, third harmonic generator, F, filter, L, lens, M, mirror, PM, off axis parabolic mirror, P, Glan polarizers, C, cell with CS_2 or chlorobenzene.[187]

The kinetic curves of the fluorescence and transient absorption decay were extracted from the time-resolved spectra recorded for various delay times by integrating the bands within the selected spectral range. The decay times were evaluated applying the deconvolution procedure.

The femtosecond transient absorption investigations were performed at the Van 't Hoff Institute for Molecular Sciences, University of Amsterdam, employing an experimental setup described in detail elsewhere.[188] Shortly, the laser system is based on a Spectra-Physics Hurricane Titanium Sapphire regenerative amplifier, which generates a 130 fs (fwhm) pulse train at 800 nm with a repetition rate of 1 kHz. This pulse was separated into two parts. One of them pumped an optical parametric amplifier (OPA 800), which was used to generate excitation pulses at 325 nm. Generation of the white light continuum from 350 to 800 nm used for

the probe pulse was accomplished by focusing the second part of the fundamental on a calcium fluoride crystal. In the present experiments magic angle conditions were used for the pump and probe beam. The circular cuvette, containing the solution of the sample, was placed in a home-made rotating ball bearing (1000 rpm), avoiding local heating by the laser beams. The probe beam was coupled into 400 μm fibre optics after passing the sample and detected by a CCD spectrometer (Ocean Optics, PC2000). The I and I_0 are provided using a chopper (Rofin Ltd., 83Hz) placed in the excitation beam. The total instrumental response was about 200 fs (fwhm) and the excitation power was kept as low as ~5 μJ per pulse using a pump spot diameter of about 1 mm. To monitor the influence of thermal effects and possible photodegradation, absorption and emission spectra before and after experiment were measured and comparison between them showed that photodegradation was not substantial. All experiments were performed at ambient temperature on solutions with an optical density of ca. 0.5 in a 1 mm cell.

Figure III.3. Schematic setup of the ultrafast spectrometer: C, chopper; D, detector (CCD or Si photodiode); DL, delay line; G, white light generator; P, polarizer; S, sample.[189]
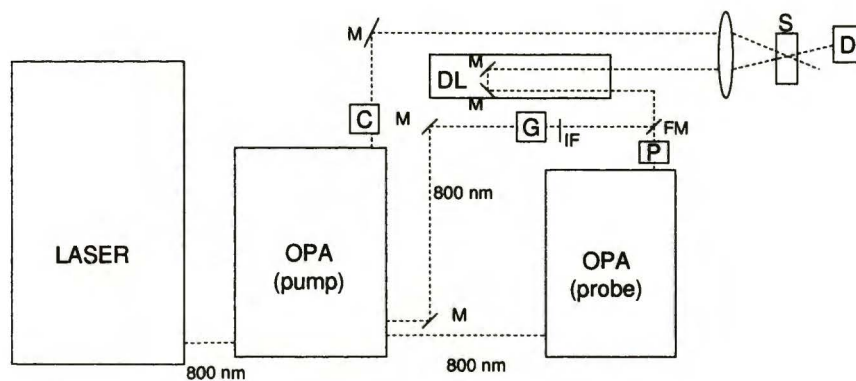
47

III.4. Supersonic jet experiments

III.4.1. Introduction

The main aim of this part of the Chapter is to explain why the supersonic jet expansion technique is attractive and useful for the spectroscopy. It is known that owing to this technique of sample cooling the range of problems which can be resolved by spectroscopy dramatically increased. The main features of the molecular beam techniques and their spectroscopic consequences are presented below.

Highly-resolved and greatly simplified molecular spectrum - the consequence of cooling of the internal degrees of freedom

In supersonic jet spectrometry, a gas expands from a high-pressure to a low-pressure region through a small orifice (Figure III.4). In the early stages of the expansion, the probability of collisions between molecules is high, and these collisions make the *velocity distribution* (related with the translational temperature) become narrow. Through the collision processes, the translational cooling is transferred to cooling of rotations and vibrations. The efficiency of energy transfer among these motions (determined by the densities of the energy levels) is different and therefore, after adiabatic expansion, the gas is not at thermodynamic equilibrium. Under the typical conditions of p_0 (He) = 3 atm, T_0 = 300 K the values of about $1 - 5$ K and $20 - 50$ K are achieved for the rotational and vibrational temperatures, respectively. At these low temperatures only a few rotational and vibrational states are appreciably populated, and therefore the gas phase spectrum changes from a broad, unresolved electronic band to a sharp spectrum where individual vibrational features are easily resolved.

The source of isolated molecule free of external perturbations

As the expansion proceeds, an isolated collision-free condition is attained. The internal energy of molecules is partly transferred into the kinetic energy of the beam. The gas may be moving with a high flow velocity, but if all molecules are moving at about the same velocity, collisions between them are unlikely. Collision-free conditions in a supersonic beam imply a considerable decrease of the inhomogeneous broadening. The Doppler effect related with the velocity distribution is dramatically reduced during the translational cooling. This effect may be further decreased by collimating the beam with a skimmer (or skimmers).
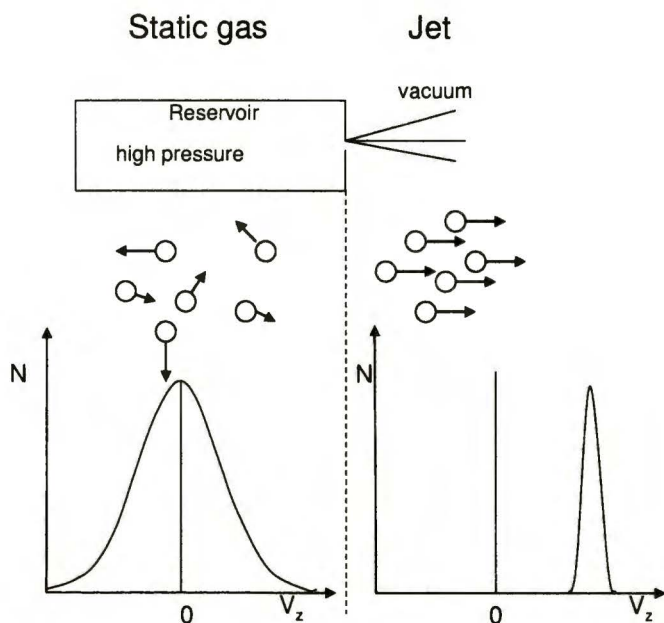
Figure III.4. Distribution of velocities in a static gas at room temperature and in a supersonic expansion.

Formation and studies of weakly bounded clusters

In a supersonic jet, where the translational temperature is low, weakly bound clusters with small dissociation energies D_e can be stabilized and can be studied spectroscopically. This is impossible at room temperature, where kT is much larger than the binding energy of the complex. Additionally, supersonic expansion allows to form molecular clusters in a controlled way. It is possible to successively add solvent molecules to the studied chromophore, one by one, in order to examine the solvation processes.

Absence of condensation

In the jet experiments a small quantity of the molecule of interest is mixed with a large amount of a carrier gas, such as helium. In this mixture, expanded to form a supersonic free jet, most of the collisions happen between carrier gas atoms. When helium or other rare gases are used as carrying medium, the interatomic forces are much weaker than they would have been in a pure molecular expansion. As a result, condensation is greatly reduced.

III.4.2. Spectroscopic laser techniques

Recently, the combination of sophisticated laser techniques and supersonic free jet expansion has offered a deeper insight into the structure and reactivity of molecules and molecular clusters. There is a large body of literature describing different types of spectroscopy that have been used to study molecules cooled in supersonic molecular beams.[162,190,191]

Laser-induced fluorescence excitation (LIF)

The energy scheme exploited in one of the most popular techniques, laser-induced fluorescence excitation (LIF) is given in Figure III.5. The fluorescence excitation spectrum is measured by monitoring the total number of fluorescent photons emitted by a molecule as a function of the excitation frequency. Since the fluorescence photon emitted by the molecule, returning to the ground state, is an indicator signaling that the molecule had absorbed a photon at a particular frequency, the LIF excitation spectrum, similarly to the absorption spectrum, can provide detailed information about optically accessible levels of electronically excited states.
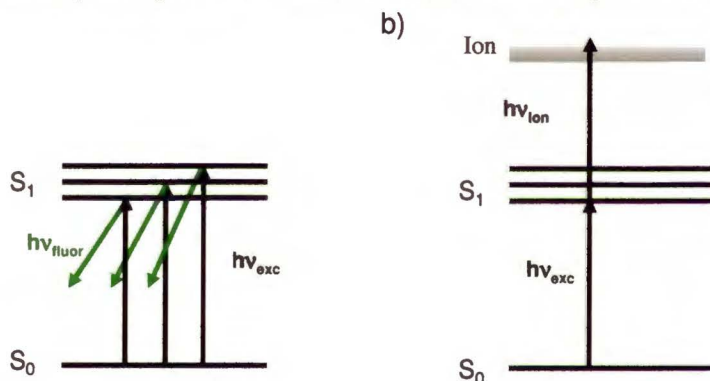
Figure III.5. Energy schemes for (a) laser-induced fluorescence (LIF) excitation and b) mass-selective resonant two-photon ionization (R2PI) spectroscopy.

Resonance-Enhanced Multiphoton Ionisation (REMPI)

In this technique one photon (or several) is used to bring the molecule to the excited state and a second photon (or several more) is then used to ionize the excited electronic state populated by the first photon. The formed ions are mass-analyzed in a time-of-flight mass spectrometer (TOF-

MS). When ionization occurs with two photons of the same frequency, the spectrum obtained is called a one-color **resonant two-photon ionization (R2PI)**. To measure R2PI spectra, the ion yield at a selected mass is recorded while scanning the wavelength of the exciting laser. In this way the vibronic spectrum of the molecular system in its S_1 state is obtained. Since the power and energy of the pump and ionizing photons may be independently varied, it is possible to study the dynamics of excited intermediates by imposing the time delay between excitation and ionization.

Double-resonance IR/R2PI ion-depletion

A very useful method to study structure and composition of hydrogen-bonded clusters is double-resonance IR/R2PI ion-depletion. This method is a combination of the structurally sensitive infrared (IR) spectroscopy with the mass-selective R2PI spectroscopy. The idea is presented in Figure III.6. The IR photon arrives prior to the UV photon, the vibrational ground state of the electronic ground state is depopulated in case of a resonant vibrational excitation, resulting in a decreasing ion signal of the R2PI. The IR/R2PI spectra are obtained by scanning IR laser and monitoring the ion yield signal (R2PI) with the wavelength from a UV laser fixed to one of the electronic transitions of the selected species. The obtained spectrum represents the IR absorption of the neutral cluster before it is ionized by R2PI. Since the vibrations in a cluster are very sensitive to its structure, the frequencies and intensities of the vibrations in different types of clusters provide information about the nature of intermolecular interactions.

Figure III.6. Scheme of a double-resonance IR/R2PI experiment.

III.4.3. Instruments

The supersonic jet experiments were performed in two laboratories. The jet spectrometer in the Laboratory of Molecular Beams, Department of Photochemistry and Spectroscopy of the Institute of Physical Chemi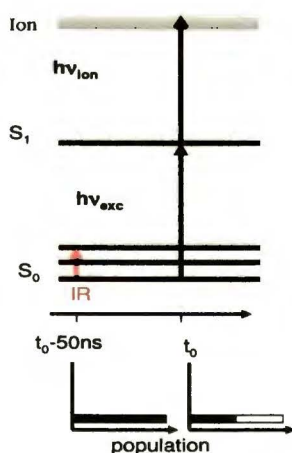stry of the Polish Academy of Sciences in Warsaw was used to measure LIF excitation spectra. R2PI, IR/R2PI depletion and IR/fsMPI measurements were carried out in the laboratory of Prof. B. Brutschy from the Institute of Physical and Theoretical Chemistry, J. W. Goethe-University in Frankfurt am Main.

A typical supersonic jet apparatus usually consists of three main components, namely: high vacuum chamber or chambers with an ejection system, the laser system for exciting the molecules under study, and the detection part. As the source of coherent narrow band light in the LIF spectrometer in Warsaw, a commercial SunliteEX (Continuum) optical parametric oscillator (OPO) was used, pumped by the third harmonic of an injection-seeded $Nd3^+$:YAG laser (Powerlite 8000 Precision), providing a spectral range of 440-1800 nm with a typical spectral linewidth < 0.2 cm^{-1}. Alternatively, two home-built, tunable dye lasers, designed by Jan Jasny,[192,193] pumped by the second harmonic of a $Nd3^+$:YAG laser (Sureline I-10) were utilized. The first dye-laser contains a prism beam expander in the resonator. The spectral width of this laser is of about 0.3 cm^{-1} and the average pulse energy, obtained from the oscillator, is typically 100–200 μJ. The other, grazing incidence dye laser system with an intracavity etalon provides about 0.1cm^{-1} bandwidth and the energy of about 150 μJ/pulse. The laser output was frequency-doubled using KDP or BBO nonlinear crystals. The spectral calibration of the lasers was carried out utilizing a high resolution grating spectrograph constructed by J. Jasny.

The experimental setup consist of a vacuum chamber evacuated by a turbomolecular pump (650 l/s) supported by a Roots pump and equipped with a pulsed valve (modified General Valve Series 9) with a 0.5 mm orifice and a compartment where the molecules of interest can be heated up to 300°C. The nozzle is controlled by a General Valve Iota One solenoid valve driver and operated with a repetition rate up to 10 Hz with typical pulse duration of 150 ÷ 700 μs. The sample heated in the compartment vaporizes and is diluted with inert gas and injected from a pulsed nozzle into a vacuum chamber to produce a supersonic jet. Here, the molecular beam is crossed perpendicularly, 5 - 8 mm downstream from the nozzle, by the excitation laser beam. The optical detection system construction of J. Jasny consists of a toroidal mirror, which collects the total fluorescence and, in order to record LIF excitation spectra, focuses it onto a Hamamatsu R2949

photomultiplier tube (PMT). The signal from the PMT is processed by a 300 MHz digital oscilloscope (LeCroy 9310) and stored in a computer. The synchronization between the devices working in the pulsed mode (lasers, pulsed jet valve) is provided by a Stanford Research DG535 delay generator.

A schematic picture of the experimental setup used to measure the R2PI spectra in the Institute of Physical and Theoretical Chemistry, J. W. Goethe-University in Frankfurt am Main, is shown in Figure III.7. The vacuum system of the supersonic beam apparatus consists of two differentially pumped vacuum chambers connected via a 5.0-mm diameter skimmer. Monomers and clusters are ionized by one-color resonant two-photon excitation and are subsequently mass-analyzed in a home-built reflectron TOF mass spectrometer in chamber 2. Ionization takes place in a two-stage parallel-plate ion source placed behind the skimmer. Excitation is provided by the frequency-doubled output of an excimer-pumped dye laser (Lambda Physik MG 103SC and LPD 3000). Alternatively, a frequency-doubled output of an optical parametric oscillator OPO (Continuum Sunlite) pumped by a Nd:YAG laser (Continuum Powerlite 8000) operated at 10 Hz is used as as the UV radiation source. The ions are amplified in a dual microchannel plate detector, of which the output is directed into a 300 MHz amplifier (Phillips, model 771) and digitized in a 300 MHz digital transient recorder (LeCroy 9310). The accumulated spectra are transferred to a PC via a general purpose interface bus (GPIB) interface.

A pulsed solenoid valve (General Valve Series 9, with a conical outlet) with a nozzle diameter of 500 μm is used as a beam source. The valve is driven by a pulse generator (Hewlett- Packard 214B) with pulses of ~75 V amplitude and ~900 μs width. A digital pulse generator (Stanford Research, DG 535) controls the triggering of the pulses for the laser, the nozzle and the fluorescence detection.

In order to study the microsolvation, the complexes of jet-cooled molecules are generated by mixing the sample vapor with the seed gas, containing the solvent at low concentration (~1% with respect to volume). To get the optimal cluster size distribution in the supersonic jet the following parameters may be adjusted: nozzle temperature, the electric driving pulse for the nozzle, the time delay between nozzle opening and laser pulse, and/or the partial pressure of the solvent in the carrier gas.
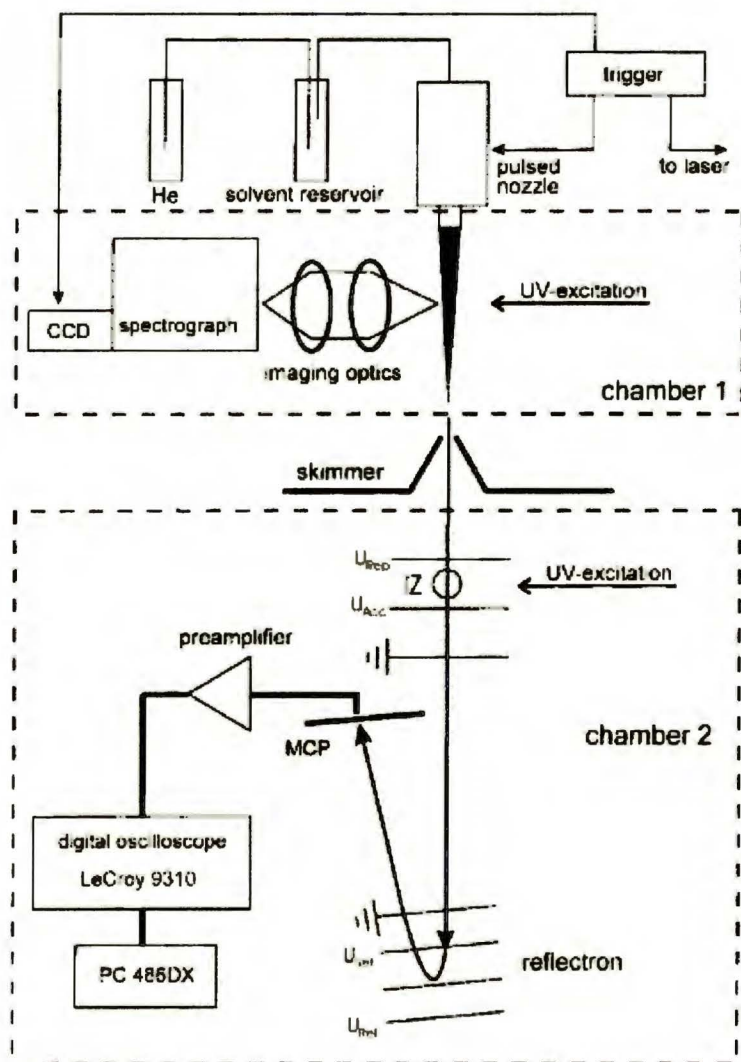
Figure III.7. Schematic picture of the experimental setup in the Institute of Physical and Theoretical Chemistry, J. W. Goethe-University in Frankfurt am Main.[194]

For the IR/R2PI experiments two counter-propagating laser beams, that of the UV ionization laser and of a tunable IR laser are focused and intersect the skimmed molecular beam at the right angle in the ionization zone of a TOF mass spectrometer, just behind the skimmer (IZ in Figure III.7). Continuously tunable IR radiation is generated by a home-built,

injection-seeded OPO using $LiNbO_3$ crystals for both the OPO and the difference-frequency mixing (DFM) stage. Its wavelength may be tuned in the range 2.7 – 4.0 µm with a bandwidth of 0.2 cm^{-1}. The typical output energy is about 5 mJ/pulse. The IR laser is fired about 50 ns before the UV laser.

The principle and the setup for the femtosecond multiphoton ionization IR/fsMPI measurements have been described previously.[162] The sample/nozzle temperature was typically maintained at 343 K. To generate REMPI signals, the tunable output of an optical parametric converter (TOPAS, Light Conversion) pumped by a femtosecond chirped-pulse amplified Ti:Sa laser system (1 kHz, 260 fs FWHM autocorrelation at 800 nm) was used. The scanning range (330-360 nm) was accomplished by applying a set of dielectric mirrors. The energy pulse was nearly constant at about 15 µJ. The UV beam was focused by an f = 30 cm fused silica lens. For the femtosecond pump-probe photoionization experiments the tunable UV laser was employed as the excitation (pump) source, and the second harmonic of the Ti:Sa fundamental was used for the ionization (probe) of the electronically excited intermediate. The sample molecules were resonantly ionized via 1×UV+2×400nm process. The total output of the Ti:Sa laser system was split into two parts, 450 µJ/pulse was directed to the TOPAS and the remaining 200 µJ/pulse was used for frequency doubling. This resulted in 80 µJ pulse energy at 400 nm. Both the UV and 400 nm beams were quasi-collinearly introduced into the detection chamber and overlapped in the ionization region of the mass spectrometer. The beams were only slightly focused by f = 4 or f = 5 m fused silica lenses. The observed ion signal was purely two-color, it was checked that each of the beams alone did not produce any ions. To regulate the time separation between the pump and probe pulses an optical delay stage was employed. Partial deuteration was performed by adding a few drops of heavy water to the sample compartment, followed by evaporation of the water in vacuum.

III.5. Theoretical methods

The quantum chemical calculations were performed using Gaussian 03^{195} or Turbomole $5.7^{196-198}$ suites of programs. Optimizations of ground state geometries of molecules and their clusters were done using density functional theory (DFT) with Lee, Yang and Parr correlation functional (B3LYP) and 6-311+G(d,p), or 6-31G(d,p) basis sets. The vibrations computed for the optimized structures contained no negative frequencies. Vertical excitation energies and oscillator strengths, as well as excited-state

dipole moments were calculated using time-dependent density functional theory (TDDFT), the B3LYP functional, and the 6-31G(d,p) basis set. The geometry optimization in the lowest electronically excited state was obtained by (CIS/6-31+G(d,p)) or (TDDFT/B3LYP/TZVP) calculations.

CHAPTER IV. Results and discussion

IV.1. Introduction. Similar electronic structure - different photophysics

The UV absorption and magnetic circular dichroism (MCD) spectra of **1**, **2**, and **3** recorded in *n*-hexane, acetonitrile and ethanol at room temperature are shown in Figs. IV.1-3, respectively. The absorption spectra of all the investigated molecules look similar and show a lowest energy broad band with the maximum at ca. 30000 cm^{-1} (**1**), 33000 cm^{-1} (**2**) and 33400 cm^{-1} (**3**) in hexane. The MCD spectra reveal the presence of at least two electronic transitions in the region of this band, with the same +,- sign pattern for all isomers. The MCD signal is weak and the spectra show the same, negative and positive, sequence of *B* terms independently of the nature of solvent (it should be recalled that a positive value of a *B* term corresponds to a negative MCD sign, and *vice versa*). Interestingly, for **2** and **3** the first absorption band is red-shifted in protic polar solvents with respect to hexane by about 500 cm^{-1} and 2300 cm^{-1}, respectively. This is not the case for **1**, which indicates that this molecule forms a strong intramolecular hydrogen bond which is not broken in alcohols.
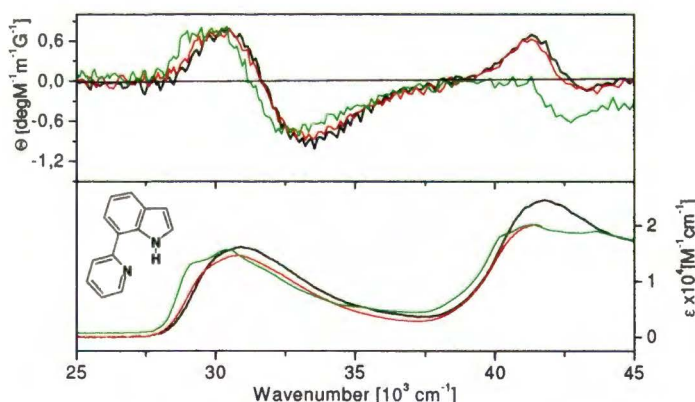
Figure IV.1. Room temperature absorption (bottom) and MCD spectra (top of **1** in *n*-hexane (green), acetonitrile (black) and ethanol (red).
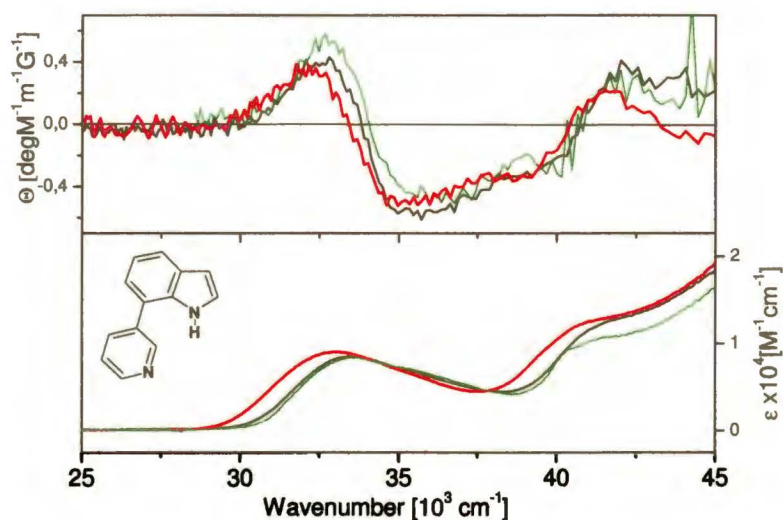
Figure IV.2. Room temperature absorption (bottom) and MCD spectra (top) of **2** in *n*-hexane (green), acetonitrile (black) and ethanol (red).
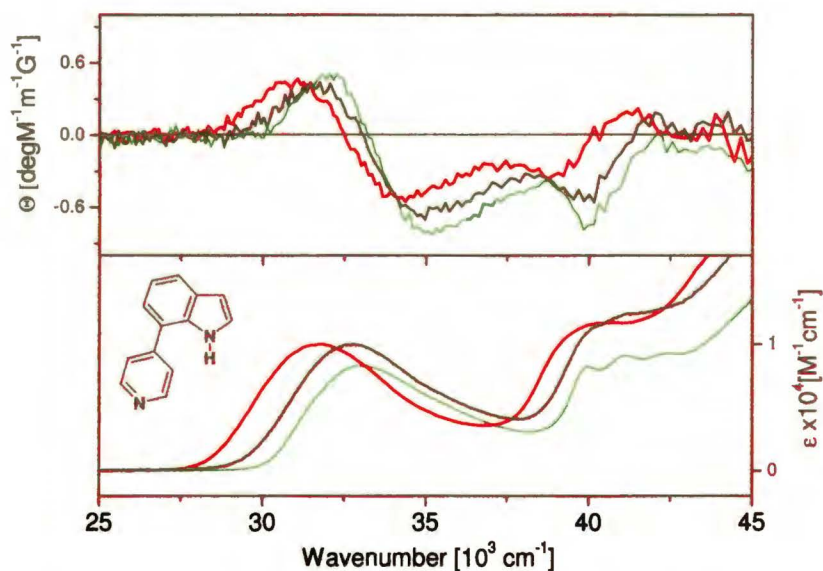
Figure IV.3. Room temperature absorption (bottom) and MCD spectra (top) of **3** in *n*-hexane (green), acetonitrile (black) and ethanol (red).

The fluorescence spectra of the three isomers of 7-(pyridyl)indole are presented in Figure IV.4. Upon changing the solvent, each compound reveals a different luminescence pattern. Compound **1** fluoresces extremely weakly: it is particularly nonfluorescent in nonpolar solvents, such as *n*-hexane. The most intense emission is observed in acetonitrile, but the quantum yield is only 0.006; it decreases in alcohols.

Totally different photophysical behaviour is observed for two other members of the series, with the indolyl moiety in the *meta* and *para* positions with respect to the pyridine nitrogen. Intense emission is now observed in hexane and acetonitrile. For both compounds, fluorescence is quenched by alcohols. However, the quenching in **3** is less effective than in **2**. The quenching increases in the series: butanol, propanol, ethanol, methanol. Interestingly, for **2** a biexponential character of fluorescence decays is observed, which points to the presence of two emitting forms.
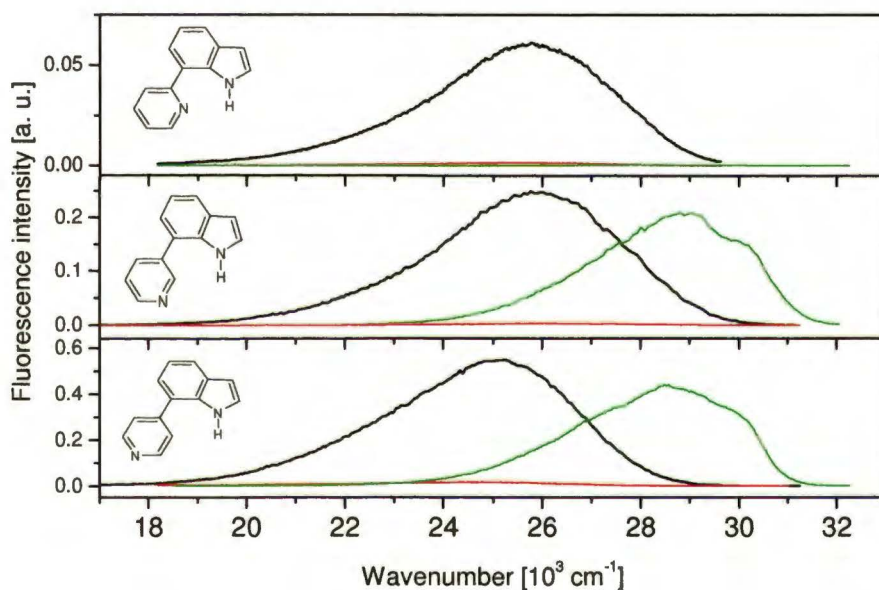
Figure IV.4. Room temperature (normalized and multiplied by the value of quantum yield) fluorescence spectra of **1**, **2** and **3** in *n*-hexane (green), acetonitrile (black) and ethanol (red).

Due to the topology of the investigated molecules, one can suspect that the deactivation process in **1** would be related with the presence of an

intramolecular hydrogen bond and, in protic solvents, with the phenomena induced by the intermolecular hydrogen bonds for **2** and **3**.

Similar to the behavior reported for many bifunctional compounds, it may be expected that the acid-base properties of **1** - **3** may change strongly upon electronic excitation. Indeed, excited state pK_a changes suggest that the electron density redistribution upon excitation leads to an increase of the acidity of the NH group and the basicity of the pyridine nitrogen (Table IV.1). Changes of pK_a upon excitation can be obtained by application of the Förster cycle[199] employing the formula:

$$\Delta pK_a = pK_a^* - pK_a^G \approx -0.00207(v_{00}^A - v_{00}^B)$$

where pK_a^* and pK_a^G denote values in the excited and ground state, respectively; the electronic transition energies in the acid (v_{00}^A) and base (v_{00}^B) forms are expressed in wavenumbers. The 0-0 transitions of both forms can be estimated from the absorption and fluorescence of the neutral and protonated species. The application of this procedure results in the finding that the excitation creates thermodynamically favorable conditions for excited state proton transfer. Due to topology, such an intramolecular reaction is possible in **1**. For **2**, one could envisage a solvent-assisted excited state tautomerization, with alcohol molecules bridging the proton donor and acceptor groups.

Table IV.1. Changes of pK_a upon $S_0 \rightarrow S_1$ excitation, calculated using the Förster cycle. Accuracy: ± 2 pK_a units.

	ΔpK_a	
	Protonation on pyridine nitrogen	Deprotonation of the NH group
1	6.4^a, 7.3^c	-14.5^a, -10.5^b, -12.1^c
2	9.5^b	-14^a
3	10.6^a, 11.3^c	-12.6^a

^{a} obtained from the absorption spectra; ^{b} from the emission spectra; ^{c} estimation of the 0-0 transition energy

60

Chapter IV. Results and discussion

The following sections are devoted to the nature of processes responsible for the deactivation of excited states of the investigated molecules. In section IV.2, the intramolecular character of fluorescence quenching related to intramolecular proton motion between the nitrogen atoms is discussed. The third section of this chapter (IV.3) addresses the problem of deactivation paths in 2,9-(di-2'-pyridyl)-4,7-di(*t*-butyl)carbazole (**4**). On the basis of the results obtained for **2** and **3**, the role of intermolecular, cyclic and noncyclic, hydrogen bonds with solvent molecules, as well as a possibility of excited state twisting and/or flattening, is analyzed in sections IV.4-5.

IV.2. Ultrafast excited state deactivation processes in 7-(2'-pyridyl)indole. Intramolecular ESPT with a twist.

7-(2'-pyridyl)indole (**1**) possesses both a hydrogen bond donor (aromatic NH group) and an acceptor (pyridine-type nitrogen atom), located in separate moieties linked by a single bond. In such molecules the hydrogen bonding centers may be located either on the same, or on the opposite sides of the molecule. These two positions correspond to *syn* and *anti* forms, respectively. There is no doubt that for **1** the dominant species corresponds to the planar, *syn* form with hydrogen atom attached to indole and forming hydrogen bond with the nitrogen atom of the pyridine ring. B3LYP/6-31G(d,p) calculations predict that an intramolecular hydrogen bond stabilizes the *syn* rotamer significantly (about 5 kcal/mol) relative to the *anti* configuration which lacks the intramolecular H-bond (Figure IV.5). In the *anti* form two rings are not coplanar (twist angle about 140°) because of pyridyl CH - indole NH steric repulsion. The crystallographic data show that the molecule exists in the *syn* conformation with the hydrogen bond between the indole NH and the pyridine nitrogen.[200] The presence of the intramolecular hydrogen bond is manifested by the red shift of the NH stretching frequency. Figure IV.6 presents the IR absorption spectra of three isomers of 7-(pyridyl)indole.
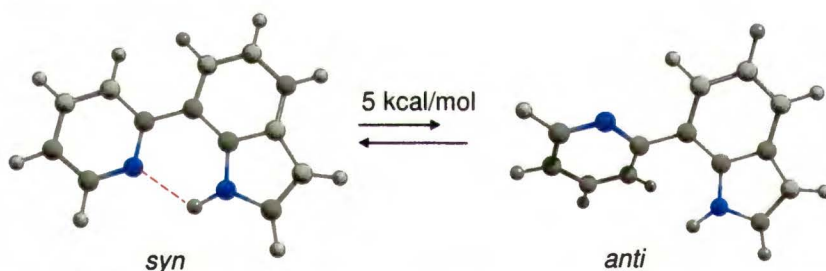
Figure IV.5. The calculated ground-state geometry of *syn* and *anti* rotamers of **1**.

The calculated ground state dipole moment values for the *syn* (2.2 D) and the *anti* (3.4 D) rotamer suggest that the latter should be stabilized in polar solvents. These predictions are consistent with the experimental findings. The fluorescence intensity and lifetimes pattern seems to confirm the presence of two different rotameric forms, of which the contributions depend on the solvent nature. Since in *n*-hexane, where only the *syn* form should be present, extremely weak fluorescence is observed (Figure IV.7), it can be proposed that the one order of magnitude larger fluorescence

quantum yield in acetonitrile is related with a small fraction of *anti* form, of which the population should be larger in polar solvents. A strong argument for such assignment is the discrepancy between the absorption and fluorescence excitation spectra (Figure IV.8).
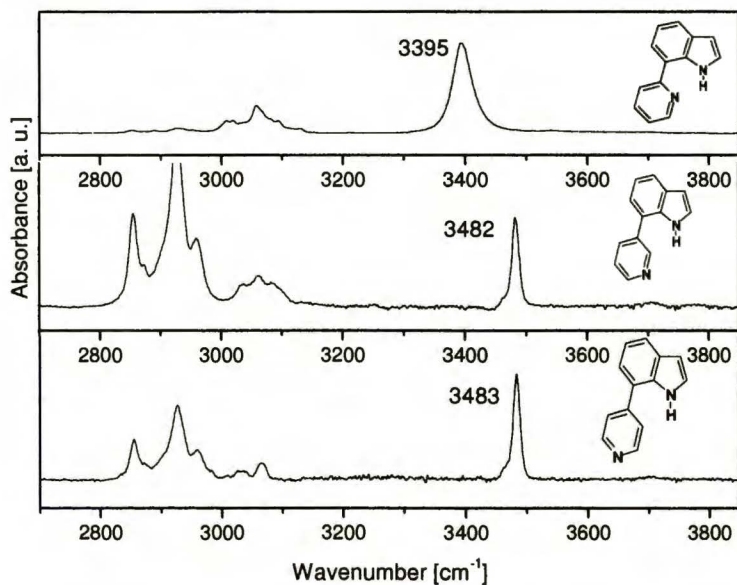
Figure IV.6. Portion of the IR absorption spectra of **1**, **2** and **3** in CCl_4.
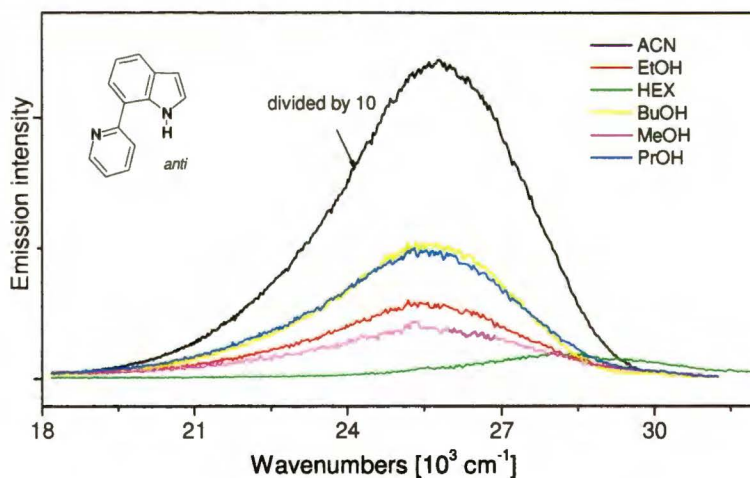
Figure IV.7. Room temperature fluorescence spectra of **1**.

The excitation spectrum in acetonitrile is blue-shifted by about 2000 cm^{-1} with respect to the absorption. The latter corresponds to the sum of the

63

absorption spectra of both rotamers: $A = f_{S_0}^a c\varepsilon_a l + f_{S_0}^s c\varepsilon_s l$, where $f_{S_0}^a$ and $f_{S_0}^s$ ($=1- f_{S_0}^a$) are the fractions of the *anti* and the *syn* forms, respectively; c denotes the concentration of the sample, ε is the absorption coefficient, and l is the optical path length. Given that $f_{S_0}^s >> f_{S_0}^a$, the absorption spectrum may be attributed to the dominant nonfluorescent *syn* rotamer, whereas the excitation spectra are due to the small fraction of the emitting *anti* form and reflect the absorption spectra of this species.
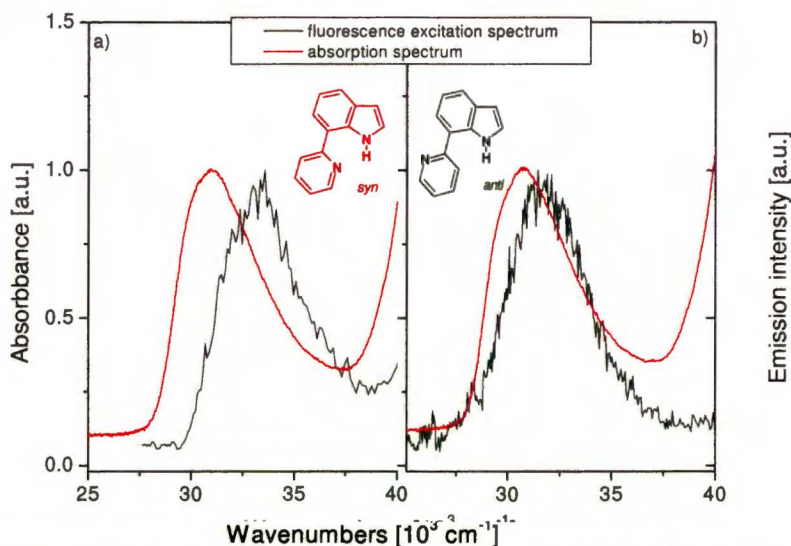
Figure IV.8. Absorption (red) and fluorescence excitation (black) spectra of **1** recorded in acetonitrile (a) and 1-propanol (b) at room temperature.

Moreover, the differences between the maxima of absorption and excitation spectra are in good agreement with the energy calculated for S_0-S_1 transitions in **1**-*syn* and **1**-*anti*. The calculations predict that the two rotamers absorb strongly at similar wavelengths, with the *anti* form absorption shifted by about 0.4 eV to the blue.[176] Another argument for the assignment of the origin of fluorescence to the *anti* form is the excitation wavelength dependence of the value of quantum yield. The quantum yield in acetonitrile changes from 0.0027, 0.006, to 0.0006 for the excitation wavelength 274 nm (36496 cm^{-1}), 300 nm (33333 cm^{-1}) and 337 nm (29673 cm^{-1}), respectively. Thus, for excitation in the blue part of the first absorption band, the quantum yield increases significantly because of the larger contribution from the *anti* population, showing that the absorption of the *anti* species is blue-shifted with respect to the absorption of the *syn*

rotamer. These considerations bring us to the conclusion that, what we observe in fluorescence is the *anti* structure. The fluorescence decays are monoexponential because the lifetime of the *syn* form is probably too short to be detected with the subnanosecond time resolution (Table IV.2).

Table IV.2. Room temperature quantum yields and fluorescence decay times of **1** in various solvents.

Solvent	Φ_{fl} [a]	τ_{fl} [ns] [b]
n-hexane	0.0005	-
acetonitrile	0.0061	4.8
butanol-1	0.0026	0.6
propanol-1	0.0025	0.6
ethanol	0.0015	0.3
methanol	0.0011	0.4

[a] accuracy: ± 20% ; [b] estimated error: ± 0.2 ns.

IV.2.1. The driving force for excited state proton transfer

The lack of detectable fluorescence from **1**-*syn* implies that nearly all the photoexcited molecules decay very rapidly. The changes of the hydrogen bonding ability of hydrogen bond centers during the excitation suggest that the excited state proton transfer may be responsible for this fast deactivation. The application of Förster cycle (Table IV.1) revealed a huge increase of the acidity of the NH group (about 11 pK_a units) and of the basicity of the pyridine nitrogen atom (about 6 pK_a units). The calculations show that the lowest excited state, of $^1(\pi,\pi^*)$ character, is mainly represented by the HOMO→LUMO excitation (Figure IV.9).

HOMO: π   **LUMO: π***
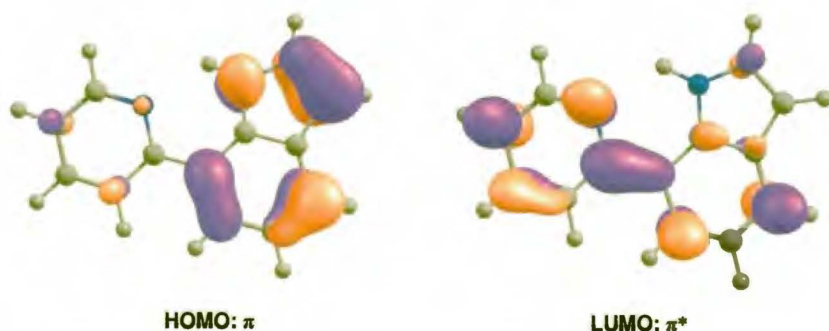
Figure IV.9. The highest occupied molecular orbital (π) and the lowest unoccupied orbital (π)*) of 7-(2'-pyridyl)indole, determined at the equilibrium geometry of the electronic ground state.

Since the HOMO orbital is localized on the indole moiety, and the LUMO is to a large extent delocalized over the whole system, the $S_0 \rightarrow S_1$ transition has some charge-transfer character. This provides a driving force for proton motion which neutralizes the electronic charge separation in the S_1 state. Usually, a direct evidence of the phototautomerization in excited state is the presence of a red-shifted fluorescence from the product of such reaction. However, no tautomeric emission in the studied range of wavelengths (350-800 nm, 28571-12500 cm^{-1}) was observed for **1**. Nevertheless, this does not necessarily exclude the presence of the photoreaction in the excited state. This observation may suggest that the tautomer is rapidly deactivated, with the rate larger than the rate of its creation. Another explanation is that the tautomeric fluorescence lies outside of the spectral range available for detection.

The calculations have shown that the tautomer of **1**-*syn* does not represent a stable minimum in the ground state and the geometry optimization of this structure restores the "normal" **1**-*syn* minimum. Concerning the fluorescence of the tautomer, calculation predict that it should be expected in the near infrared range.[176]

IV.2.2. ESIPT in condensed phase. Femtosecond transient absorption measurements

To investigate the dynamical processes occurring in the excited states, the transient absorption measurements with femtosecond time resolution have been performed. Figures IV.10-12 present the transient absorption spectra of **1** taken in different solvents. The results of global and target analysis of the spectra were also included as an inset. The definition

global means a simultaneous analysis of multiple spectra in two dimensions (wavelength, time), whereas target refers to the applicability of a particular target model. Here a sequential kinetic model with increasing lifetimes was assumed, where each component corresponds to a species which is transformed into the next, longer-decaying form. Using such a model applied to transient absorption results, the spectra may be viewed as evolution-associated difference spectra (EADS). They represent the temporal evolution of the spectra e.g., the spectrum of A decays with the first lifetime, the B spectrum rises with the first lifetime and decays with the second lifetime, etc.
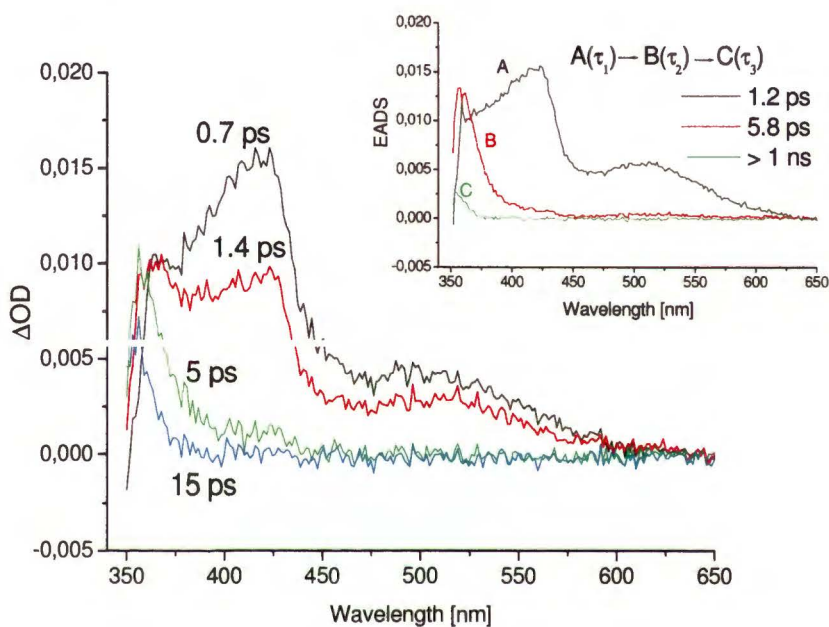
Figure IV.10. Transient absorption spectra of **1** in *n*-hexane at 293 K; inset,results of global and target analysis.
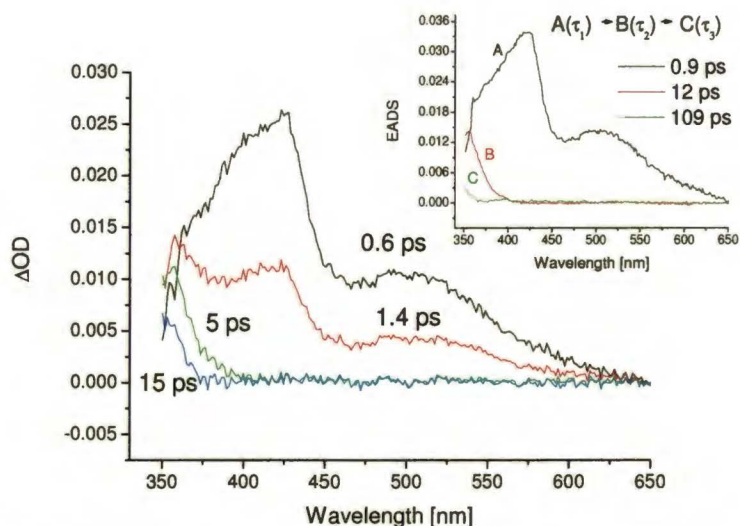
Figure IV.11. Transient absorption spectra of **1** in acetonitrile at 293 K for several delay times; inset, results of global and target analysis.
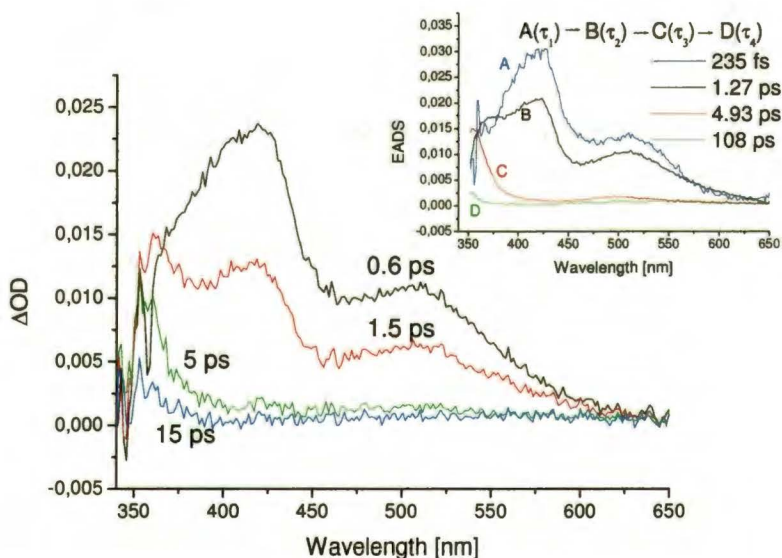
Figure IV.12. Transient absorption spectra of **1** in methanol at 293 K; inset, results of global and target analysis.

The initially excited species reveals a characteristic TA spectrum with two bands centered at 420 nm and 500 nm, respectively. The decay of this

spectrum occurs in about 1.0 ± 0.2 ps. After this time, only a weak signal around 360 nm, in the whole available spectral range, is observed. This component is found decaying in a few ps. We propose to assign this spectrum (slightly shifted to the red with respect to stationary absorption) to the unrelaxed molecule in the ground state and its decay to the vibrational cooling.

The TA spectra have provided two most important findings. First, the lack of a measurable transient species, except the (probably vibrationally hot) ground state form, explains the fact that no fluorescence from either **1-***syn* or from the phototautomer could be detected. Second, essentially the same spectrum and decay time are observed in solvents differing in polarity and proticity: *n*-hexane, acetonitrile, methanol, methanol-OD, propanol-1, ethylene glycol, and decanol. This suggests that in **1**, which is intramolecularly H-bonded, no solvent is necessary to induce the ultrafast depopulation of the initially excited form. The somewhat slower decay time, 1.7 ps, in decanol may point to the fact that such solvent parameter as viscosity may be important for the deactivation process.

IV.2.3. ESIPT under supersonic jet conditions

To understand the mechanism and dynamics of intramolecular excited state proton transfer the investigations in supersonic jets were performed. However, applying a standard setup with the nanosecond lasers it was impossible to record the signal from photoexcited **1** using mass, as well as fluorescence detection. These unsuccessful attempts indicated a very short lifetime of the excited state of **1** and suggested that lowering the temperature does not stop a rapid depopulation of S_1. Therefore, the jet setup was modified: the nanosecond laser has been replaced with a femtosecond one in order to shorten the excitation/ionization pulses. The molecules were ionized resonantly via S_1, using one UV photon for excitation and two photons of 400 nm for ionization steps (in two-color scheme). The one color scheme was also employed. The resonance-enhanced multiphoton ionization spectra of isotopomers of **1,** obtained by using lasers pulses of about 200 fs duration, are given in Figure IV.13. These spectra are similar to absorption observed at room temperature.
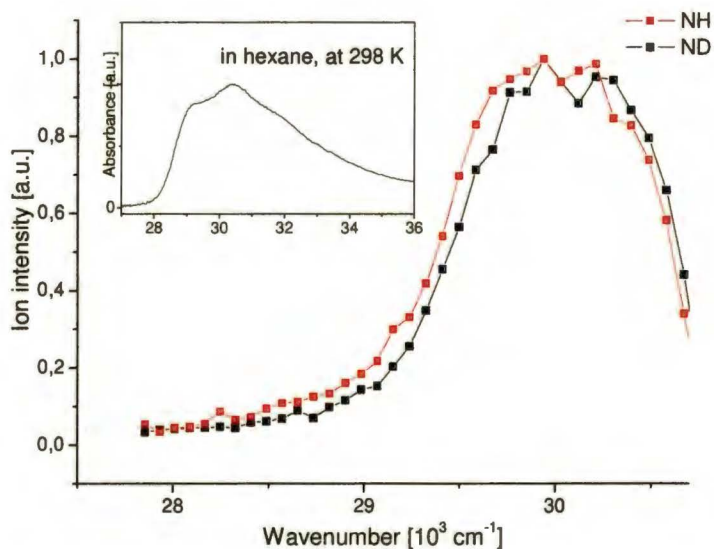
Figure IV.13. One color REMPI spectra of jet-cooled **1** and its ND isotopomer. Inset, room temperature absorption in *n*-hexane.
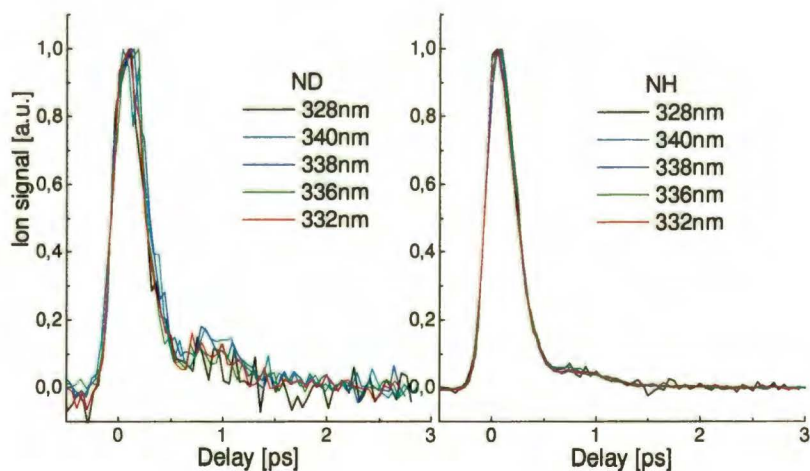
Figure IV.14. The pump-probe spectra of the ND/NH isotopomers (UV +2*400 nm) at different pump (UV) wavelengths.

The crucial piece of information was provided by the pump–probe photoionization experiments. The kinetic profiles of the ion signal are

presented in Figures IV.14-15. The spectra do not essentially depend on the pump wavelength. Both NH and ND species do not decay monoexponentially and reveal a small peak in the transient signal at about 1 ps delay time (Figure IV.15). The pump-probe spectra were fitted by convolution of the cross-correlation function (gaussian) with a harmonically modulated monoexponential decay: $(1+a*\cos(\omega t+\varphi))*\exp(-t/\tau)$. This fitting procedure allowed to extract the very fast decay of ion signal. The lifetimes of the initially excited NH molecule and of the N-deuterated species were found to be 280 fs and 390 fs, respectively. The deuterium isotope effect was estimated to be about 1.4 ± 0.2. The cosine frequency was about 34 cm^{-1} in both cases (Figure IV.16). The calculations (B3LYP/6-31G(d,p)) suggest that this frequency may be related to a vibrational mode (calculated at the 29 cm^{-1} as a lowest vibration in **1**-*syn*) corresponding to torsional motions of the indole and pyridine moieties, occurring with the period of about 1 ps.
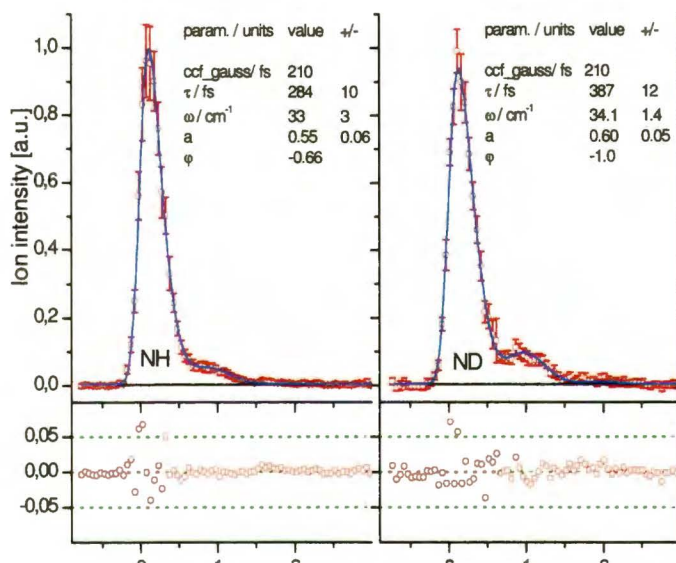
Figure IV.15. The pump-probe REMPI spectra (circles) obtained in a supersonic jet for **1** and its N-deuterated analogue; solid lines, results of the fitting procedure.
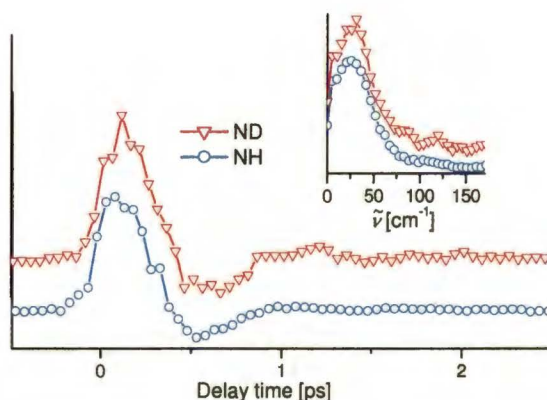
Figure IV.16. The oscillatory signal components and their Fourier
transforms (inset).

The dominant presence of the *syn* structure of **1** under jet conditions
was confirmed by employing the IR/ fsMPI technique.[162] The IR absorption
spectrum in the NH stretch region was recorded by detecting the
femtosecond multiphoton ionization. Figure IV.17 presents the comparison
of IR/fsMPI spectrum of **1** and IR/R2PI spectrum of 7-(3'-pyridyl)indole
(**2**). The lower NH stretching vibrational frequency (3412 cm^{-1}) of **1** in
relation to **2** (3513 cm^{-1}) and bare indole (3525 cm^{-1})[201] indicates a fairly
strong red shift due to the formation of an intramolecular hydrogen bond.
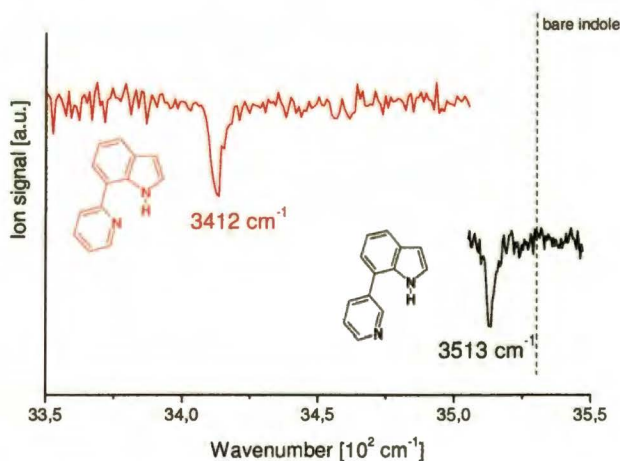
Figure IV.17. Comparison of the IR/fsMPI (1-color, 335nm) spectrum of **1**
(red) and the IR/R2PI spectrum of **2** (black).

72

IV.2.4. The model of deactivation based on the experiments and calculations

The rather unusual finding that the photoreaction is faster in a cold, supersonic jet-isolated molecule than in room temperature solutions may seem at first rather odd. However, all the experimental observations in solution as well as in the jet and the calculations are consistent, and comparison of them allowed us to propose a model of the excited state deactivation of this molecule involving a sequence of coupled events occurring after electronic excitation.[202] The analysis of the excited state potential energy profile obtained at the CC2/cc-pVDZ level suggests that the excitation of 1-*syn* results in a barrierless reaction of proton transfer.[176] Interestingly, this process is coupled to the indole-pyridine torsional coordinate. The proton-transferred structure is not stable with respect to the inter-ring twisting. For the CCCN dihedral angle of 33° a shallow minimum was calculated on the S_1 potential energy, placed only 1.2 eV above the ground state energy. Around the perpendicular orientation of the rings ($\theta \approx 90°$) the conical intersection between S_1 and S_0 appeared. This intersection provides very effective mechanism of ultrafast radiationless decay of the tautomer to the ground state. Similarly to the reaction in the excited state, the back proton reaction is also barrierless, and thus **1** performs a closed, reversible reaction cycle.

The experimental results perfectly match these computational predictions. After excitation, charge transfer from the indole to the pyridyl moiety occurs, followed by a rapid (about 1 ps at 293 K in solution and about 280 fs in the jet) proton transfer to the pyridyl nitrogen. The difference of decay times can be explained by the fact that the proton transfer is coupled with twisting, and therefore tautomerization should be sensitive to changes in the torsional potential. In a condensed phase, the solvent may create the barrier for twisting, resulting in a somewhat longer lifetime of the excited molecule. Jet environment offers different conditions: the molecule is isolated, essentially free of interactions with the surroundings. The deuterium isotope effect, equal, within experimental accuracy, to the square root of two, suggests that under jet conditions phototautomerization is barrierless. The phototautomer undergoes an even faster internal conversion to the ground state. The process is accompanied by twisting about the 7,2'-bond which leads to a conical intersection. This feature makes the process so efficient that no traces of the excited tautomeric form can be detected in transient absorption and emission experiments.

IV.2.5. Short spectroscopic characteristics of the *anti* rotamer

It is interesting that, since the *syn* rotamer is nonfluorescent, a minor fraction of the *anti* form is readily observed. In the case of **1** rotamerization has important photophysical consequences since the *anti* form cannot undergo fast depopulation processes characteristic for the *syn* structure. Therefore, the two rotamers can be distinguished because of different fluorescence quantum yields and lifetimes. One can estimate, using the results of the absorption, fluorescence and lifetimes experiments, assuming similar absorption coefficients for both rotamers, that the *anti* population in the ground state in acetonitrile does not exceed 2%. It should be stressed that the quantum yields given in Table IV.2 provide only a lower limit for the fluorescence quantum yield of the *anti* form. Since the observed quantum yield is described by the expression: $\Phi_{fl} = \Phi_a f_{S_1}^a + \Phi_s (1 - f_{S_1}^a)$,

where $f_{S_1}^a$ is the fraction of the *anti* forms in the excited state, the real values of the quantum yields of the *anti* form can be much higher. Assuming that $f_{S_1}^a$ equals 0.02 and $\Phi_s = 0$, the quantum yield of *anti* form becomes 0.305 in acetonitrile.

Interestingly, fluorescence is significantly quenched by alcohols. The quantum yields decrease along the series: butanol, propanol, ethanol, methanol, from 0.0026 to 0.0011. This quenching trend may be correlated with proton donating abilities of the alcohols, which increase in the same order. The fluorescence decay in acetonitrile is 4.8 ns, while the values in alcohols are much shorter, of the order of 0.5 ns or below. The quenching would involve formation of hydrogen bonds between the alcohol and the pyridine nitrogen and the NH group. One can envisage the following 1:1 and 1:2 complexes:
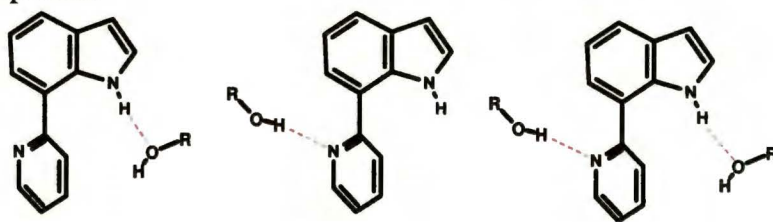
Figure IV.18. Possible alcohol complexes of **1**-*anti*.

This assumption is supported by the difference between fluorescence excitation spectra in acetonitrile and alcohols. In the latter, red shift is observed with respect to the former, pointing to a specific hydrogen bond

interaction. The quenching process in alcohol is strongly temperature-dependent (Figure IV.19). Lowering the temperature leads to the recovery of the radiative properties of the molecule. The increase of the intensity of fluorescence seems to be too large in light of the fact that *syn* rotamer is nonfluorescent and the fraction of *anti* form is small. However, it may be explained by assuming that the radiative rate constant becomes larger when the medium is sufficiently rigid. Such situation may occur when the relative twisting of the indole and pyridyl moieties takes place in the excited state. Lowering of temperature is accompanied by viscosity increase and, as a consequence, decreases of the probability of twisting. The deactivation of the excited state may be viscosity-dependent, as indicated by the temperature measurements and the fact that in octanol the quantum yield of fluorescence is 0.0044, nearly twice the value of 0.0026 obtained in less viscous butanol. The activation energy of the quenching process was found to be correlated with the activation energy of the viscous flow of the solvent. Such behavior of the emission suggests that deactivation process may involve rearrangement of the alcohol molecules around the excited chromophore or/and torsional motion of the pyridyl ring. As discussed later in more detail, similar behavior was observed for other molecules studied in this work.
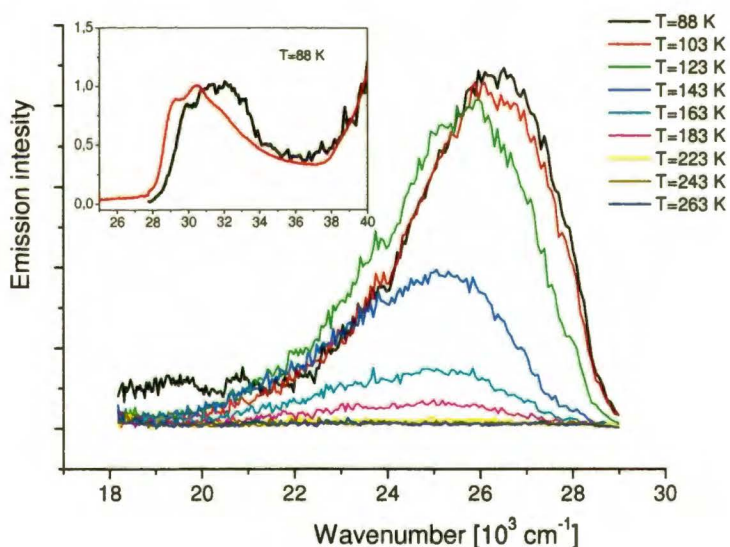
Figure IV.19. Temperature dependence of the emission of 7-(2'-pyridyl)indole in ethanol:methanol (1:1); inset, the absorption and fluorescence excitation spectrum (monitored at 25000 cm^{-1}) recorded at 88 K.

IV.2.6. Summary

The results of experimental and theoretical investigations presented above strongly suggest that the photoinduced proton transfer in 7-(2´-pyridyl)-indole (**1**) is accompanied by mutual twisting of the pyridyl and indole moieties. The proton transfer process is coupled with torsional motion, which leads to the S_1-S_0 conical intersection providing a very efficient channel for ultrafast excited state deactivation. Similar scenario of depopulation of excited state was theoretically predicted for other ESIPT systems: salicylic acid,[203] methyl salicylate,[204] and 2-(2´-hydroxyphenyl)benzotriazole.[205] Perhaps, this deactivation pattern is quite general.

The phenomenon of solvent-induced rotamerization was observed: two forms of **1**, *syn* and *anti* were detected. The possibility to form intra-(*syn*) or intermolecular (*anti*) hydrogen bonds imposes different patterns of excited state deactivation and allows the two rotamers to be spectroscopically distinguishable.

IV.3. Excited state deactivation path in 2,9-(di-2'-pyridyl)-4,7-di(*t*-butyl)carbazole. Separation between ESIPT and twisting.

As discussed in chapter IV.2, very efficient radiationless deactivation via excited state intramolecular proton transfer along the hydrogen bond formed between the acceptor and donor group was observed for 7-(2'-pyridyl)indole. It seemed interesting to check what will happen when the number of intramolecular hydrogen bond acceptors will be doubled and the NH proton will have a choice of two partners to create hydrogen bonds. Such a case was realized in 2,9-(di-2'-pyridyl)-4,7-di(*t*-butyl)carbazole (**4**). Our goal was to answer the question: is the photophysical behavior of **4**, a molecule structurally related to **1**, analogous to that occurring in **1**?

It was shown previously that dipyrido[*2,3-a:3',2'-i*]carbazole (**DPC**), a molecule structurally similar to **4**, reveals an efficient photoinduced intermolecular double proton transfer process with hydroxylic partners, but not an intramolecular reaction.[152] However, it is known that for similar proton donor/acceptor strengths, the intramolecular hydrogen bonding is stronger in six- than in five-membered quasi-rings due to steric and orientation effects. Additionally, **DPC** is more rigid

dipyrido[2,3-a:3',2'-i]carbazole (**DPC**)

due to lack of single bonds between the proton donor and acceptor groups and this fact may also have a great importance for the photophysics of these systems.
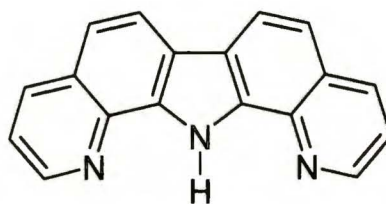
IV.3.1. Room temperature absorption and fluorescence

The absorption and emission spectra of **4** in *n*-hexane, acetonitrile, and methanol at 293 K are shown in Figure IV.20. In contrast to **1**, dual emission is observed for each solvent. Apart from a fluorescence band with a small Stokes shift (F_1), a red emission (F_2), separated from the maximum of F_1 by about 10000 cm^{-1} is also detected. The values of F_1/F_2 intensity ratio are given in Table IV.3. It was found that this ratio is practically the same in *n*-hexane, acetonitrile, and methanol, while it increases twice in more viscous propanol. Fluorescence excitation spectra measured at F_1 and F_2 coincide with each other and with absorption, showing that both

77

emissions originate from the same ground state precursor (Figure IV.21). The intensity of both emissions is very weak. We assign F_1 to the primarily excited species and F_2 to the product of an excited state intramolecular proton transfer reaction, in which the NH proton is shifted to the pyridyl nitrogen.
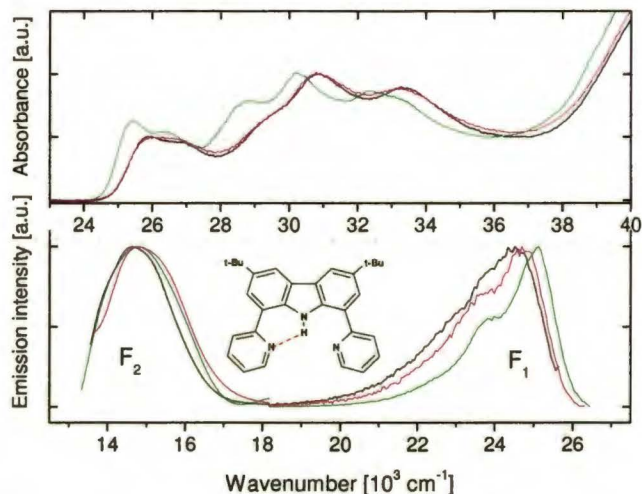
Figure IV.20. Room temperature absorption (top) and emission (bottom) of **4** in *n*-hexane (green), acetonitrile (black) and methanol (magenta). Intensity of F_1 and F_2 are normalized, in fact the F_2 is significantly weaker than F_1, see Table IV.1.
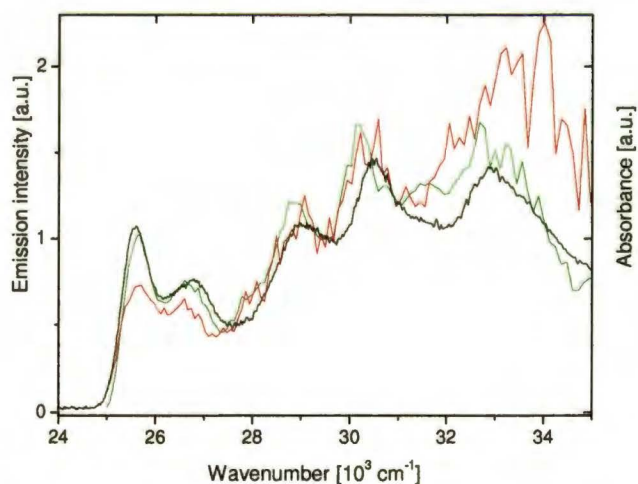
Figure IV.21. Absorption (black) and excitation spectra of F_1 (green) and F_2 (red) for **4** in the 1:1 MeOH/EtOH mixture at 88 K.

Table IV.3 presents the quantum yield values which indicate very effective radiationless deactivation of the initially excited state of **4**, a similar behavior as in **1**. The excited phototautomer undergoes rapid deactivation, too. However, the process is not as efficient as in **1** and now the fluorescence of the phototautomeric product is detectable.

Table IV.3. The photophysical data (maximum of the lowest absorption band, maximum of F_1 and F_2 fluorescence, fluorescence (F_1) quantum yields of **2** in different solvents at room temperature.

Solvent	$\nu_{abs}{}^a$ $[10^3\,cm^{-1}]$	$\nu_{F_1}/\nu_{F_2}{}^a$ $[10^3\,cm^{-1}]$	$\Phi_{fl}{}^b$ $[\times10^{-4}]$	F_2/F_1
Hexane	25.40	25.00/14.70	7.0	0.048
Acetonitrile	25.80	24.60/14.80	4.5	0.053
Propanol	26.00	25.00/15.00	8.0	0.10
Methanol	25.80	24.70/14.70	3.9	0.058
MeOD:EtOD	26.00	24.30/15.00	23.8	0.05
BuCN	25.70	25.00/15.00	6.9	0.10

[a] the error is estimate to be $\pm 200\ cm^{-1}$, [b] accuracy $\pm 20\%$

Time-resolved fluorescence measurements performed in acetonitrile at room temperature have shown that F_1 and F_2 emissions are short-lived. Both bands rise and decay very rapidly, below the time resolution of our instrument, estimated as 5-10 ps (Figure IV.22).
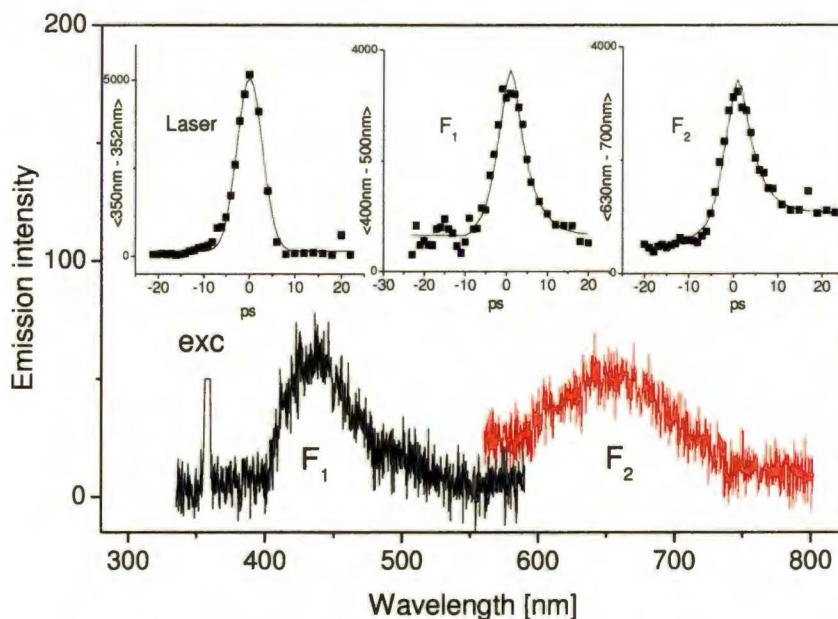
Figure IV.22. Bottom, room temperature fluorescence of **4** in acetonitrile registered 1 ps after excitation; top, temporal profiles of F_1, F_2, and the excitation source intensities.

IV.3.2. Temperature and deuterium isotope effects

Interesting results were provided by measurements of the temperature dependence of the emission. Lowering the temperature from 293 to 90 K of a 1:1 v/v methanol:ethanol solution of **4** leads to a strong increase of the primary fluorescence, by a factor of 134 (Figure IV.23). Interestingly, the lower energy emission also becomes stronger, by a factor of 17. Similar behavior was observed in 3-methylphentane (3MP), however the increase of F_2 was less prominent. This increase of F_1 indicates that the yield of proton transfer, the dominant process of deactivation in the initial excited species, becomes smaller. The gain of F_2 emission intensity upon lowering of the temperature may be interpreted as a manifestation of stronger temperature dependence of the depopulation rate of the phototautomer than that of the ESIPT. The tautomeric emission is observed even at 88 K, indicating a small barrier for the process and, most probably, the importance of tunneling. The fact that the F_2 emission starts to increase when the medium becomes rigid suggests that the deactivation of the

phototautomer may be viscosity-dependent. Another argument for that is the F_2/F_1 intensity ratio obtained in *n*-propanol. This value is nearly two times larger than the value in less viscous *n*-hexane, acetonitrile, and methanol (Table IV.3).
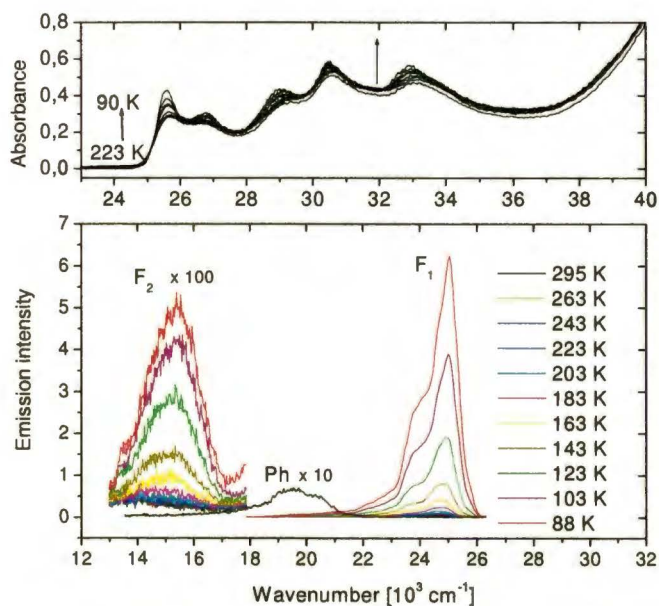
Figure IV.23. The temperature dependence of the absorption (top) and emission (bottom) of **4** in MeOH:EtOH (1:1 v/v). Excitation energy: 26700 cm^{-1}. The spectra are not corrected for the spectral response of instrument.
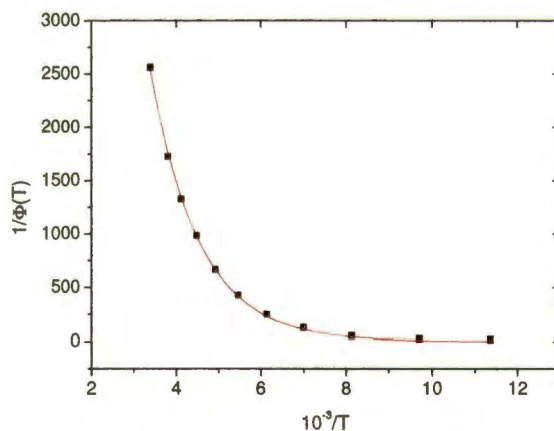
Figure IV.24. Plot of $1/\Phi$ vs. $1/T$ for **4** in MeOH:EtOH (1:1 v/v). The squares show the experimental values, the solid line, the result of the fitting.

81

If one assumes that the temperature dependence of F_1 intensity is governed by the proton transfer rate, fitting the experimental data to equation: $1/\Phi(T))= 1 + (k^0_{nr}/ k_r) + (k'/k_r)\exp(-\Delta E/RT))$ allows one to estimate ΔE, the activation energy for the process. An example of the fit is given in Figure IV.24 The activation energy obtained using this procedure was found to be 1.8 ± 0.1 kcal/mol in MeOH:EtOH solution and 2.0 ± 0.1 kcal/mol in 3MP.

In general, if the proton transfer reaction involves potential energy barrier, the reaction may occur via a combination of a "classical" transfer over the barrier and quantum mechanical tunneling through the barrier, the latter resulting from the small mass of the proton and its isotopes. If the motion or tunneling of the proton governs the transfer, the rate of the process is expected to reveal a deuterium isotope effect. Thus, deuterium substitution provides a tool for studying the nature of proton transfer. In order to deuterate **4,** a 1:1 EtOD:MeOD mixture was used. From the temperature dependence of the emission in this solution $\Delta E = 2.3 \pm 0.2$ kcal/mol was obtained. If one makes a reasonable assumption that the radiative rate is the same in deuterated and nondeuterated species, the ratio $\Phi_{F_1(D)} / \Phi_{F_1(H)}$ can be expressed as $(k_0^H + k_{PT}^H)/ (k_0^D + k_{PT}^D)$, where Φ is the quantum yield of F_1 in deuterated and nondeuterated molecule, k_{PT} is the proton transfer rate and k_0 includes all the depopulation processes other than tautomerization. This ratio, at least in the higher temperature range can be approximated as k_{PT}^H/ k_{PT}^D, thus yielding the isotope effect on the tautomerization rate (Figure IV.25). The value of the isotope effect obtained in this way increases from 6.1 at 293 K to 16.9 at 163 K, which strongly suggests that tunneling plays an important role in the phototautomerization process.
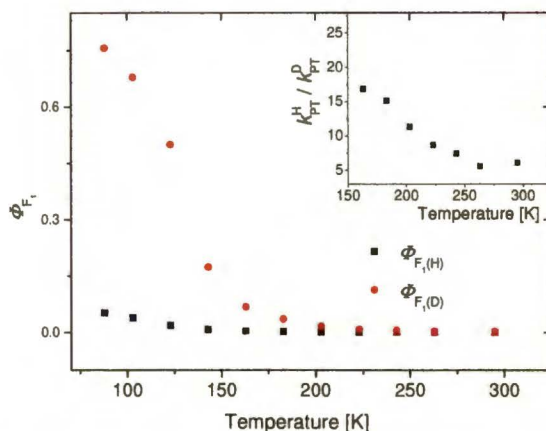
Figure IV.25. The changes of F_1 quantum yield of **4** in MeOH:EtOH (black squares) and in MeOD:EtOD (red dots); inset, the isotope effect vs. temperature.

IV.3.3. Intermolecular interaction?

After deuteration of **4** the quantum yield of F_1 becomes larger. Simultaneously, the quantum yield of the tautomeric fluorescence is four times larger than in nondeuterated alcohols. It may suggest that radiationless deactivation of the tautomeric form involves forming an intermolecular hydrogen bond with alcohol molecules. One can envisage such situation in a *syn-anti* form - one of three possible rotameric forms of **4** (Table IV.4). X-ray studies show that **4** exists in a *syn-syn* structure (**4a**) with both pyridyl nitrogen atoms forming bifurcated hydrogen bonds with the NH proton.[200] Ground state energy optimizations of possible forms of **4** reveal that, apart from the most stable *syn-syn* geometry, the forms with one (*syn-anti*, **4b**) and two (*anti-anti*, **4c**) pyridyl nitrogens in the *anti* conformation with respect to the NH group with energy higher by 3.01 and 8.86 kcal/mol, respectively (3.09 and 8.78 kcal/mol after inclusion of zero-point energies) may also exist (Table IV.4). The calculation was done for molecule **4** with hydrogen atoms instead of the *t*-butyl groups in positions 2,9 (**4H**). Since **4b** is characterized by a larger dipole moment, 4.25 D vs. 2.27 D for **4a**, in polar alcohol solvents **4b** should be stabilized with respect to **4a**. Another factor which makes the *syn-anti* structure preferentially stabilized in protic media are specific hydrogen bonding interactions, which seem thermodynamically more favorable for the *anti* conformation of the pyridyl group.

However, the analysis of the results (obtained so far) does not provide a direct evidence for the existence of **4b**-solvent complexes. The decay times in propanol and butyronitrile measured as a function on temperature look similar and do not suggest the forming of the intermolecular hydrogen bonds. The comparison of F_1/F_2 intensity ratio in hexane and alcohols does not reveal any additional effect related with intermolecular interaction with alcohols.

Table IV.4. Results of B3LYP/6-31G(d,p) ground state geometry optimization of **4H**.
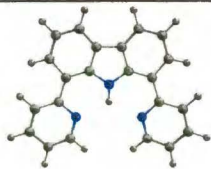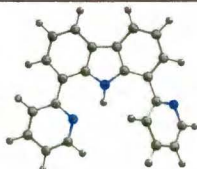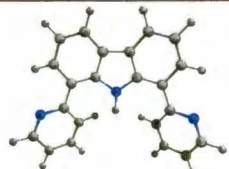
	syn-syn (**4a**)	*syn-anti* (**4b**)	*anti-anti* (**4c**)
Energy [kcal/mol]	0.00	3.09 (3.01)	8.86 (8.78)
Torsional angles $\Theta_{C-P1}/\Theta_{C-P2}$	0.0/0.0	0.0/150.4	148.8/148.8
Dipole moment [D]	2.27	4.25	3.76

Table IV.5. Photophysical parameters of **4** in propanol as a function of temperature.

Temperature [K]	Φ_{F_1} [a] $[10^{-3}]$	τ_{S_1} [b] [ps]	k_r $[10^7 s^{-1}]$	k_{nr} $[10^{10} s^{-1}]$
294	0.8	10 ± 1	8.0	10
173	4.8	61 ± 5	8.0	1.63
153	9.6	127 ± 10	7.6	0.8
133	16.0	230 ± 34	7.0	0.41
113	30.0	400 ± 41	7.5	0.24

[a] accuracy ± 30 %, [b] Obtained from transient absorption

IV.3.4. Similarities and differences in the deactivation path of 4 and 1

The changes of fluorescence quantum yield (Figure IV.26 and Table IV.5) and lifetimes of S_1 in propanol accompanying decreasing of temperature show that the radiative rate constant is independent on temperature, whereas the nonradiative processes are slowed down by cooling (Table IV.5). An example of the kinetic curve of the transient absorption signal decay and the TA spectra recorded for two selected delay times are given in Figure IV.27.
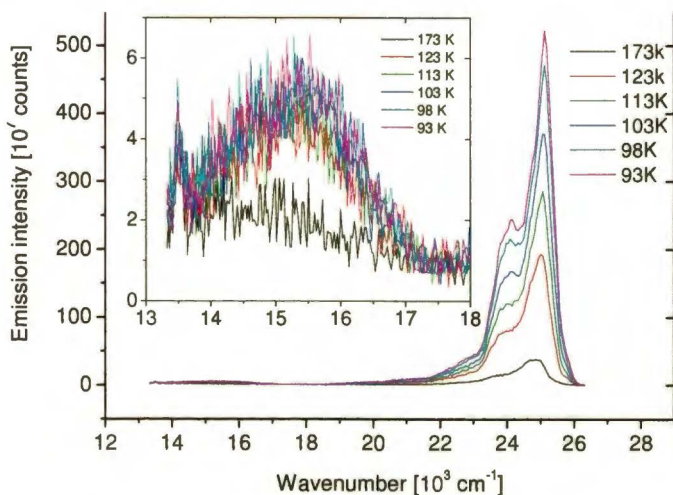
Figure IV.26. The temperature dependence of the emission of **4** in propanol.

Keeping in mind the assumption that the deactivation of the primarily excited population is mainly governed by proton transfer reaction, one can conclude that a barrier for this process exists. The apparent activation energy for tautomerization (in a few solvents) was estimated to be almost 2 kcal/mol, in contrast to **1**, where the proton transfer was found to be barierrless. For **1** the process in the excited state was so fast that it was impossible to determine whether the proton transfer precedes twisting or whether both processes happen simultaneously. The experimental results and calculations allowed to claim only that both processes are coupled to each other. Whereas in **4**, the rate of proton transfer is sufficiently slowed down to enable separation of these two processes. On the basis of the presented results one can propose the following model for the excited state deactivation of this molecule (Figure IV.28). After electronic excitation, the

ESPT along the intramolecular hydrogen bond takes place (about 10 ps). The phototautomer undergoes very efficient and fast depopulation to the ground state, most probable induced by twisting about the bond linking the donor and acceptor moieties. The optimization of the ground state tautomeric structure for **4a** was not successful. Similarly to **1**, the calculations led to the optimized geometry of the initial form, showing that the tautomer is not stable in S_0.

Preliminary jet studies revealed that neither fluorescence nor ion signals could be detected using nanosecond lasers. This situation may be similar to that of **1**, and thus in order to observe short-lived species the femtosecond pulse excitation/ionization should be used
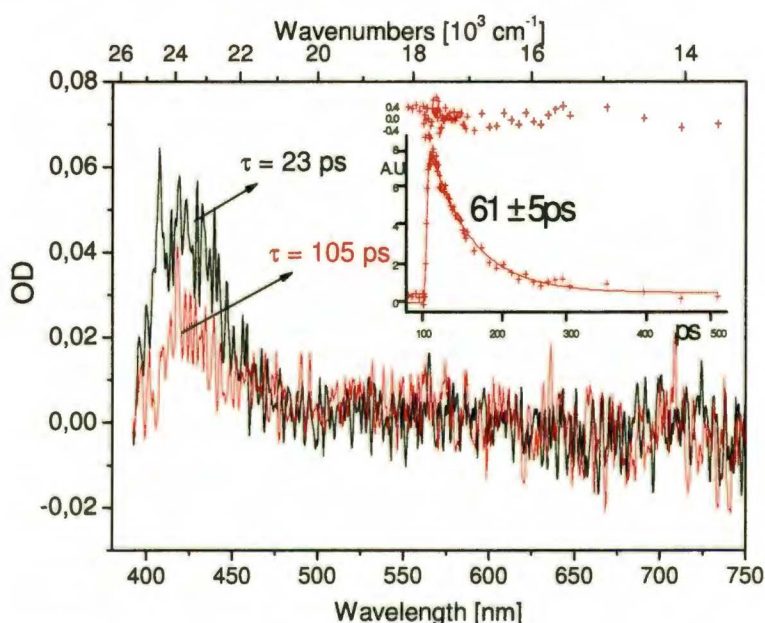
Figure IV.27. Transient absorption spectra of **4** in propanol measured at 173 K, 23 ps and 105 ps after excitation. The temporal profile of transient absorption signal intensity (integrated between 415 and 460 nm) and the results of the fitting procedure are inset.
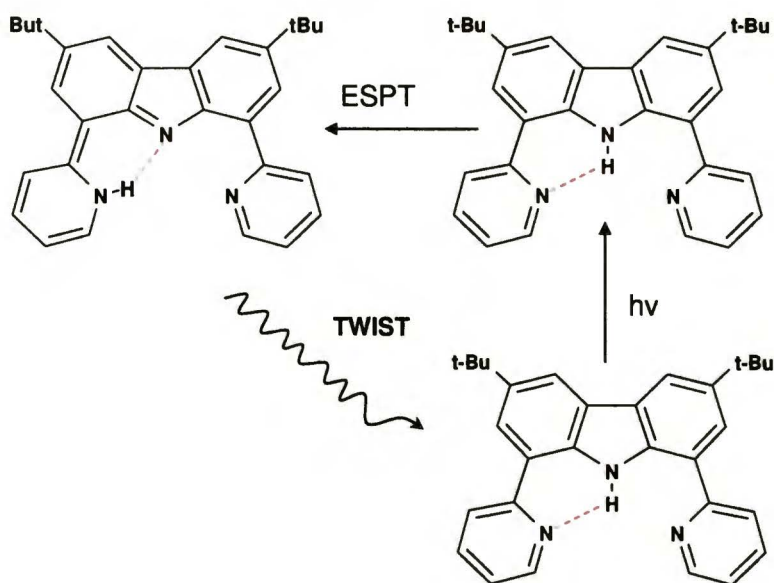
Figure IV.28. The model proposed for the excited state deactivation path of **4**.

IV.3.5. Substitution effect on the ESIPT dynamics. Preliminary studies

The IR absorption spectra presented in ref. 200 suggest that the change in the size of substituent in position 4, 7 may have some influence in the excited state reaction. Upon passing from the R= H, R= CH_3 to R= *t*-butyl group, the strength of the intramolecular hydrogen bond is changed, which could be reflected in the change of the ESIPT rate. Although the studies on this aspect are at a very initial stage, the results obtained for 2,9-(di-2'-pyridyl)carbazole (**4H**) and **4** have shown that the ratio of F_2/F_1 is larger in former whereas the quantum yields of F_1 are rather the same. It suggests that the rate of the deactivation of the tautomer occurs on a longer time scale in **4H**.

An important result was obtained in a polymer medium (PMMA) for the derivative of **4** for which the *t*-butyl groups are replaced by hydrogen. Room temperature emission spectra of **4H** in acetonitrile and polymer are presented in Figure IV.29. A dramatic increase of the F_2 emission intensity is observed for the polymer film. This result is called here because it nicely confirms the model that postulates the importance of twisting for the deactivation of the phototautomer; the experiment shows that this process is

strongly inhibited in a viscous medium. Assuming that the quantum yield of tautomer formation in excited state is 100%, one can deduce from the ratio of F_2 intensities that the tautomer in polymer lives much longer, by about an order of magnitude.
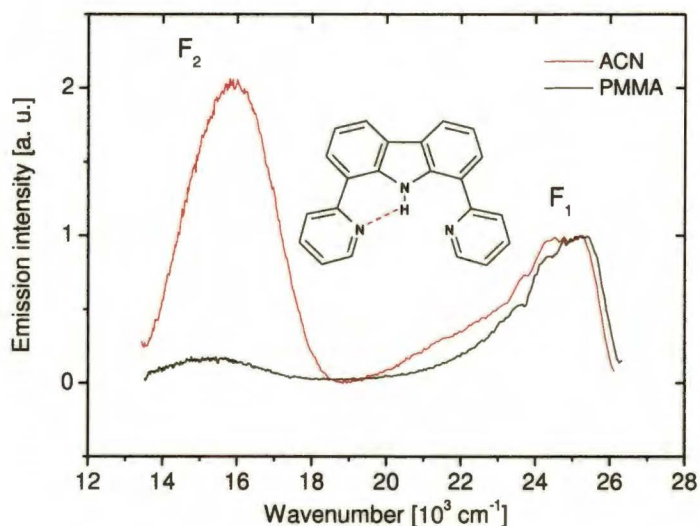
Figure IV.29. Room temperature emission spectra of **4H** in acetonitrile and polymethyl-methacrylate.

IV.3.6. Summary

2,9-(di-2'-pyridyl)-4,7-di(*t*-butyl)carbazole similarly to **1**, reveals ESPT along the intramolecular hydrogen bond. However, the rate of the reaction is slower in the case of **4** and contrary to **1**, the tautomeric fluorescence is observed. The radiationless deactivation of the phototautomer was found to be strongly dependent on temperature and viscosity, suggesting the important role of twisting. The deuterium substitution has shown that the tunneling contributes to phototautomerization.

In order to more carefully analyse the problem of intermolecular interaction, supersonic jet studies of hydrogen-bonded clusters with protic solvent are planned.

IV.4. Intermolecular character of fluorescence quenching in 7-(4'-pyridyl)indole

As was mentioned in the introduction to this chapter, moving the hydrogen-bonding centers one or two bonds away from each other results in drastical changes of the photophysics of 7-(pyridyl)indoles. Whereas for **1** the solvent is practically not necessary to observe rapid depopulation of the excited state, the photophysics of 7-(3'-pyridyl)indole (**2**) and 7-(4'-pyridyl)indole (**3**) seem to be governed by specific and nonspecific interactions with the solvent and, therefore, its role and nature cannot be neglected.

Since the case of **2** seems to be more complicated by the possible presence of two different rotamers, we decided to first present the results obtained for 7-(4'-pyridyl)indole (**3**) and, keeping these in mind, try to understand the photophysics of **2**.

IV.4.1. Solvent-dependent emission pattern

Both X-ray analysis[200] and calculations show that the ground state equilibrium structure of **3** is not planar as in **1**, but corresponds to a conformation with the twist angle between the donor and acceptor moieties being about 45°. In contrast to **1**, strong fluorescence is observed in aprotic, polar and nonpolar solvents (Table IV.6). In alcohols the maximum of the lowest absorption band is red-shifted in respect to nonpolar solvents (Figure IV.30) and the fluorescence becomes weak, with the same pattern of intensities as observed for **1**, i.e., the largest quantum yield in butanol and the smallest in methanol. However, in the case of **3** this tendency is much more pronounced. The fluorescence quantum yield of **1** decreases two times upon passing from butanol to methanol, whereas for **3** it becomes several dozen times weaker. Additionally, comparing the quantum yields and fluorescence lifetimes in aprotic and protic polar solvents one can see that they change differently with polarity. In a series of aprotic solvents Φ and τ increase with solvent polarity, whereas in protic solvents both parameters decrease when the polarity is growing. Interestingly, upon passing from nonpolar hexane to polar acetonitrile the quantum yield of fluorescence does not change excessively, whereas the lifetime becomes several times longer, indicating a smaller value of the radiative constant in the latter. Similar results were obtained for DMSO and BuCN.
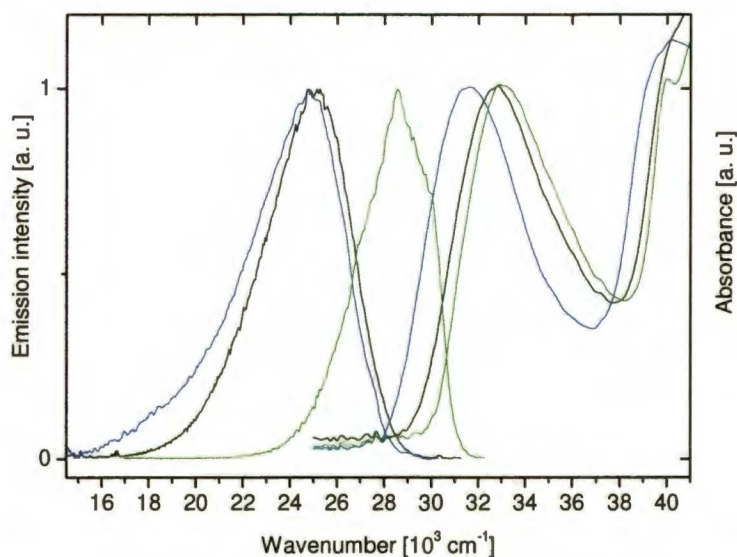
Figure IV.30. Room temperature absorption and fluorescence spectra of **3** in *n*-hexane (green), acetonitrile (black) and propanol (blue).

Table IV.6. Photophysical data (maximum of the lowest absorption band, maximum of fluorescence, fluorescence quantum yields and lifetimes) of **3** in different solvents at room temperature.

Solvent	$\nu_{abs}{}^{a}$ $[10^3\,cm^{-1}]$	$\nu_{fl}{}^{a}$ $[10^3\,cm^{-1}]$	$\Phi_{fl}{}^{b}$	$\tau_{fl}{}^{c}$ [ns]	k_r $[10^8\,s^{-1}]$	k_{nr} $[10^8\,s^{-1}]$
n-Hexane	33.00	28.57	0.44	1.2	3.67	4.6
Acetonitrile	32.70	24.75	0.55	5.8	0.95	0.77
Butanol	31.50	25.25	0.10	0.8	1.25	11.25
Propanol	31.50	24.69	0.046	0.6	0.77	15.9
Ethanol	31.70	24.87	0.018	0.2	0.9	49.1
Methanol	31.80	24.87	0.0034	0.03	1.1	332.2
DMSO	32.00	24.6	0.67	9.6	0.70	0.34
Water	32.50	24.81	0.0027	-	-	-
BuCN	33.00	25.00	0.4	4.6	0.87	1.3

[a] the error is estimated to be ± 200 cm⁻¹, [b] accuracy ± 20%, [c] the error does not exceed 10% for ns decays and becomes somewhat larger for ps lifetimes

90

The value of the radiative decay rate constant, k_r, obtained from the Φ/τ ratio, decreases by a factor of four upon passing from nonpolar n-hexane to polar solvents (Table IV.6). Such behavior may be interpreted in terms of relative twisting of the indole and pyridine moieties in the excited state, activated by polar media. It is generally known that the radiative constant is a function of the twist angle (Θ) and decreases when the value of Θ changes from 0° to 90°, where the two moieties involved in the charge transfer are orbitally decoupled and, as a consequence, the transition is forbidden and k_r becomes practically zero. This picture has been confirmed for **2** and **3** by B3LYP/6-31G(d,p) TDDFT calculations of the transition energies, carried out for fixed values of Θ changing from 0° to 90° in steps of 15°. The oscillator strength for the S_0-S_1 absorption decreases from 0.17 for $\Theta = 0$° to 0.005 for $\Theta = 90$°. Changing the values of Θ from 30° to 75° results in more than fivefold decrease of the oscillator strength; this trend agrees with the fourfold difference in radiative rates observed for **3** between n-hexane and polar solvents.

The differences between the pK_a values in the ground and excited states (Table IV.1), as well as the results of calculations show that the absorption of photon is accompanied by electron density redistribution, making the $S_0 \rightarrow S_1$ transition charge-transfer in character. The dipole moment of **3** increases significantly in the S_1 state (10.88 D vs. 2.03 D in S_0). As this highly polar state is stabilized with a growing polarity of solvent, the red shift of the fluorescence band is observed.

High values of the fluorescence quantum yield in acetonitrile, butyronitrile and in DMSO - polar aprotic solvents - show that excited state twisting in these media does not activate any radiationless deactivation processes. The results obtained in alcohol solutions, showing that the quantum yield of fluorescence drops drastically (by 2 orders of magnitude in methanol), suggest that besides twisting, some other channel of radiationless deactivation is being switched on. Upon passing from polar aprotic to polar protic solvent the nonradiative rate constant increases significantly, becoming the largest in methanol, the least viscous and the most acidic and polar alcohol among those used in the experiments. Since the lifetimes in alcohols at room temperature appeared to be comparable with the nanosecond time resolution of our instrument (or even shorter in the case of methanol), time-resolved fluorescence measurements were performed using a picosecond time correlated single-photon counting setup (SPC). The experiments carried out with better time resolution revealed that besides the main components of 0.6 ns in propanol and 0.27 ns in ethanol, a second, shorter time, contributes to the emission decay. For methanol, the dominance of the 30 ps component was clearly demonstrated. The most

important and interesting is that the lifetimes with the largest contribution to fluorescence decay in alcohols are correlated with the longest relaxation time of alcohols, underlining the important role of solvent in depopulation of excited state (Table IV.8).

Table IV.8. Comparison the decay times of fluorescence with relaxation time of solvents.

Solvent	Decay time of fluorescence [ps]	Relaxation time [ps]
propanol	590	329^a, 430^b
ethanol	270	163^a
methanol	30	51^a

[a] values taken from [206]; [b] values taken from [207]

IV.4.2. Transient absorption measurements

The femtosecond transient absorption spectra (Figures IV.31-33) revealed that, in contrast to **1**, the shape of the absorption spectra of an initially excited species of **3** depends on the nature of solvent. In the case of **1**, when the strong intramolecular hydrogen bond makes the possibility of intermolecular interactions with solvent unlikely, the TA spectra in polar solvents look very similar to those in nonpolar ones. It is not the case for **3**. Transient absorption spectra, which can provide an evidence for all the species involved in the excited state process, measured in acetonitrile do not reveal any spectral changes (Figure IV.32). Kinetic traces of transient absorption recorded at the maximum of the band indicate a rapid relaxation to a long-lived state (>1ns). The TA spectra in hexane measured after 900ps should be treated as a sum of S_1-S_n and T_1-T_n spectra, which explains their slightly different shape from the spectra measured at short time delays.
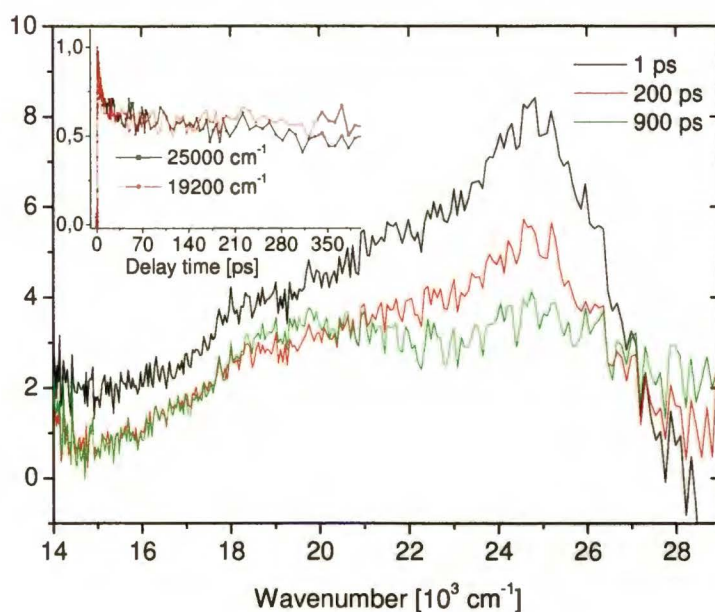
Figure IV.31. Transient absorption spectra of **3** in *n*-hexane at 293 K; inset, kinetic traces measured at 25000 cm^{-1} and 19200 cm^{-1}.
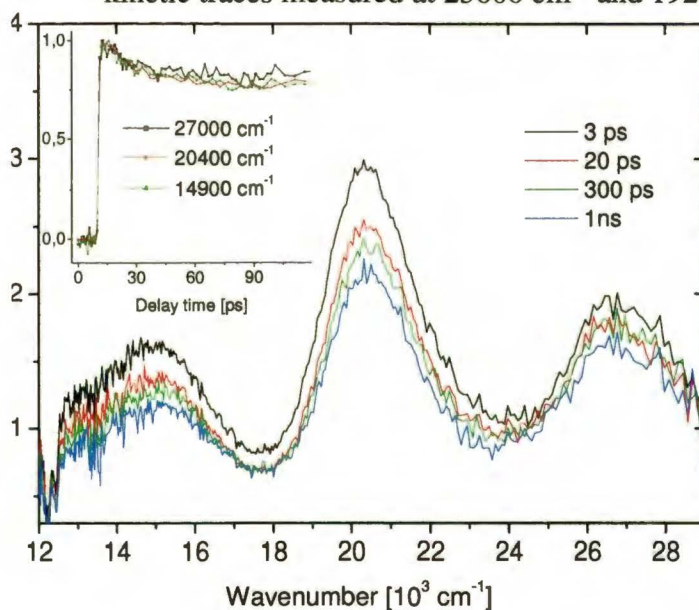
Figure IV.32. Transient absorption spectra of **3** in acetonitrile at 293 K; inset, kinetic traces measured at 27000 cm^{-1}, 20400 cm^{-1} and 14900cm^{-1}.
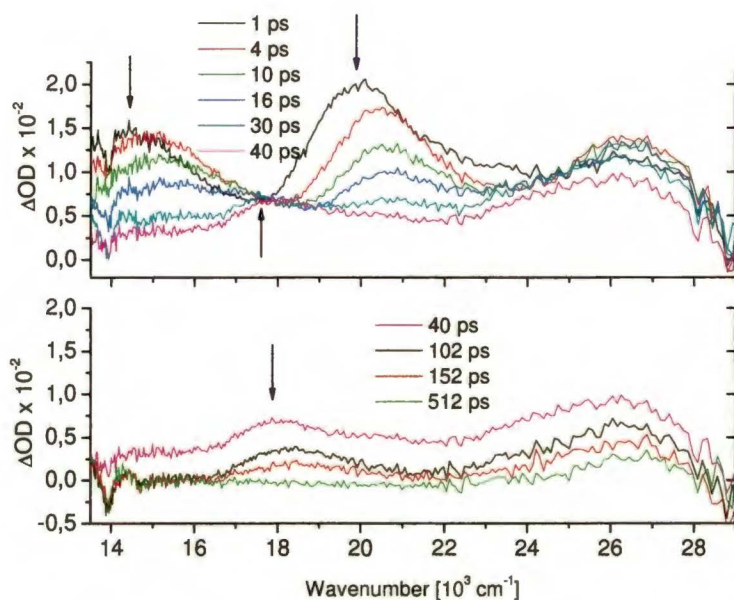
Figure IV.33. Transient absorption spectra of **3** in methanol at 293 K.

The TA spectra recorded shortly after excitation in polar acetonitrile and methanol look similar. The main features are three absorption bands with maxima at about 27000 cm^{-1}, 20400 cm^{-1} and 14900cm^{-1} (Figures IV.32-33). However, the TA spectra recorded for longer delay times reveal differences between these two solvents. In methanol the band at 27000 cm^{-1} remains, while the two other features (at 20400 cm^{-1} and 14900cm^{-1}) disappear. Additionally, after 40 ps delay, a band at 18200 cm^{-1} appears, of which the lifetime is ca. 70 ps. At the present stage of studies it is difficult to state what the structure of this transient species is. However, it is undoubtedly related to specific, hydrogen bonding interactions with the solvent. As discussed above, the changes of pK_a accompanying excitation clearly show that both hydrogen bonds become stronger in the excited state. Since the efficient radiationless deactivation is not observed in DMSO, which forms a hydrogen bond with the NH group, it is the pyridine nitrogen which provides a rapid deactivation channel. Another possibility is that of cooperative role of both intermolecular hydrogen bonds, suggested by the results obtained for **2**, discussed below.

IV.4.3. The effect of temperature on the fluorescence

Temperature measurements confirm the importance of solvent relaxation for excited states deactivation. Upon lowering the temperature the relaxation times become longer and the molecule recovers its radiative properties. In 1:1 ethanol:methanol solution the intensity of fluorescence increases about 100 times, showing that the quenching process is effectively slowed down by decrease of temperature or increase of viscosity (Figure IV.34). Another important feature of the variable-temperature spectra is the substantial blue shift observed upon formation of the optical glass: the emission maximum shifts by about 2000 cm^{-1}, from ca. 24000 cm^{-1} at 298 K to ca. 26000 cm^{-1} at 103 K. Further decreasing of the temperature does not change the position of the spectrum. The spectral evolution takes place in a narrow range of temperatures (120-100 K) where the glass transition occurs. It may be explained in terms of solute-solvent interactions, to which the emission spectra are sensitive. At low temperature, when the solvent is frozen, the relaxation processes are hindered. The relaxation processes may include reorientation of polar solvent molecules to their equilibrium configuration in the field of the excited state of the polar solute, as well as relaxation via intramolecular twisting. Both mentioned processes are slowed down when the viscosity of the medium is large and, as a consequence, fluorescence occurs from the Franck-Condon state, which explains the blue shift of the spectrum. At 88 K, phosphorescence is observed. The excitation spectra suggest that both fluorescence and phosphorescence originate from the same ground state precursor. At low temperature, the processes responsible for the deactivation of S_1 at room temperature become slow and the probability of intersystem crossing increases.

The fluorescence decays measured at 203 K and lower temperatures are biexponential. Both decay times increase with decreasing temperature. Similar results were obtained in propanol. However, for this solvent the values of lifetimes reveal the maximum around the temperature where propanol becomes rigid. An example of decay of fluorescence and the results of the fitting procedure are given in Figure IV.35. Further decreasing of temperature leads to shorter lifetimes (Table IV.9). The comparison of the lifetimes measured at different wavelengths of fluorescence shows that down to 183 K the decay components are practically independent on v_{obs}. However, with decreasing temperature the situation changes and both lifetimes becomes longer when λ_{obs} increases. This behavior may be related to the increasing relaxation time of the solvent. The decay of fluorescence measured at its red edge is monoexponential down to 163 K, and only below this temperature a second component is observed (Table IV.10).

In order to analyze these results, we recall that **3** interacts with protic solvent molecules via hydrogen bonds, forming various types of complexes which may differ in lifetimes and emission spectra.
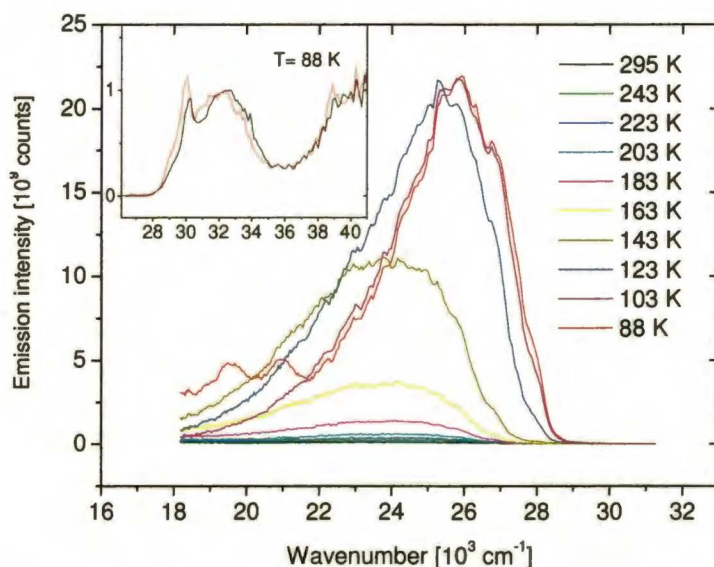
Figure IV.34. Temperature dependence of the emission of 7-(4'-pyridyl)indole in ethanol:methanol (1:1); inset, the fluorescence (in red) and phosphorescence (in black) excitation spectra recorded at 88 K.

Table IV.9. Fluorescence lifetimes of **3** in alcohols as a function of temperature.

Temperature [K]	Ethanol:methanol (1:1)[a] [ns]			Propanol[a] [ns]		
	τ_1	τ_2	A_2/A_1	τ_1	τ_2	A_2/A_1
223				1.8	0.3	0.6
203	1.20	0.34	49	3.6	0.8	0.5
183	1.34	0.72	5.6	6.5	1.9	0.6
163	2.60	0.78	0.8	8.5	3.3	0.9
143	7.10	2.1	0.9	7.6	3.7	1.1
123	9.20	4.6	1.1	6.4	3.7	1.3
103	8.04	4.6	2.0	6.1	3.5	1.8
88	8.30	4.6	2.7			

[a] the error was estimated to be ca. 10%

Table IV.10. Decay times of fluorescence of **3** in propanol measured at different emission wavelengths.

T [K]	τ[ns]	ν_{obs} [cm^{-1}]			
		27800	27000	25000	22700
203	τ_1	1.1	1.1	1.4	-
	τ_2	3.5	3.5	3.6	3.8
188	τ_1		1.6	1.7	-
	τ_2		5.4	5.8	6.1
183	τ_1		2.1	2.6	-
	τ_2		6.3	6.7	6.8
173	τ_1		2.6	3.9	-
	τ_2		7.2	8.3	9.5
163	τ_1	2.6	3.2	4.9	6.5
	τ_2	6.6	7.7	9.5	10.2

Figure IV.35. Kinetic curve of fluorescence of **3** in propanol monitored at 22200 cm^{-1} at 143 K (black) and the result of the fitting procedure (blue). The instrument response function is also shown for comparison; bottom, the plot of residuals.

97

The fluorescence intensity of **3** in polar aprotic BuCN increases progressively with decreasing temperature and reaches a constant level corresponding to maximal fluorescence quantum yield of 0.8, which is two times larger than at room temperature (Figure IV.36). Simultaneously, a small red shift of the fluorescence maximum is observed, reflecting the stabilization of the excited state with increasing polarity of the solvent. However, when the medium becomes sufficiently rigid, the maximum of the emission shifts to the blue (Figure IV.37). This behavior can be related to the fact that under such conditions, the probability of modification of molecular structure via twisting after excitation is very low and, consequently, the fluorescence occurs from the solute which maintains the ground state geometry.

If one assumes that the nonradiative rate of the excited singlet state deactivation may be expressed as a sum of a temperature-independent and a temperature-dependent processes, $k^0_{nr} + k' \exp(-\Delta E/RT)$, an Arrhenius-type expression results: $1/\Phi(T) = 1 + (k^0_{nr}/k_r) + (k'/k_r)\exp(-\Delta E/RT))$

The activation energy obtained from fitting the experimental results to this equation was found to be 2.4 ± 0.1 kcal/mol, This value is very similar to the energy of viscous flow of BuCN (2.2 kcal/mol),[208] which suggests that the influence of the environment, its viscosity in particular, may be crucial in the deactivation process.
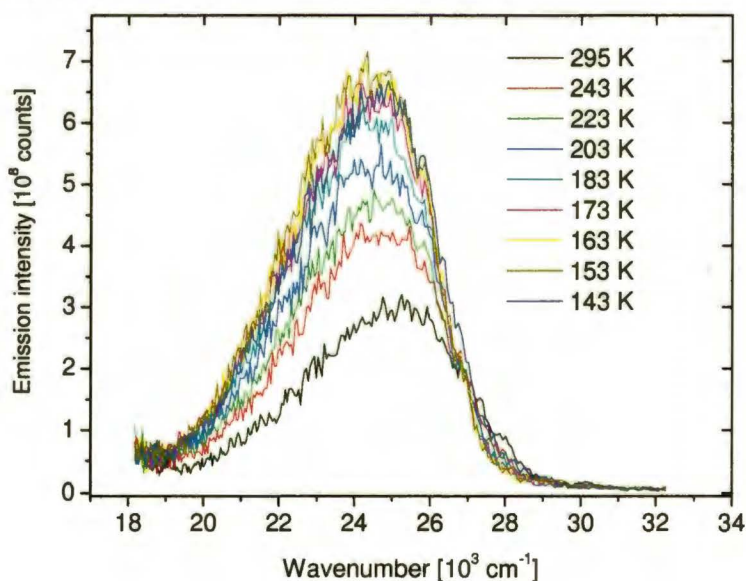
Figure IV.36. Temperature dependence of the emission of **3** in butyronitrile.
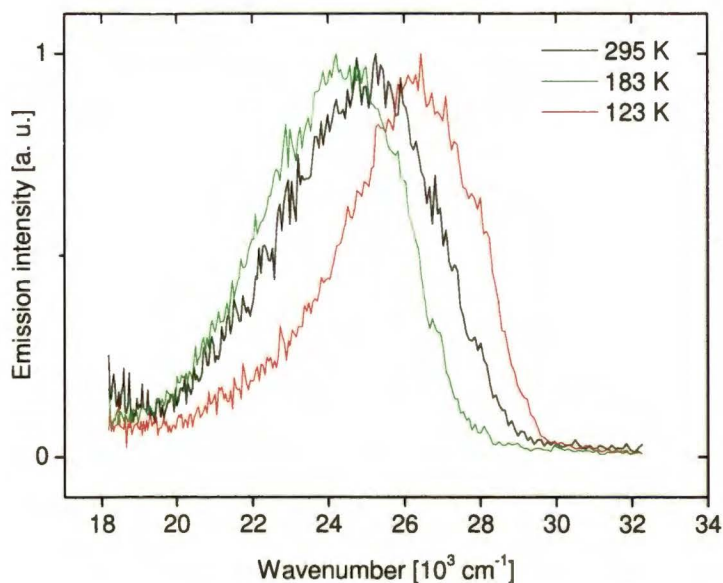
Figure IV.37. The changes in the position of the maximum of fluorescence band of **3** in butyronitrile accompanying temperature decrease.

The lifetime of fluorescence measured at different temperatures allows to state that the radiative rate constant is temperature-independent in the range 293-143 K. Similar to fluorescence intensity, the decay times of **3** increase initially with decreasing temperature and approach a constant value. Interestingly, for temperatures lower than 153 K the decay time becomes shorter (Figure IV.38). It may reflect the fact that twisting in the excited state is hampered and consequently the radiative constant at low temperatures is larger. It should be mentioned that in the temperature range of 153-110 K the decays of fluorescence become bi- or even triexponential, depending on the wavelength of emission. Similar effects for BuCN were observed by Rettig and coworkers.[209] It is known from literature that the relaxation times of butyronitrile in this range of temperature become very long,[210] and it is therefore possible that the additionally observed decay times are related to solvent relaxation. One cannot also exclude effects due to hindered rotational relaxation of the solute.
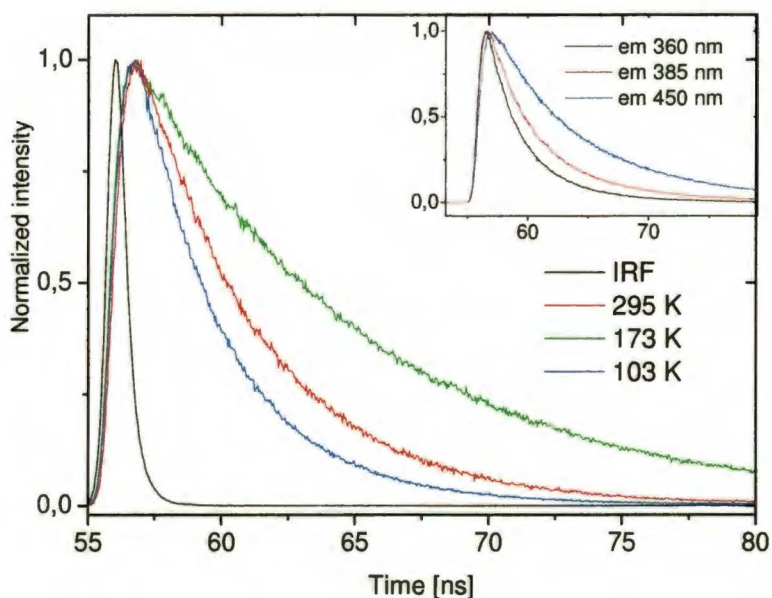
Figure IV.38. Kinetic curves of fluorescence of **3** in butyronitrile: monitored at 22200 cm^{-1} as a function of temperature. The instrument response function is also shown for comparison. Inset, Kinetic curves of fluorescence of **3** in butyronitrile monitored at 27800 cm^{-1}, 26000 cm^{-1}, 22200 cm^{-1} recorded at 133 K.

Low temperature experiments were undertaken also in nonpolar glass-forming solvents, such as methylcyclohexane and 3-methylpentane. However, these solvents turned out to be not sufficiently dry and additional effects, like complexation of protic impurities (most probably water) at lower temperatures, complicated the interpretation. A triexponential function was required to fit the decay profile adequately in the low-temperature region.

IV.4.4. Supersonic jet studies

According to the differences in the radiative rate constants in polar and nonpolar solvent (about four times larger in the latter) and the results of temperature measurements the conclusion is the following: in polar solvents, the twisting in excited state takes place. In order to answer the question whether the molecule can become more flat in the excited state when it is free from interactions with the solvent (as is suggested by calculations

100

performed for the isolated molecule) one can envisage experiments in supersonic jets, analogous to those reported for 2-phenylindole (**PI**) by Philips and co-workers.[211,212] The torsional potentials in S_0 and S_1 states may be determined from the laser induced fluorescence excitation and various single vibronic level fluorescence (SVLF) spectra. The spectrum of **PI** exhibits a relatively weak origin and is dominated by a strong torsional 64 cm^{-1} mode. The long progression in this mode (up to 15 quanta) was interpreted as a result of a significantly different geometry along the torsional coordinate in the S_0 and S_1 electronic states. It was shown that the interplanar angle tends to zero value upon electronic excitation, similarly to other biaromatic systems linked by a single bond.[213-216] One can suspect that **PI** may serve as a good reference molecule for the compound **3**. The insertion of pyridine atom into the phenyl ring does not change significantly the mass of the molecule. However, it induces a rather large perturbation as far as the electronic density distribution is concerned. The character of the lowest excited state of **3** becomes definitely more charge-transfer-like.

The laser-induced fluorescence excitation (LIF) spectra of **3** in supersonic jets are shown in Figure IV.39.
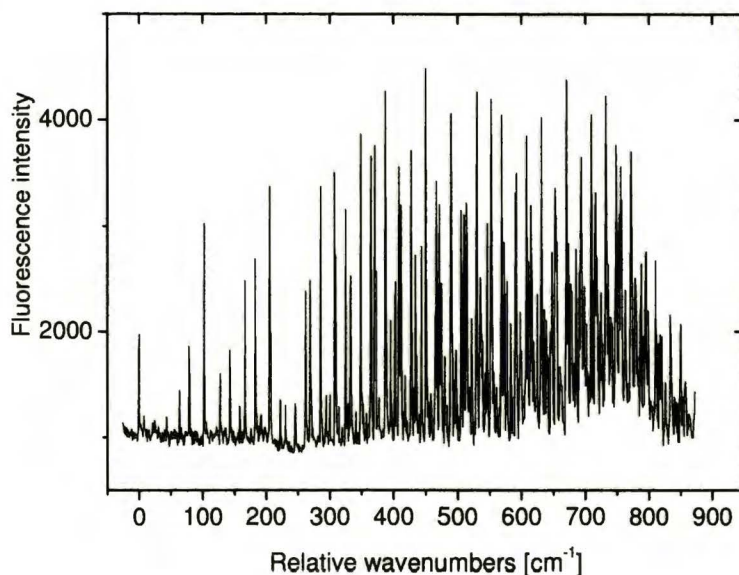
Figure IV.39. Fluorescence excitation spectrum of jet-cooled **3**. The 0_0^0 band is located at 32202 cm^{-1}.

The lowest energy transition at 32202 was ascribed to the $S_0 \rightarrow S_1$ origin. The intensity of this band is medium with respect to other vibrational

101

transitions, which means that the conformation of the molecule changes in the electronically excited state with regard to that in the ground state and that overlapping of the vibrational eigenfunctions of the electronic states involved in the transition takes place. Due to a large number of modes, the excitation spectrum is congested and difficult to assign completely. Thus, in the present study the vibrational analysis has been limited to the low frequency spectral region (Figure IV.40). All major transitions observed in the excitation spectrum of **3** up to 500 cm^{-1} are listed in Table IV.11. Most of the features may be described by the combinations of three low frequency modes: 63.7 cm^{-1}(A), 78.8 cm^{-1} (B) and 102.5 cm^{-1} (C).
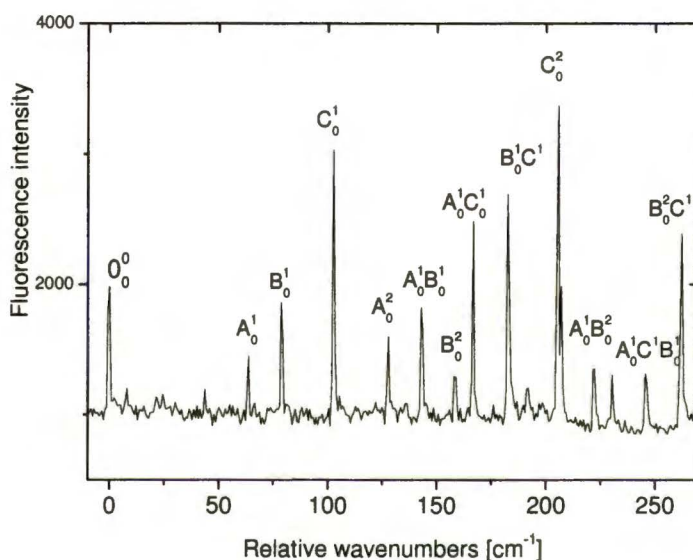
Figure IV.40. Low frequency region of fluorescence excitation spectrum of jet-cooled **3**.

The most prominent progression occurs at 0_0^0+102.5 cm^{-1}. The progression of this mode, built practically on all overtones and combination bands of A and B vibrations was found in the LIF spectrum (Table IV.11).

The calculations for S_1 predict three vibrations with frequencies below 100 cm^{-1}, in very good agreement with experiment (Table IV.11). The comparison between the calculated and experimentally observed vibrational transitions allows to assume that the low-frequency progressions observed in the excitation spectrum can be attributed to the torsional motion of the pyridyl ring with respect to the indole moiety.

102

Detailed investigations of the structural changes accompanying electronic excitation of **3** are in progress. In order to obtain information on the S_0 torsional potential, measurements of vibrationally-resolved dispersed fluorescence spectra, obtained for excitation into specific vibronic levels (SVLF) are planned. The comparison of LIF and SVLF spectra with results of quantum-chemical calculations should allow a detailed description of the vibrational structure of **3** in its ground and lowest excited singlet electronic states and help answering the question considering conformational changes. The initial results of the quantum chemical calculations demonstrate that the dihedral angle Θ between the indole and pyridyl rings equals 46° in the equilibrium ground state (B3LYP/6-31+G(d,p)), and approaches 22.3° (CIS/6-31+G(d,p)) or 33.9° (TDDFT/TZVP) in the electronically excited state. These results suggest that the isolated molecule becomes more flat in S_1, thus adding credibility to the previous comparison of oscillator strengths between a structure more flat than in S_0 (the molecule in a nonpolar solvent) and more twisted than in the ground state (the same molecule in a polar environment).

IV.4.5. Summary

In conclusion, the photophysics of **3** is governed by the specific and nonspecific interactions with the solvent. In polar aprotic solvents, the excitation is accompanied by relative twisting of pyridyl and indole rings, however the excited state twisting in these media does not activate any radiationless depopulation processes. The intermolecular interaction with molecules of protic solvents provides a fast deactivation channel, namely the S_1-S_0 internal conversion of hydrogen-bonded complexes. No quenching was observed in DMSO, which points to the important role of the pyridine nitrogen atom in deactivation. Surprisingly, the initial calculations predict the cyclic structure for complexes of **3** with two molecules of water. In order to verify the computational results the structure of possible complexes will be studied by IR/R2PI. The supersonic jet experiments performed so far for the monomer of **3** strongly suggest that the geometry of the isolated molecule in the electronically excited state differs from that in the ground state.

103

Table IV.11. Transition energies, intensity and initial assignments of the bands in the LIF excitation spectrum of **3** relative to the $S_0 \rightarrow S_1$ origin at 32202 cm^{-1}.

Δv [cm^{-1}]	Relative intensity	Assignment	Δv [cm^{-1}]	Relative intensity	Assignment
0 (32202)	1	0-0	332.8	1.3	A^2C^2
63.7 (62.8)[a]	0.7	A^1	340.8	0.6	
78.8 (82.4)[a]	0.9	B^1	348.8	1.9	$A^1B^1C^2$
102.5 (98.0)[a]	1.5	C^1	364.9	1.8	B^2C^2
127.7	0.8	A^2	370.8	1.9	A^1C^3
142.8	0.9	A^1B^1	372.9	1.3	$A^3 B^1C^1$
158.6	0.6	B^2	377.4	0.7	
166.6	1.2	A^1C^1	387.6	2.2	B^1C^3 ,
182.5	1.4	B^1C^1	389.1	sb	$A^2B^2C^1$
205.6	1.0	C^2	395.6	1.0	A^3C^2
207.0	1.0	A^2B^1	403.0	1.2	$A^1B^3C^1$
222,3	0.6	A^1B^2	408,8	1.8	C^4
230.3	0.6	A^2C^1	411.8	1.6	$A^2B^1C^2$
245.5	0.7	$A^1B^1C^1$	417.6	0.8	
262.2	1.2	B^2C^1	427.2	1.9	$A^1B^2C^2$
268.7	1.2	A^1C^2	433.8	1.4	A^2C^3
271.0	sb	A^3B^1	436.0	0.9	
285.5	1.7	B^1C^2	443.3	1.4	
287.0	sb	A^2B^2	450.7	2.3	$A^1B^1C^3$
294,2	0.7	A^3C^1	458.7	0.7	
300.0	0.7	A^1B^3	466.8	1.7	B^2C^3
307.3	1.8	C^3	472.0	1.6	A^1C^4
310,2	0.7	$A^2B^1C^1$	474.9	1.2	
313.8	0.6		480.1	0.9	
324.8	1.6	$A^1B^2C^1$	489.6	2.0	B^1C^4

[a] TDDFT/TZVP calculations, frequencies scaled by 0.956.

IV.5. The consequences of solvent-induced *syn-anti* rotamerisation in 7-(3'-pyridyl)indole on intermolecular fluorescence quenching.

7-(4'-pyridyl)indole (**3**), with the electron/proton acceptor in the *para* position serves as an ideal reference molecule for other members of the series, especially for the *meta*-substituted derivative (**2**), of which the photophysics is enriched by the finding of *syn-anti* rotamerisation. The consequence of conformational changes is a possibility to form, with protic solvents, a large number of different types of (cyclic and noncyclic) complexes. For each of such complexes, different processes may decide about the path of excited state deactivation, making the interpretation of photophysical behavior quite challenging.

Figure IV.41 presents room temperature electronic absorption and emission spectra of **2** for selected solvents, differing in polarity and the ability to form hydrogen bonds. Table IV.12 contains relevant photophysical parameters for all studied solvents.
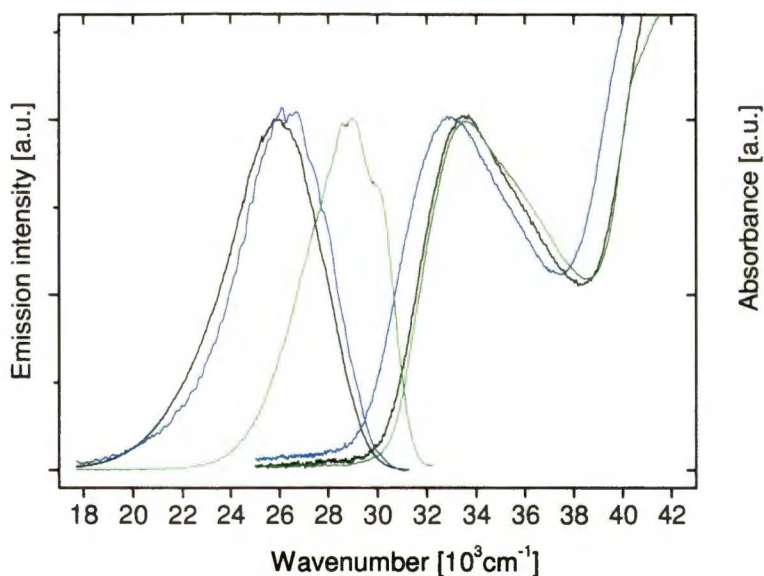
Figure IV.41. Room temperature absorption and fluorescence spectra of **2** in *n*-hexane (green), acetonitrile (black) and propanol (blue).

Upon passing from a nonpolar, through polar aprotic to a polar protic solvent the first absorption band reveals a red shift denoting a specific hydrogen bond interaction. The formation of hydrogen bonds with alcohol

105

molecules leads to fluorescence quenching. Similarly as in **3**, intense emission is observed in hexane and acetonitrile. In alcohols the quantum yield decreases drastically and the efficiency of quenching increases in the series: butanol, propanol, ethanol, methanol. This behavior is characteristic for all members of the series. However, the difference between the quantum yield in aprotic and protic solvents is the largest in the case of **2**. This suggests that there is some feature characteristic for **2** only which makes the quenching in alcohols more effective and, probably, it may be traced to the possibility of formation of cyclic hydrogen bonds.

Table IV.12. The photophysical data (maximum of the lowest absorption band, fluorescence maximum, fluorescence quantum yield) of **2** in different solvents at room temperature.

Solvent	ν_{abs} [a] $[10^3\,cm^{-1}]$	ν_{fl} [a] $[10^3\,cm^{-1}]$	Φ_{fl} [b]
Hexane	33.50	29.00	0.21
Acetonitrile	33.50	26.00	0.25
Butanol	32.80	26.40	0.015
Propanol	32.90	26.40	0.011
Ethanol	32.90	26.40	0.0036
Methanol	33.00	26.30	0.0011
Octanol	32.50	27.00	0.046
DMSO	33.00	25.30	0.41
BuCN	33.25	26.40	0.30

[a] the error is estimated to be ± 200 cm^{-1}, [b] accuracy ± 20%,

The calculations predict that **2** may exist in two rotameric forms, *syn* and *anti* (Figure II.1). The respective molecular structures computed for **2** are both nonplanar, with the indole and pyridine moieties twisted with respect to each other by about 45°. The conformers should have similar energies, the *syn* form being more stable only by less than 0.5 kcal/mol. The calculated ground state dipole moment is higher in the *anti* form, 2.98 D vs. 1.63 D in the *syn* structure. Thus, the *anti* form should be stabilized in polar solvents. The TDDFT-computed energies of vertical transitions suggest that both rotamers should absorb at very similar wavelengths, with similar

oscillator strengths for low-energy transitions. After absorption of the photon the electron density is moved from the indole to the pyridine ring. Figure IV.42 presents the HOMO and LUMO orbitals for *syn* and *anti* forms which are involved in the lowest energy transition. The TDDFT calculations predict that, upon excitation to S_1, the dipole moment of both forms significantly increases (to about 9 and 12 D for the *syn* and *anti* species, respectively), due to charge transfer from the indole onto the pyridine moiety.
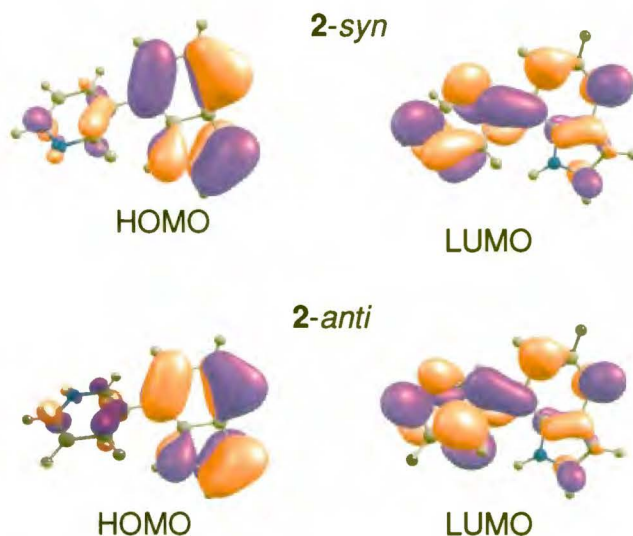
Figure IV.42. The shapes of HOMO and LUMO molecular orbitals (B3LYP/6-31G(d,p)) involved in the lowest transition of **2**-*syn* (top) and **2**-*anti* (bottom).

The similarities of the two forms make them difficult to be distinguished spectroscopically. The comparison between the excitation of fluorescence and absorption spectra, presented in Figure IV.43, does not give direct evidence for the presence of two emitting forms.
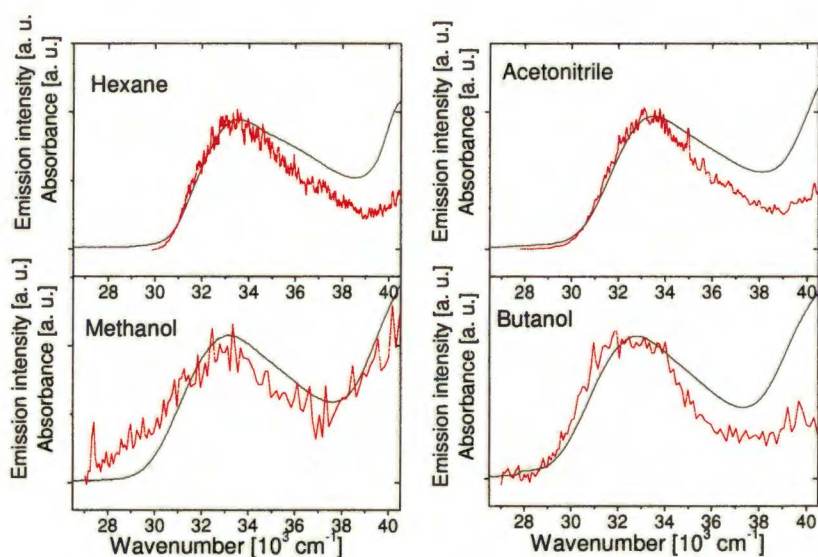
Figure IV.43. Room temperature absorption (black) and fluorescence excitation (red) spectra of **2**.

IV.5.1. Time-resolved fluorescence measurements

However, the presence of two different species of **2** could be established by time-resolved fluorescence measurements. The fitting of the fluorescence decay in DMSO solution yields two times: 7.1 ns and 3.4 ns, with the relative amplitudes of 0.69 and 0.31, respectively. In ACN and BuCN two forms are also observed; however, the lifetimes of 3 ns and ca. 1.3 ns differ from those in DMSO and the much larger amplitude of the former suggest that the long-lived population dominates. Practically, it is difficult to state without any doubt that in ACN and BuCN the second form actually exists, whereas it is unquestionable in DMSO and alcohols. This fact may point to the role of specific interactions as a factor which can make two forms distinguishable from each other. Upon passing from polar aprotic to protic solvents the longer decay time does not change significantly, in contrast to the second component, which becomes clearly shorter. The amplitudes show that in alcohols the short-lived structures definitely prevail. It should be noted that the error in the determination of the relative contributions of the two emissions becomes very large if one of the decays is too short to be determined exactly; this is the reason why the amplitudes were not included in Table IV.13. These results may suggest that one of the possible forms of **2** is much more stabilized by forming hydrogen bonds

with alcohol molecules. It would seem justified to attribute the longer decay time to the *anti* form, which is stabilized in polar solvents. However, one should take into consideration that the specific interactions of protic solvents with the *syn* form, which is able to form cyclic complexes, can also lead to energy lowering.

The fluorescence in hexane decays monoexponentialy. It could indicate that only one form is present in nonpolar solvent. However, taking the similarities of two forms into consideration, one cannot exclude the existence of both of them, indistinguishable in this kind of experiment. The presented results of time-resolved measurements suggest which factors can be used to differentiate between the two forms. Manipulating such parameters of the solvent as polarity and/or hydrogen bonding ability creates a possibility to preferentially stabilize one of them.

The lifetime of fluorescence in hexane and the longer component measured for polar aprotic solvent reveal the same tendency of changes as in **3** (Table IV.6); however the effect is a bit weaker in **2**. Similarly to **3**, it may be interpreted in terms of possible relative twisting of the donor and acceptor moieties in excited state.

Table IV.13. Decay times of fluorescence of **2** measured in different solvents at room temperature; (d) indicates a dominant population.

Solvent	τ_1 [ns][a]	τ_2 [ns][a]
Hexane	1.2	-
Dimethylsulfoxide	7.1 (d)	3.4
Acetonitrile	2.8 (d)	1.3
Butyronitrile	2.9 (d)	1.5
Propanol	2.9	0.1 (d)
Ethanol	2.4	0.05 (d)
Methanol	3.2	0.02 (d)

[a] the error does not exceed 10% for ns decays and become somewhat larger for ps lifetimes

IV.5.2. Temperature dependence of the emission intensity and decay times

Lowering the temperature leads to the recovery of the emissive properties of **2** in alcohols (Figure IV.44). More intense fluorescence in alcohol glasses may suggest that a large number of ground state structures are not prepared for a fast excited state deactivation process, and the

reorganization of solvent around the excited molecule is necessary. In other words, the process which is responsible for fast deactivation of excited state becomes slower in the regime of cold, rigid alcohol glasses. Actually, the importance of alcohol relaxation is indicated already by the room temperature data obtained for a viscous octanol (Table IV.12): the fluorescence maximum lies definitely higher in energy than for other alcohols, suggesting that the emission occurs from a nonrelaxed state.

The temperature dependence of the emission looks similar to that observed for **3** in alcohols. Besides growing of intensity, the position of the emission maximum moves to the blue with decreasing temperature. In a rigid medium fluorescence originates from the solvent-unrelaxed state, i.e., an excited molecule with the environment arrangement identical or close to that of the ground state. Fluorescence occurs before full relaxation of the excited molecule to its equilibrium configuration. At intermediate viscosities fluorescence arises from a partly relaxed excited molecule. At 88 K phosphorescence appears and the excitation spectra suggest the same ground precursor for both emissions.
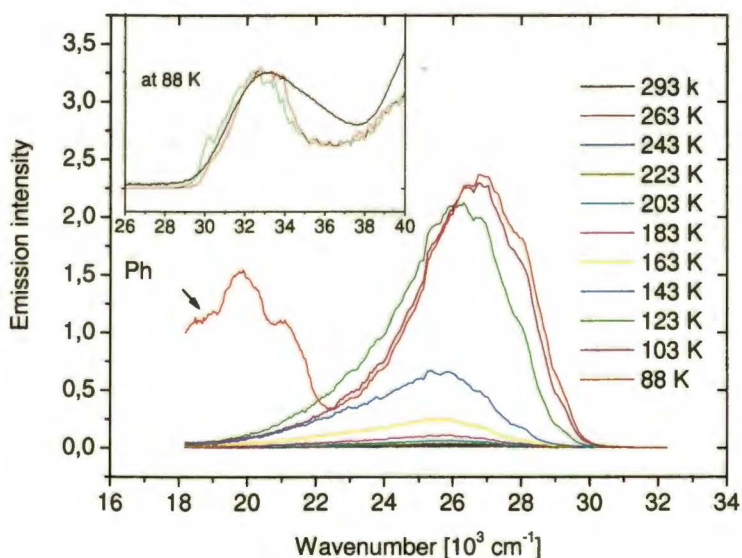
Figure IV.44. The temperature dependence of the emission of **2** in MeOH:EtOH (1:1 v/v). Excitation energy: 33300 cm^{-1}. Inset, the comparison of absorption (black), fluorescence (red) and phosphorescence (green) excitation spectra at 88 K.

The time-resolved fluorescence spectra recorded in ethanol:methanol (1:1), as well as in propanol and BuCN as a function of temperature,

110

revealed that the fluorescence decays are biexponential. Both observed times become longer when the temperature decreases. However, when the medium becomes sufficiently rigid the process of times elongation is stopped and even the shortening of times is observed. In BuCN this process is accompanied by changes in the position of fluorescence maximum similar to those observed for **3**. Lowering of temperature leads to an increase of emission intensity and, simultaneously, the position of the maximum of fluorescence is moved slightly to the red (Figure IV.45). The temperature decrease leads to a larger dielectric constant of the solvent, which more strongly stabilizes the polar excited state of the solute. This results in the red shift of the emission. However, below 153 K, besides the above-mentioned shortening of decay times, a blue shift of the emission is observed. It may suggest that, similarly to **3**, the twisting may have some influence in the deactivation processes of the lowest excited singlet state of **2**. The activation energy calculated from the $1/\Phi$ dependence of $1/T$ in BuCN appeared to be slightly smaller than the activation energy of the viscous flow in a given solvent (1.9 ± 0.1 kcal/mol and 2.2 kcal/mol,[208] respectively). The comparison of decay times measured in alcohol and in aprotic solvents, such as BuCN, showed that the form with a shorter lifetime behaves in a different way in both types of solvents when the temperature decreases. One can suppose that the lifetime of this form in alcohols is much more sensitive to temperature and viscosity.
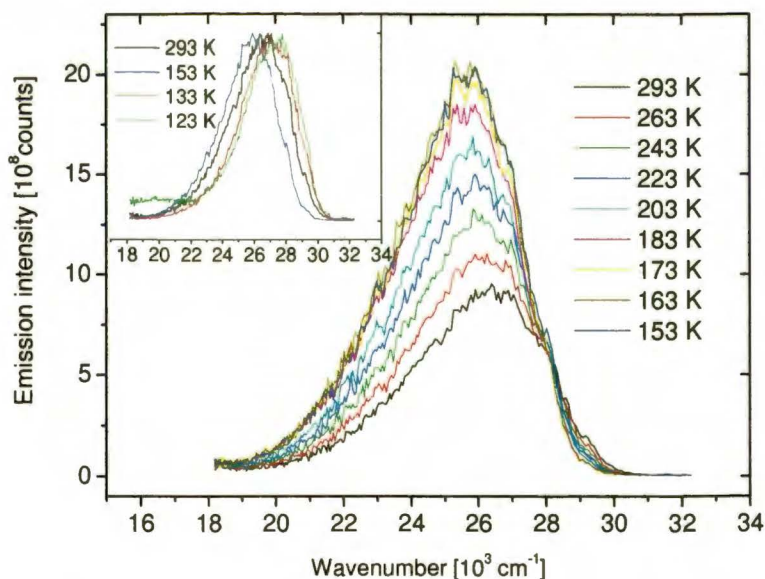
Figure IV.45. Temperature dependence of the emission of **2** in butyronitrile.

It should be mentioned that the fluorescence decay times in alcohols measured as a function of the wavelength of observation (emission) differ: a general trend is the elongation of both components for lower emission energies. Keeping in mind that **2** may exist in two rotameric forms, and each of them possesses two sites which can act as hydrogen bond donor or acceptor, this behavior may be explained by the presence of different type of complexes. Given different possibilities of complexation, it is especially interesting to investigate the size-selected hydrogen-bonded complexes of **2** isolated under supersonic jet conditions. Such experiment may be treated as a link between the bulk solvent and the gas phase.

IV.5.3. Supersonic jet studies

One can suspect that two rotamers with similar energies should be present under jet conditions. Using the results of calculations, according to the Boltzmann distribution, at 393 K (a typical nozzle temperature in jet experiments) the fractions of *syn* and *anti* forms should be 65% and 45%, respectively, and similar vibrational patterns for both species are expected. Since both rotamers are of C_1 point group symmetry, all vibrations (69) can be active in the spectrum. The TDDFT calculations predict the $S_0 \rightarrow S_1$ transition of the *anti* form to be blue-shifted by about 70 cm^{-1} with respect to that of the *syn* rotamer. The LIF excitation spectra of **2** measured in the range 32000-33100 cm^{-1} are given in Figure IV.46 together with the one-color R2PI spectrum recorded in the m/e=194 Da channel. Unfortunately, the spectra are not corrected for the laser intensity, which explains the differences between them. However, vibronic structures measured by application of fluorescence and ion detections are very similar.

The spectra are crowded; however, the comparison with the LIF spectrum of **3** suggests that they should not be treated as the superposition of two spectra that belong to different rotameric forms (Figure IV.47). **2** and **3** (which exists in only one form) reveal very similar vibronic patterns. To verify the possibility of coexistence of two conformers of **2** under supersonic jet conditions, a double-resonance UV/UV fluorescence-depletion and IR/R2PI–hole burning experiments were performed. In these experiments, an IR laser beam excited the NH stretching vibration, located at 3513 cm^{-1}, 50 ns prior to UV laser scanning the R2PI spectrum. Unfortunately, very small signal to noise ratio did not allow to draw definite conclusions from these experiments and the problem is still under study. Its solution could be helpful in interpreting the investigations concerning the geometrical structure of jet-cooled **2** clusters with protic "partners", which are presented below.
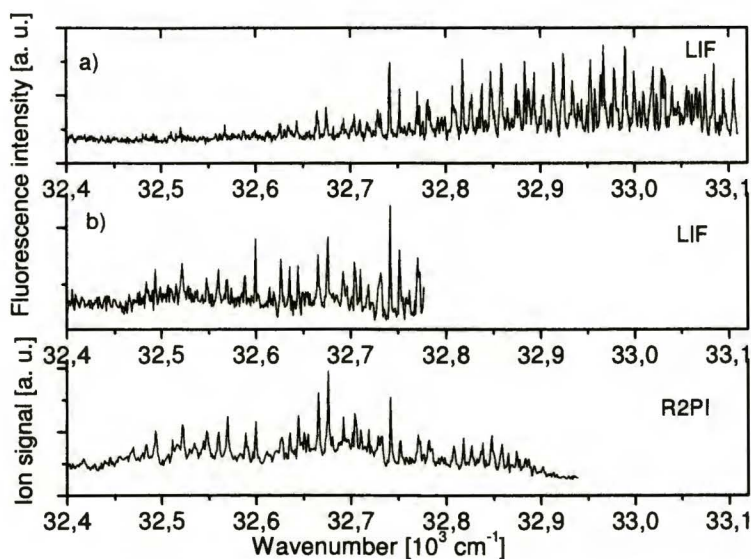
Figure IV.46. Fluorescence excitation and one-color R2PI spectra of jet-cooled **2**. The two upper spectra were measured in different laboratories: Warsaw (a) and Frankfurt (b).
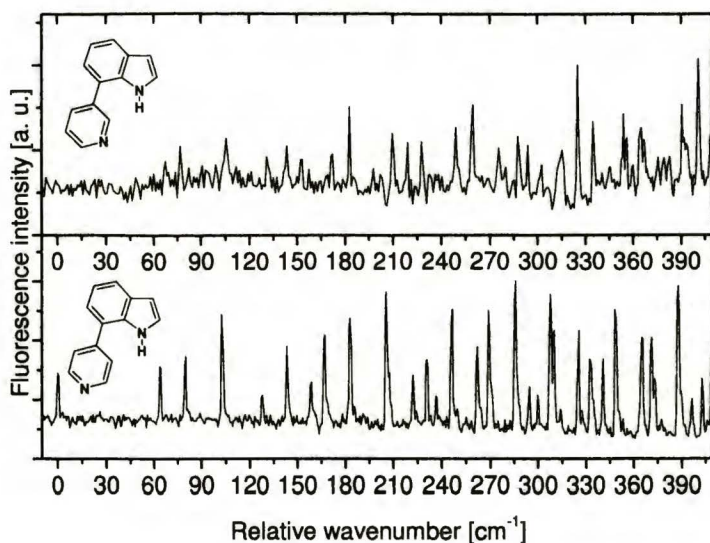
Figure IV.47. Comparison of the fluorescence excitation spectra of **2** and **3** in the vicinity of the $S_1 \leftarrow S_0$ transition. The relative energy shifts are presented with respect to the 0-0 transitions (in cm^{-1}).

At the present stage of study one can conclude that, most probably, the dominant isomer stabilized in the supersonic jet conditions is the *syn* form. The very weak $S_0 \rightarrow S_1$ electronic origin of **2** detected at 32426 cm^{-1} and long progressions may be treated as evidence of geometry changes upon excitation along the torsion coordinate. The most prominent vibronic transitions observed in the range of 0- 400 cm^{-1} are listed in Table IV.14. Similarly as for **3**, the spectrum is dominated by three low frequency vibrations. The longest progression is observed for $0_0^0 + 76.9$ cm^{-1} transition. The TDDFT calculations of S_1 frequencies show that these three modes may be described mainly as motions changing the torsional angle between the pyridyl and indole rings/are composed of significant torsional character.

Table IV.14. Transition energies, intensities and initial assignments of the bands in the LIF excitation spectrum of **2** relative to $S_0 \rightarrow S_1$ origin at 32426 cm^{-1}.

Δv [cm^{-1}]	Relative intensity	Assignment	Δv [cm^{-1}]	Relative intensity	Assignment
0 (32426)	vw	0-0	287	m	B^1C^2, A^2B^2, B^1D^1
67.4 (65.9)[a]	w	A^1	294	m	A^1B^3
76.9 (76.1)[a]	w	B^1	302	m	F^1
105.4 (99.9)[a]	w	C^1	315.2	m	C^3
130.9	w	A^2	324.8	s	$A^1B^2C^1$, E^1B^1
143.6	w	A^1B^1	335.6	m	
153.1	w	B^2	353.8	m	
172	w	A^1C^1	356.3	m	
182	s	B^1C^1	365.0	m	B^2D^1
210.5	m	C^2, D^1	366.5	m	
219.0	m	A^1B^2	375.3	m	
227.6	m	B^3,	378.3	m	B^1F^1
250.0	s	$A^1B^1C^1$, E^1	382.2	s	
259.6	s	B^2C^1	392.0	s	
275.6	m	A^1C^2	401.0	m	B^2E^1

[a] TDDFT/TZVP calculations, frequencies scaled by 0.956.

IV.5.3a. Size-selected hydrogen-bonded clusters

In order to obtain hydrogen-bonded solute-solvent complexes in a supersonic jet, vapor of the protic solvent was added to the expanding mixture of an inert carrier gas (helium) and the solute. The partial pressure of the solvents was controlled by temperature. Laser-induced resonant two-photon ionization spectroscopy (R2PI) was used to select a particular cluster size from the beam. The size and composition of an ionized cluster was determined via its mass in a time of flight mass spectrometer (TOF).

The presence of **2**:water complexes was manifested by very broad bands with the maximum at about 31700 cm^{-1} (1:1) and 30700 cm^{-1} (1:2) in the R2PI spectra. The complexes exhibit a red-shift with respect to the 0-0 transition of the monomer and the absence of distinct vibrational structure in their absorption spectra (Figure IV.48). This behavior may have multiple origins, such as the occurrence of many ground-state complexes with different geometries, as well as the short lifetime of the excited Franck-Condon state, due to a rapid deactivation processes.
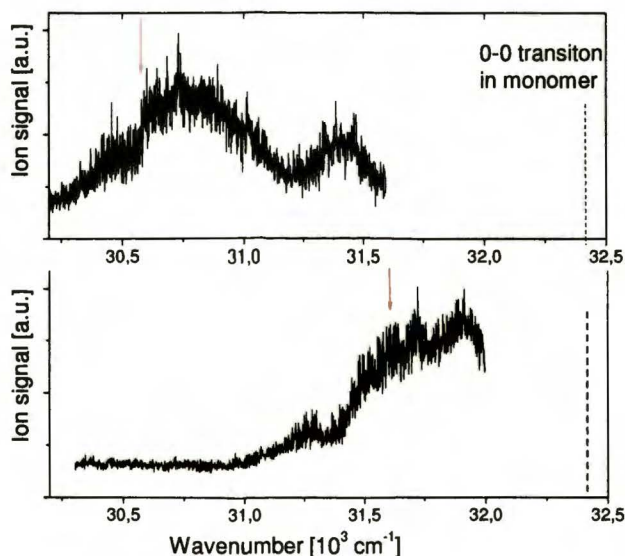
Figure IV.48. One color R2PI spectrum of the **2**:H_2O complexes (bottom) and **2**·2H_2O complexes (top). The arrows indicate the wavelength of the UV laser chosen for excitation in IR/R2PI experiments.

However, using these spectra and the corresponding time-of-flight mass selected spectra, which show the ion size distribution allowed to find

115

proper conditions for IR/R2PI investigation of the structure of **2**:(water)$_n$ complexes where n = 1, 2. The IR/R2PI spectrum of the monomer (Figure IV.49) was recorded upon selective excitation at the vibronic transition located 153 cm^{-1} above the origin. This spectrum possesses a single strong transition at 3513 cm^{-1} due to the N–H stretch fundamental which serves as a reference for the **2**:water cluster IR transitions.

Figure IV.49 displays the IR dip spectrum of **2**:H_2O measured by fixing the ionising laser at 31595 cm^{-1} (Figure IV.48), where the TOF spectra showed a large contribution from 1:1 structures (the fragmentation effect was also taken into account). This spectrum shows four dips at 3722, 3555, 3436, and 3398 cm^{-1}, which reveals that different types of 1:1 complexes are present. The assignment can be made on the basis of DFT calculations and the experimental data for similar H-bonded systems. The comparison of B3LYP/6-311+G(d,p) computed spectral positions of the vibrational bands of possible **2**:H_2O complexes suggests that the spectrum is dominated by vibrations involved in a cyclic structure formed by the *syn* rotamer of **2** (*syn*H_2O), predicted as the most stable one (Table IV.15 and Figure IV.50)
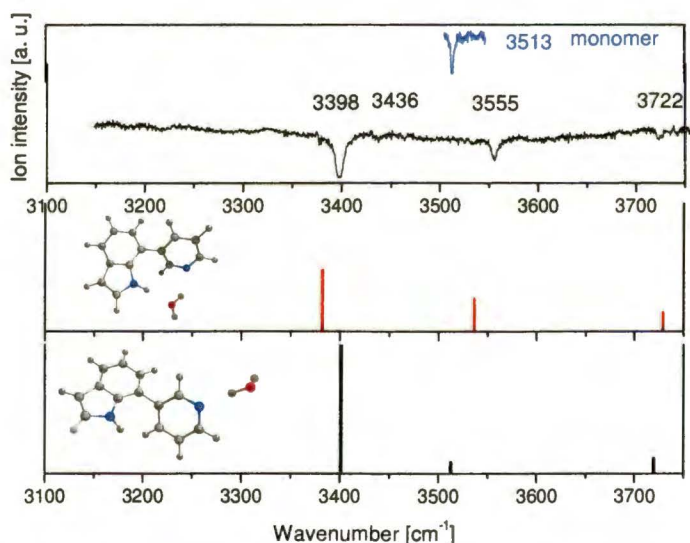
Figure IV.49. IR/R2PI spectra of the monomer of **2** (top), and of the 1:1 water complexes of **2** (bottom). The vertical lines correspond to the calculated spectral positions in two lowest energy complexes of **2**; the frequencies are scaled by a factor of 0.958, obtained as a ratio of the observed to the calculated frequency of the NH stretching in the monomer; this factor is similar to those typically used.[217]

The highest frequency band observed at 3722 cm^{-1} is assigned to the free OH stretching vibration of water. This mode is red-shifted by 34 cm^{-1} with respect to the antisymmetric stretch of free water (v_{as} = 3756 cm^{-1}).[218] The red shift of free water OH stretch frequency to about 3772 cm^{-1} seems to be typical for clusters in which the water molecule is attached to the pyridine atom or when water is involved in a cyclic complex.[219-223] The dip observed at 3555 cm^{-1} may be related to the symmetric stretch vibration of water hydrogen-bonded to the pyridine nitrogen. The energy of this vibration is red-shifted by 102 cm^{-1} with respect to the symmetric stretch of free water (v_s = 3657 cm^{-1}). This shift is rather small in comparison with that observed for the cyclic structure of the jet-cooled isolated 1:1 complexes of 7-azaindole (282 cm^{-1}),[219] 2-aminopyridine (254 cm^{-1})[221] and 2-hydroxypyridine (283 cm^{-1})[223] with water. It suggests that the geometry of the hydrogen bonds in **2** makes them weaker with respect to these complexes.

Table IV.15. Binding energies (in kcal mol^{-1}) of the ground state **2** complexes with water, calculated at B3LYP/6-31G(d,p) level[a]

1:1 water complexes of **2**

	*syn*H$_2$O	*anti*H$_2$Oa	*anti*H$_2$Od
ΔE^N	-13.16	-11.26	-11.49
ΔE^B	-12.17	-10.18	-10.94
ΔE^C	**-10.06**	**-7.57**	**-8.16**

[a]ΔE^N and ΔE^B represent the binding energies without and with BSSE correction, respectively. ΔE^C *is* the ZPVE-corrected ΔE^B

Figure IV.50. The two lowest energy B3LYP/6-311+G(d,p) optimized structures of the H-bonded complexes between **2** and one water molecule.

The most intense vibration at 3398 cm^{-1} belongs to the hydrogen-bonded NH stretch fundamental, red-shifted by 115 cm^{-1} with respect to this vibration in the monomer. Similar NH frequency shifts were observed in cyclic complexes of azaindole and carbazole. Another band located at 3436 cm^{-1} may be treated as a manifestation of the existence of clusters formed by the *anti* form of **2**, with water attached to the pyridine nitrogen. The calculations predict that the binding energy for this structure is lower by 1.9 kcal/mol in respect to the *syn* complex. (Table IV.15). The calculated vibrational transitions imply that observed dip most probably belongs to the hydrogen-bonded OH stretch; a weak intensity of the calculated transition may explain the lack of the trace of free NH stretch. The computational prediction for another possible (*anti*H$_2$Oa) complex, the *anti* form with the water molecule hydrogen-bonded to the NH group, suggests that such a structure should be less strongly bonded (by 2.5 kcal/mol) in comparison with the most stable cluster. The IR/R2PI spectrum does not reveal the presence of such type of complexes under experimental conditions.

To measure the IR absorption spectra of 1:2 water complexes of **2** the UV source, which creates a constant ion signal, was fixed to 30667 cm^{-1} (Figure IV.48). Such excitation energy was chosen in order to maximize the ion signal for the depletion experiment. The IR spectrum of 2:2H$_2$O (Figure IV.51) exhibits seven main features. Similarly as for 1:1 complexes, using the literature data base and DFT calculations one can try to deduce the geometry or at least the number of different types of complexes observed under such conditions. However, it should be stressed that in the case of 1:2 complexes the measurements, repeated several times, have shown that the relative intensity of the depleted ion signal shoud be treated with caution. The dip at 3717 cm^{-1} may be attributed to the antisymmetric stretching vibration in free water. A weak, lowest frequency band (3070 cm^{-1}) is most

probably related to C–H stretch fundamentals. Among the rest of the observed transitions located at 3160 cm^{-1}, 3238 cm^{-1}, 3325 cm^{-1}, 3365 cm^{-1}, 3420 cm^{-1} one can look for the hydrogen-bonded N-H indole stretching mode and the OH stretching of water involved in different types of hydrogen bonds. On the basis of experimental data for similar hydrogen-bonded systems (2-(2'-pyridyl)pyrrole, 1H-pyrroloquinoline[162]) and the results obtained for 1:1 complexes, one could claim that such pattern of dips may indicate the presence of cyclic 1:2 complexes in which the NH stretching vibration burns at 3238 cm^{-1}, and the dips at 3160 and 3325 cm^{-1} may be attributed to the OH stretch vibrations engaged in the hydrogen bond to pyridine, and in the water bridge, respectively. The calculated IR spectra of the *syn*2H$_2$O complex, where the two water molecules form a bridge between the indole and the pyridine ring, predicts three intense bands in the NH and OH stretch regions, attributed to the hydrogen bonded NH stretch (3303 cm^{-1}), and the OH stretch fundamentals: one involved in the hydrogen bond with the pyridine nitrogen (3193 cm^{-1}) and the other in the water dimer (3368 cm^{-1}). A comparison between the calculated and observed frequencies is given in Figure IV.51. The match-up between experiment and calculation seems to be sufficiently good to confirm our assignment of 2:2H$_2$O complex as *syn*2H$_2$O.
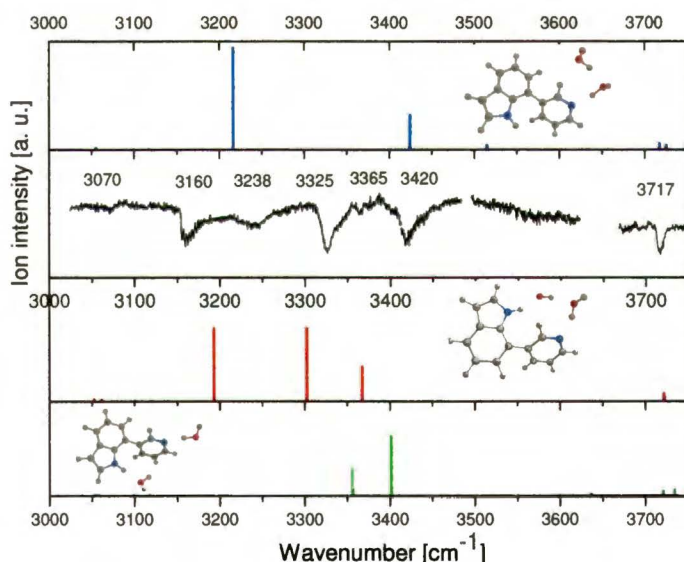
Figure IV.51. IR/R2PI spectra of 1:2 water complexes of **2**. The vertical lines correspond to the spectral positions in the spectra calculated for diferent complexes of **2**; scaling factor is 0.958.

However, the spectrum reveals additional dips which should be treated as a sign of other type of complexes. Table IV.16 presents the binding energies for a few of the most probable structures of 1:2 water complexes of **2**. Interestingly, the calculations suggest that when the dimer of water is attached to the NH indole group of the *anti* rotamer of **2** the structure becomes cyclic and very similar to the *syn*2H$_2$O (Figure IV.52). The calculated vibrational transitions for the presented clusters and the comparison with experimental results show that one cannot definitively exclude the presence of any of them. It should be stressed that the observed dips are broad and one cannot exclude that in some cases two close-lying transitions overlap and are unjustly treated as a single vibration. Keeping this in mind, the band at 3238 cm^{-1}, although attributed to *syn*2H$_2$O, may be interpreted also as a sign of the *anti*(H2O)$_2$d complex. Similarly, a deep dip burnt at 3420 cm^{-1} may come from at least two different geometries of 1:2 complexes. The origin of this band may be (i) the OH stretch of water being a hydrogen bond donor in the complex consisting of the *anti* rotamer and two water molecules independently attached, one to the NH group and the other to the pyridine nitrogen (*anti*2H$_2$O), or (ii) the symmetric OH stretch in the water dimer attached to the pyridine nitrogen atom (*anti*(H2O)$_2$d).

syn2H$_2$O

anti(H$_2$O)$_2$d

anti2H$_2$O
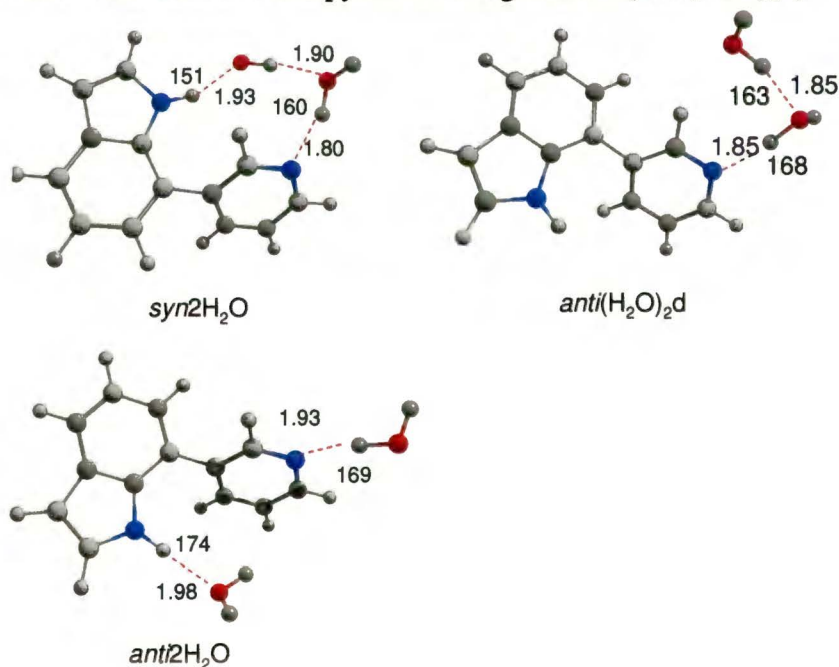
Figure IV.52. The B3LYP/6-311+G(d,p) optimized structures of the H-bonded complexes between **2** and two water molecules.

Table IV.16. Binding energies (in kcal mol^{-1}) of the ground state of 1:2 water complexes of **2**, calculated at the B3LYP/6-31G(d,p) level[a]

1:2 water complexes of **2**

	syn2H$_2$O	anti2H$_2$O	anti(H$_2$O)$_2$d
ΔE^N	-26.67	-18.23	-20.68
ΔE^B	-24.31	-16.60	-18.94
ΔE^C	**-19.58**	**-13.34**	**-14.84**

[a] ΔE^N and ΔE^B represent the binding energies without and with BSSE correction, respectively. ΔE^C is the ZPVE-corrected ΔE^B

In summary, an unequivocal description of the IR/R2PI spectrum of 1:2 complexes is not trivial. However, there is no doubt that at least two types of complexes with 1:2 stoichiometry are present under experimental conditions. Moreover, the most plausible assignment (*syn*2H$_2$O) seems reliable, not only due to the agreement between experimentally observed and computed IR transition frequencies, but also because it corresponds to the structure with the lowest calculated energy. The observed and B3LYP/6-311+G(d,p) calculated vibrational frequency shifts of the OH and NH stretching modes in complexes of **2** with respect to those of the free solvent molecules are summarized in Table IV.17.

The jet experiments are in progress and a clear explanation of problems related to *syn–anti* rotamerisation needs additional investigations combined with theoretical studies of the ground and excited states of **2**.

IV.5.4. Summary

The presented results have shown that 7-(3'-pyridyl)indole can exist in two rotameric forms. The specific and nonspecific interactions with the solvent may preferentially stabilize one of them. The studies of solvation effects on jet-cooled **2** revealed that under experimental conditions the cyclic complexes of the *syn* rotamer are preferentially formed. This observation may explain the most effective quenching of fluorescence of **2** in comparison with other members of the series of 7-pyridylindoles studied

in protic solvents. The communication between the hydrogen bond centers seems to be the clue for fast deactivation processes. The cyclic complexes are efficiently deactivated in S_1, via internal conversion. These rapid deactivation channels are not available in the *anti* rotamer of **2** and in **3**, which cannot form cyclic 1:1 complexes. Similar effects were recently observed for 2-(2'- pyridyl)indole.[108] In the case of molecules which reveal strong fluorescence quenching in alcohols and simultaneously do not exhibit dual emission the "unsuccessful chemical reaction mechanism"[107] for rapid deactivation in cyclic 1:1 complexes can be postulated. According to this mechanism, cooperative movement of protons occurs in the excited chromophore; however, before achieving the tautomeric form, the conical intersection between the S_1 and S_0 potential energy surfaces is encountered, which brings the excited system back into the ground state.

Table IV.17. Comparison of the observed and B3LYP/6-311+G(d,p) calculated vibrational frequencies of the OH and NH stretching modes in the complexes **2**:water.

species	freq calc [cm^{-1}]	freq exp [cm^{-1}]	Δv^a [cm^{-1}]	mode description^b
2		3513		NH
1:1 stoichiometry				
*syn*H$_2$O	3382	3398	105	NH…O
	3537	3555	115	HO…N ss
	3729	3722	34	HO as free
*anti*H$_2$Od	3513			NH
	3402	3436	221	OH…N ss
	3720			OH as free
*anti*H$_2$Oa	3358			NH…O
	3626			OH ss free
	3732			OH as free
1:2 stoichiometry				
*syn*2H$_2$O	3193	3160	419	OH…N ss
	3302	3238	353	NH…O
	3368	3325	332	OH…O ss
	3723	3717	39	OH as free (asym in water dimer)
	3722			OH as free (sym in water dimer)
anti(H$_2$O)$_2$d	3216			OH…N ss
	3424			OH…OH ss
	3515			NH
	3718			OH as free in water HB to pyridine
	3726			OH as free
*anti*2H$_2$O	3357	3365^c		NH…O
	3401	3420^c		OH…N
	3637			OH ss free (water as acceptor)
	3722			OH as free (water as donor)
	3735			OH as free (water as acceptor)

$^{a)}$ For experimental values the wavenumber shifts with respect to monomer of **2** or free water molecule was given; $^{b)}$ ss, as -symmetric and antysymmetric stretch, respectively; $^{c)}$ tentative assignment

123

CHAPTER V. Summary and outlook

Ground and excited state processes induced by hydrogen bond formation have been studied and discussed for heteroazaaromatic compounds which possess both a proton donor (the NH group) and an acceptor (pyridine-type nitrogen). The results revealed extremely rich photophysics, dependent both on the solvent properties (viscosity, polarity and ability to form hydrogen bonds with the solute) and on the position of the donor and acceptor relative to each other.

V.1. Main conclusions

In this work, the focus was on (i) ground and excited state structure of isolated and complexed chromophores; (ii) the phenomena related to the excited state deactivation. The photophysical studies of three isomeric 7-(pyridyl)indoles allowed to describe the influence of intra- and intermolecular hydrogen bonding on excited state depopulation processes, as well as the relations between geometrical structure and excited state properties. The main results and conclusions obtained during the research presented in this work are listed below.

ESIPT with a twist

The *syn* form of 7-(2-pyridyl)indole (**1**) undergoes ultrafast excited state proton transfer along the intramolecular hydrogen bond (ESIPT). This process proceeds in a barrierless fashion and is coupled with mutual twisting of the pyridine and indole moieties. It results in an unusual finding that the reaction is slower in a condensed phase at room temperature than in the supersonic jet-isolated molecule (1 ps vs. about 300 fs). In solution, the solvent molecules hinder torsion, thus slowing down the reaction. The phototautomer is efficiently deactivated by a radiationless channel which may be defined in terms of S_1/S_0 conical intersection along the proton transfer/twisting coordinate.

2,9-(di-2'-pyridyl)-4,7-di(*t*-butyl)carbazole (**4**), contrary to the structurally related **1**, exhibits dual fluorescence in nonpolar and polar, protic and aprotic solvents. These results are interpreted as a manifestation of intramolecular excited state tautomerization along the pre-existing hydrogen bond, which occurs on a time scale of 5-10 ps. The measurements

of fluorescence temperature dependence have shown that in condensed phase **4** appears to have a small barrier to tautomerization and revealed the importance of tunneling, confirmed also by the isotope effect, large and more pronounced at lower temperatures. The product of this reaction undergoes very fast radiationless deactivation. However, in **4**, the photoreaction is sufficiently slow to allow the distinction between two consecutive steps: after excitation, an ESIPT take place, followed by the twisting about the bond linking the pyridyl and carbazole rings. This torsional motion seems to be responsible for the deactivation of the phototautomerization product. Because of an ultrafast rate of deactivation, such separation of the sequence: proton transfer - twisting was impossible in the case of **1**.

Syn-anti rotamerization induced by solvent

The phenomenon of solvent-induced *syn-anti* rotamerization has been observed for two molecules. 7-(2'-pyridyl)indole (**1**) and 7-(3'-pyridyl)indole (**2**) have been found to exist in different rotameric forms, depending on the solvent. In polar, both protic and aprotic media, *syn* and *anti* species are detected, whereas in nonpolar solvents the *syn* structure definitively dominates. Two rotamers could be distinguished owing to their different excited state deactivation patterns.

Structure of hydrogen-bonded complexes

The studied molecules possess two sites which may act as hydrogen bond centers and, as a consequence, in bulk alcohols they are able to form a wide range of hydrogen-bonded structures. The supersonic jet experiments revealed that **2** tends to form cyclic structures even with one molecule of water, which seemed at first to be a bit surprising. However, this finding was verified by comparing the IR/R2PI experimental data with DFT calculations. Besides the 1:1 complex, also a 1:2 cyclic species has been identified. These studies point to the tendency of **2** to form the hydrogen bonds with geometric parameters deviating from those characteristic for a typical hydrogen bond.

Cyclic intermolecular hydrogen bonds as the origin of effective nonradiative channel.

The photophysical behavior of **2** and 7-(4'-pyridyl)indole (**3**) clearly proves that the deactivation processes of their excited states are governed by specific and nonspecific interaction with the solvent. The fluorescence of both compounds is strongly quenched in alcohols, due to the appearance of an efficient nonradiative channel, most probably connected with internal conversion in intermolecularly hydrogen-bonded complexes. The rate and efficiency of this process is influenced by temperature or solvent properties, such as viscosity, and becomes negligible in low temperature rigid alcohol glasses. The comparison of results obtained for **2** and **3** shows that internal conversion is more efficient in cyclic solvates, with alcohol molecules forming a bridge between the proton donor and the acceptor groups of an excited chromophore. Only the *syn* form of **2** is able to form such types of 1:1 complexes. It is known that in cyclic, 1:1 doubly hydrogen-bonded complexes another channel of deactivation is possible, namely a solvent-assisted excited state double proton transfer. However, this process could not be detected in complexes of **2**. The origin of enhanced S_1-S_0 internal conversion, being the major channel of excited state depopulation in protic solvents, may be tentatively attributed to "aborted double proton transfer",[107] most probably involving complexes of 1:2 stoichiometry.

Excited state twisting or flattening?

Another interesting result of this work is the observation of tendency of all studied molecules to undergo conformational changes in the excited states. The difference in radiative rates observed between *n*-hexane and polar solvents shows that in the latter, a molecule, after excitation, becomes more twisted than in the ground state. Additionally, the supersonic jet experiments performed for **2** and **3** suggest a different geometry along the torsional coordinate in S_0 and S_1 states. On the other hand the, calculations for the isolated molecules predict more flat geometry in S_1. Given that, it is especially interesting to perform detailed investigations concerning the structural changes following S_0-S_1 excitation. The analysis and assignment of torsional progressions observed in LIF and SVLF spectra (supported by calculations) and fitting these data to a one-dimensional potential of the form $V(\Theta) = (1/2)\Sigma_n V_n(1 - \cos n\Theta)$ will allow reconstructing the ground and excited state potential surfaces.

126

V.2. Open questions and perspectives

Besides the unfinished problem of quantitative characterization of conformational changes in the excited state, this thesis leaves open other questions, and generates new ones, which could not have been answered in the present work and which might be a subject of future research.

The problem of *syn-anti* rotamerization of the monomer of **2** under supersonic jet condition was not definitively explained. Although no effort has been spared to clarify this issue, the previously performed experiments repeated with better signal to noise ratio, supported by additional experiments, such as single vibronic level fluorescence (SVLF), may help solving the question about the coexistence of rotamers.

Futher studies are planned to explore the mechanism of fluorescence quenching in protic solvents. In order to prove the crucial role of cyclic structures in efficient deactivation, experiments involving complexes with various protic solvents for **2** and **3** should be designed. This would enable identification of their stoichiometry and structure by IR/R2PI, IR/LIF techniques, combined with calculations. As far as the presence of cyclic complexes of **2**-*syn* could have been expected, the computational prediction of such complexes in the case of **3** seems somewhat surprising, and further investigations in supersonic jets are needed to address this problem. The studies on the role of protic solvents will be supported by molecular dynamics simulations.

To check whether **4** behaves in a similar way to **1** in a supersonic jet, in particular whether the rate of phototautomerization is larger than in condensed phases, femtosecond multiphoton ionization (fsMPI), and femtosecond pump-probe photoionization measurements are planned.

Finally, it should be mentioned that the photophysical properties of the investigated chromophores, especially those of **1,** suggest that they can be considered as possible photostabilizers. For **1** and **4**, the time scale of the excitation-proton transfer-deactivation-back proton transfer cycle is similar, or even shorter than in well-known proton-transferring polymer-stabilizing systems, such as Tinuvin[69] or 2,2'-bipyridyl-3,3'-diol.[224]

REFERENCES

(1)   Cleland, W. W. *Low barrier hydrogen bonds and low fractionation factor bases in enzymatic reactions* Biochemistry **1992**, *31*, 317-319.

(2)   Cleland, W. W.; Frey, P. A.; Gerlt, J. A. *The low barrier hydrogen bond in enzymatic catalysis* J. Biol. Chem. **1998**, *273*, 25529-25532.

(3)   Weiss, M. S.; Brandl, M.; Suhnel, J.; Pal, D.; Hilgenfeld, R. *More hydrogen bonds for the (structural) biologist* Trends Biochem. Sci. **2001**, *26*, 521-523.

(4)   Steiner, T.; Koellner, G. *Hydrogen bonds with π–acceptors in proteins: frequencies and role in stabilizing local 3D structure* J. Mol. Biol. **2001**, *305*, 535-557.

(5)   *The hydrogen bond. Recent developments in theory and experiments*; Schuster, P.; Zundel, G.; Sandorfy, C., Eds.; North-Holland Publishing Company-Amsterdam: New York, **1976**.

(6)   Arnaut, L. G.; Formosinho, S. J. *Excited-state proton transfer reactions I. Fundamentals and intermolecular reactions* J. Photochem. Photobiol., A **1993**, *75*, 1-20.

(7)   Formosinho, S. J.; Arnaut, L. G. *Excited-state proton transfer reactions II. Intramolecular reactions* J. Photochem. Photobiol., A **1993**, *75*, 21-48.

(8)   Rehm, D.; Weller, A. *Kinetics of fluorescence quenching by electron and H-atom transfer* Isr. J. Chem. **1970**, *8*, 259-271.

(9)   Chou, P. T.; Martinez, M. L.; Clements, J. H. *Reversal of excitation behavior of proton-transfer vs. charge-transfer by dielectric perturbation of electronic manifolds* J. Phys. Chem. **1993**, *97*, 2618-2622.

(10)   Douhal, A.; Kim, S. K.; Zewail, A. H. *Femtosecond molecular dynamics of tautomerization in model base pairs* Nature **1995**, *378*, 260-263.

(11)   Ormson, S. M.; Brown, R. G. *Excited state intramolecular proton transfer. Part 1: ESIPT to nitrogen* Prog. React. Kinet. Mech. **1994**, *19*, 45-91.

(12)   Chou, P. T. *The host/guest type of excited-state proton transfer; A general review* J. Chin. Chem. Soc. **2001**, *48*, 651-682.

(13)   Waluk, J. *Proton and electron transfer in hydrogen-bonded systems* J. Mol. Liq. **1995**, *64*, 49-56.

References

(14)   Waluk, J. *Hydrogen-bonding-induced phenomena in bifunctional heteroazaaromatics* Acc. Chem. Res. **2003**, *36*, 832-838.

(15)   Raczyńska, E. D.; Kosińska, W.; Ośmiałowski, B.; Gawinecki, R. *Tautomeric equilibria in relation to pi-electron delocalization* Chem. Rev. **2005**, *105*, 3561-3612.

(16)   Jeffrey, G. A. *An introduction to hydrogen bonding.*, Oxford University Press: New York, **1997**.

(17)   Huppert, D.; Gutman, M.; Kaufmann, K. J. *Laser Studies of Proton Transfer* in *Adv. Chem. Phys.*; Jortner, J., Levine, R. D., Rice, S. A., Eds., **1981**; Vol. 47.

(18)   Ireland, J. F.; Wyatt, P. A. H. *Acid-base properties of electronically excited states of organic molecules* Adv. Phys. Org. Chem. **1976**, *12*, 131-221.

(19)   Bardez, E. *Excited-state proton transfer in bifunctional compounds* Isr. J. Chem. **1999**, *39*, 319-332.

(20)   Weller, A. *Fast reactions of excited molecules* Prog. React. Kinet. **1961**, *1*, 188-214.

(21)   Lim, E. C. *Proximity effect in molecular photophysics: dynamical consequences of pseudo- Jahn-Teller interactlon* J. Phys. Chem. **1986**, *90*, 6770-6777.

(22)   Mataga, N.; Kaibe, Y.; Koizumi, M. *Equilibrium of hydrogen-bond formation in the excited state* Nature **1955**, *175*, 731.

(23)   Agmon, N. *Elementary steps in excited-state proton transfer* J. Phys. Chem. A **2005**, *109*, 13-35.

(24)   Waluk, J. *Conformational aspect of intra- and intermolecular excited-state proton transfer* in *Conformational analysis of molecules in excited states*; Waluk, J., Ed.; Wiley-Vch: New York, **2000**.

(25)   *The IUPAC Compendium of Chemical Terminology (Gold Book).* **2006**; http://goldbook.iupac.org/about.html.

(26)   *Hydrogen-Transfer Reactions* Hynes, J. T.; Klinman, J. P.; Limbach, H. H.; Schowen, R. L., Eds.; Wiley-Vch: Weinheim, **2007**; Vol. 1.

(27)   Weller, A. *Quantitative Untersuchungen der Fluoreszenzumwandlung bei Naphtholen* Z. Elektrochem. **1952**, *56*, 662-668.

(28)   *Ultrafast hydrogen bonding dynamics and proton transfer processes in the condensed phase*; Elsaesser, T.; Bakker, H. J., Eds.; Kluwer Academic Publishers: Dordrecht, **2002**; Vol. 23.

(29)   Kasha, M. *Proton-transfer spectroscopy. Perturbation of the tautomerization potential* J. Chem. Soc., Faraday Trans. 2 **1986**, *82*, 2379 - 2392.

References

(30) Chudoba, C.; Lutgen, S.; Jentzsch, T.; Riedle, E.; Woerner, M.; Elsaesser, T. *Femtosecond studies of vibrationally hot molecules produced by intramolecular proton transfer in the excited state* Chem. Phys. Lett. **1995**, *240*, 35-41.

(31) Kijak, M.; Nosenko, Y.; Singh, A.; Thummel, R. P.; Waluk, J. *Mode-selective excited-state proton transfer in 2-(2'-pyridyl)pyrrole isolated in a supersonic jet* J. Am. Chem. Soc. **2007**, *129*, 2738-2739.

(32) O'Connor, D. B.; Scott, G. W.; Coulter, D. R.; Yavrouian, A. *Temperature dependence of electronic energy transfer and quenching in copolymer films of styrene and 2-(2'-hydroxy-5'-vinylphenyl)-2H-benzotriazole* J. Phys. Chem. **1991**, *95*, 10252-10261.

(33) Crawford, J. C. *2(2-Hydroxyphenyl)2H-benzotriazole ultraviolet stabilizers* Progr. Polymer Sci. **1999**, *24*, 7-43.

(34) O'Connor, D. B.; Scott, G. W.; Coulter, D. R.; Gupta, A.; Webb, S. P.; Yeh, S. W.; Clark, J. H. *Direct observation of the excited-state proton transfer and decay kinetics of internally hydrogen-bonded photostabilizers in copolymer films* Chem. Phys. Lett. **1985**, *121*, 417-422.

(35) Otterstedt, J.-E. A. *Photostability and molecular structure* J. Chem. Phys. **1973**, *58*, 5716-5725.

(36) Weller, A. *Intermolekularer protonenübergang in angeregten zustand* Z. Elektrochem. **1956**, *60*, 1144-1147.

(37) Marsh, J. K. *XLIX.—Studies in fluorescence spectra. Part II. Phenol and phenolic ether vapours* J. Chem. Soc., Trans. **1924**, *125*, 418-423.

(38) Acuña, A. U.; Catalán, J.; Toribio, F. *Photon energy relaxation and thermal effects on gas-phase electronically excited methyl salicylate* J. Phys. Chem. **1981**, *85*, 241-245.

(39) Bisht, P. B.; Petek, H.; Yoshihara, K.; Nagashima, U. *Excited state enol-keto tautomerization in salicylic acid: A supersonic free jet study* J. Chem. Phys. **1995**, *103*, 5290-5307.

(40) Heimbrook, L.; Kenny, J. E.; Kohler, B. E.; Scott, G. W. *Lowest excited singlet state of hydrogen-bonded methyl salicylate* J. Phys. Chem. **1983**, *87*, 280-289.

(41) Nishiya, T.; Yamauchi, S.; Hirota, N.; Baba, M.; Hanazaki, I. *Fluorescence studies of intramolecularly hydrogen-bonded o-hydroxyacetophenone, salicylamide, and related molecules* J. Phys. Chem. **1986**, *90*, 5730-5735.

References

(42) Herek, J. L.; Pedersen, S.; Banares, L.; Zewail, A. H. *Femtosecond real-time probing of reactions. IX. Hydrogen-atom transfer* J. Chem. Phys. **1992**, *97*, 9046-9061.

(43) Felker, P. M.; Lambert, W. R.; Zewail, A. H. *Picosecond excitation of jet-cooled hydrogen-bonded systems: Dispersed fluorescence and time-resolved studies of methyl salicylate* J. Chem. Phys. **1982**, *77*, 1603-1605.

(44) Douhal, A.; Lahmani, F.; Zewail, A. H. *Proton-transfer reaction dynamics* Chem. Phys. **1996**, *207*, 477-498.

(45) Lahmani, F.; Zehnacker-Rentien, A. *Effect of substitution on the photoinduced intramolecular proton transfer in salicylic acid* J. Phys. Chem. A **1997**, *101*, 6141-6147.

(46) Lahmani, F.; Zehnacker-Rentien, A. *Spectroscopic study of jet-cooled heterodimers of salicylic acid with acetic and trifluoroacetic acids* Chem. Phys. Lett. **1997**, *271*, 6-14.

(47) Goodman, J.; Brus, L. E. *Proton transfer and tautomerism in an excited state of methyl salicylate* J. Am. Chem. Soc. **1978**, *100*, 7472-7474.

(48) Acuña, A. U.; Toribio, F.; Amat-Guerri, F.; Catalán, J. *Excited state proton transfer: A new feature in the fluorescence of methyl 5-chlorosalicylate and methyl 5-methoxysalicylate* J. Photochem. **1985**, *30*, 339-352.

(49) Catalán, J.; Toribio, F.; Acuña, A. U. *Intramolecular hydrogen bonding and fluorescence of salicylaldehyde, salicylamide, and o-hydroxyacetophenone in gas and condensed phase* J. Phys. Chem. **1982**, *86*, 303-306.

(50) Toribio, F.; Catalán, J.; Amat, F.; Acuña, A. U. *Electronically induced proton-transfer reactions in salicylic acid esters and salicyloyl chloride* J. Phys. Chem. **1983**, *87*, 817-822.

(51) Klopffer, W.; Naundorf, G. *On the fluorescence of methyl salicylate in hydrogen bonding solvents* J. Lumin. **1974**, *8*, 457-461.

(52) Klopffer, W.; Kaufmann, G. *Absorption and fluorescence spectra of methyl salicylate in the vapor phase* J. Lumin. **1979**, *20*, 283-289.

(53) Orton, E.; Morgan, M. A.; Pimentel, G. C. *Photorotamerization of methyl salicylate and related compounds in cryogenic matrixes* J. Phys. Chem. **1990**, *94*, 7936-7943.

(54) Morgan, M. A.; Orton, E.; Pimentel, G. C. *Characterization of ground and electronically excited states of o-hydroxybenzaldehyde and its non-hydrogen-bonded photorotamer in 12 K rare gas matrixes* J. Phys. Chem. **1990**, *94*, 7927-7935.

131

(55)   Gebicki, J.; Krantz, A. *Photochemical behaviour of matrix-isolated salicylaldehyde and its derivatives. Trapping of a non-hydrogen-bonded conformer* J. Chem. Soc., Faraday Trans. 2 **1984**, 1617-1621.

(56)   Pant, D. D.; Joshi, H. C.; Bisht, P. B.; Tripathi, H. B. *Dual emission and double proton transfer in salicylic acid* Chem. Phys. **1994**, *185*, 137-144.

(57)   Lopez-Delgado, R.; Lazare, S. *Fluorescence properties of methyl salicylate in vapor, liquid, and solution* J. Phys. Chem. **1981**, *85*, 763-768.

(58)   Sandros, K. *Hydrogen bonding effects on the fluorescence of methyl salicylate* Acta Chem. Scand. **1976**, *30*, 761-736.

(59)   Heimbrook, L. A.; Kenny, J. E.; Kohler, B. E.; Scott, G. W. *Dual fluorescence excitation spectra of methyl salicylate in a free jet* J. Chem. Phys. **1981**, *75*, 5201-5203.

(60)   Acuña, A. U.; Amat-Guerri, F.; Catalán, J.; Gonzalez-Tablas, F. *Dual fluorescence and ground state equilibriums in methyl salicylate, methyl 3-chlorosalicylate, and methyl 3-tert-butylsalicylate* J. Phys. Chem. **1980**, *84*, 629-631.

(61)   Kuper, J. W.; Perry, D. S. *Spectroscopy and intramolecular relaxation of methyl salicylate in its first excited singlet state* J. Chem. Phys. **1984**, *80*, 4640-4645.

(62)   Sanchez-Cabezudo, M.; De Paz, J. L. G.; Catalán, J.; Amat-Guerri, F. *Photoinduced intramolecular proton transfer in methyl salicylates: a theoretical study with spectroscopic support* J. Mol. Struct. **1985**, *131*, 277-289.

(63)   Orttung, W. H.; Scott, G. W.; Vosooghi, D. *Investigation of ground and excited state properties of internally hydrogen-bonded aromatic carbonyls using molecular orbital methods* J. Mol. Struct. **1984**, *109*, 161-176.

(64)   Nagaoka, S.-i.; Nagashima, U. *Intramolecular proton transfer in various electronic states of o-hydroxybenzaldehyde* Chem. Phys. **1989**, *136*, 153-163.

(65)   Nagaoka, S.; Nagashima, U.; Ohta, N.; Fujita, M.; Takemura, T. *Electronic-state dependence of intramolecular proton transfer of o-hydroxybenzaldehyde* J. Phys. Chem. **1988**, *92*, 166-171.

(66)   Nagaoka, S.; Nagashima, U. *Effects of nodal plane of wave function upon photochemical reactions of organic molecules* J. Phys. Chem. **1990**, *94*, 1425-1431.

(67)   Nagaoka, S.; Nagashima, U. *Effects of node of wave function upon photochemical reactions of organic molecules. 2* J. Phys. Chem. **1991**, *95*, 4006-4008.

References

(68) Smith, K. K.; Kaufmann, K. J. *Picosecond studies of intramolecular proton transfer* J. Phys. Chem. **1978**, *82*, 2286-2291.

(69) Heller, H. J.; Blattmann, H. R. *Some aspects of stabilization of polymers against light* Pure Appl. Chem. **1973**, *36*, 141-161.

(70) Förster, T. *Die pH-abhangigkeit der Fluoreszenz von Naphthalinderivaten* Z. Elektrochem. **1950**, *54*, 531-535.

(71) Wiechmann, M.; Port, H.; Laermer, F.; Frey, W.; Elsaesser, T. *Excited-state proton transfer in a benzotriazole photostabilizer investigated by femtosecond spectroscopy* Chem. Phys. Lett. **1990**, *165*, 28-34.

(72) Wiechmann, M.; Port, H.; Frey, W.; Laermer, F.; Elsaesser, T. *Time-resolved spectroscopy on ultrafast proton transfer in 2-(2'-hydroxy-5'-methylphenyl)benzotriazole in liquid and polymer environments* J. Chem. Phys. **1991**, *95*, 1918-1923.

(73) Frey, W.; Elsaesser, T. *Femtosecond intramolecular proton transfer of vibrationally hot molecules in the electronic ground state* Chem. Phys. Lett. **1992**, *189*, 565-570.

(74) Rieker, J.; Lemmert-Schmitt, E.; Goeller, G.; Roessler, M.; Stueber, G. J.; Schettler, H.; Kramer, H. E. A.; Stezowski, J. J.; Hoier, H.; et al. *Ultraviolet stabilizers of the 2-(hydroxyphenyl)benzotriazole class: influence of substituents on structure and spectra* J. Phys. Chem. **1992**, *96*, 10225-10234.

(75) Chudoba, C.; Riedle, E.; Pfeiffer, M.; Elsaesser, T. *Vibrational coherence in ultrafast excited state proton transfer* Chem. Phys. Lett. **1996**, *263*, 622-628.

(76) Lenz, K.; Pfeiffer, M.; Lau, A.; Elsaesser, T. *Resonance Raman and femtosecond absorption studies of vibrational relaxation initiated by ultrafast intramolecular proton transfer* Chem. Phys. Lett. **1994**, *229*, 340-346.

(77) Pfeiffer, M.; Lenz, K.; Lau, A.; Elsaesser, T. *Resonance Raman studies of heterocyclic aromatic compounds showing ultrafast intramolecular proton transfer* J. Raman Spectrosc. **1995**, *26*, 607-615.

(78) Pfeiffer, M.; Lau, A.; Lenz, K.; Elsaesser, T. *Anharmonicity effects in the resonance Raman spectra of heterocyclic aromatic molecules showing photoinduced intramolecular proton transfer* Chem. Phys. Lett. **1997**, *268*, 258-264.

(79) Laermer, F.; Elsaesser, T.; Kaiser, W. *Femtosecond spectroscopy of excited-state proton transfer in 2-(2'-hydroxyphenyl)benzothiazole* Chem. Phys. Lett. **1988**, *148*, 119-124.

133

References

(80) Lochbrunner, S.; Wurzer, A. J.; Riedle, E. *Microscopic mechanism of ultrafast excited-state intramolecular proton transfer: A 30-fs study of 2-(2'-hydroxyphenyl)benzothiazole* J. Phys. Chem. A **2003**, *107*, 10580-10590.

(81) Arthen-Engeland, T.; Bultmann, T.; Ernsting, N. P.; Rodriguez, M. A.; Thiel, W. *Singlet excited-state intramolecular proton tranfer in 2-(2'-hydroxyphenyl) benzoxazole: spectroscopy at low temperatures, femtosecond transient absorption, and MNDO calculations* Chem. Phys. **1992**, *163*, 43-53.

(82) Stock, K.; Bizjak, T.; Lochbrunner, S. *Proton transfer and internal conversion of o- hydroxybenzaldehyde: coherent versus statistical excited-state dynamics* Chem. Phys. Lett. **2002**, *354*, 409-416.

(83) Rini, M.; Kummrow, A.; Dreyer, J.; Nibbering, E. T. J.; Elsaesser, T. *Femtosecond mid-infrared spectroscopy of condensed phase hydrogen-bonded systems as a probe of structural dynamics* Faraday Discuss. **2002**, *122*, 27-40.

(84) de Vivie-Riedle, R.; De Waele, V.; Kurtz, L.; Riedle, E. *Ultrafast excited-state proton transfer of 2-(2 '-hydroxyphenyl)benzothiazole: Theoretical analysis of the skeletal deformations and the active vibrational modes* J. Phys. Chem. A **2003**, *107*, 10591-10599.

(85) Lochbrunner, S.; Stock, K.; Riedle, E. *Direct observation of the nuclear motion during ultrafast intramolecular proton transfer* J. Mol. Struct. **2004**, *700*, 13-18.

(86) Bulska, H. *Intramolecular cooperative double proton transfer in [2,2'-bipyridyl]-3,3'-diol* Chem. Phys. Lett. **1983**, *98*, 398-402.

(87) Borowicz, P.; Grabowska, A.; Wortmann, R.; Liptay, W. *Tautomerization in fluorescent states of bipyridyl-diols: A direct confirmation of the intramolecular double proton transfer by electro-optical emission measurements* J. Lumin. **1992**, *52*, 265-273.

(88) Zhang, H.; vanderMeulen, P.; Glasbeek, M. *Ultrafast single and double proton transfer in photo-excited [2,2'-bipyridyl]-3,3'-diol* Chem. Phys. Lett. **1996**, *253*, 97-102.

(89) Marks, D.; Prosposito, P.; Zhang, H.; Glasbeek, M. *Femtosecond laser selective intramolecular double-proton transfer in [2,2'-bipyridyl]-3,3 '-diol* Chem. Phys. Lett. **1998**, *289*, 535-540.

(90) Lochbrunner, S.; Stock, K.; Schriever, C.; Riedle, E. *Ultrafast double proton transfer: symmetry breaking wavepacket motion and absence of deuterium isotope effect* in *Ultrafast Phenomena XIV*; Kobayashi, T., Okada, T., Nelson, K., De Silvestri, S., Eds.; Springer-Verlag: Berlin, **2005**.

(91) Stock, K.; Schriever, C.; Lochbrunner, S.; Riedle, E. *Reaction path dependent coherent wavepacket dynamic in excited state intramolecular double proton transfer* Chem. Phys. **2008**, *349*, 197-203.

(92) Watson, J. D.; Crick, F. H. C. *Genetical implications of the structure of deoxyribonucleic acid* Nature **1953**, *171*, 964-967.

(93) Mataga, N.; Miyasaka, H. *Photoinduced charge transfer phenomena: Femtosecond-picosecond laser photolysis studies* Prog. React. Kinet. Mech. **1994**, *19*, 317-430.

(94) Yatsuhashi, T.; Inoue, H. *Molecular mechanism of radiationless deactivation of aminoanthraquinones through intermolecular hydrogen-bonding interaction with alcohols and hydroperoxides* J. Phys. Chem. A **1997**, *101*, 8166-8173.

(95) Biczók, L.; Valat, P.; Wintgens, V. *Effect of molecular structure and hydrogen bonding on the fluorescence of hydroxy-substituted naphthalimides* Phys. Chem. Chem. Phys. **1999**, *1*, 4759-4766.

(96) Waluk, J. *Hydrogen-bonding-induced phenomena in bifunctional heteroazaaromatics* Acc. Chem. Res. **2004**, *36*, 832-838.

(97) Waluk, J.; Grabowska, A.; Pakuła, B. *Proton additon to excited diazaphenanthrenes topology determined molecular properties* J. Lumin. **1980**, *21*, 277-291.

(98) Lim, E. C. *Vibronic interactions and luminescence in nitrogen-heterocyclic and aromatic carbonyl compound*; Academic: New York, **1976**.

(99) Waluk, J.; Komorowski, S. J.; Herbich, J. *Excited-state double proton transfer in 1-azacarbazole-alcohol complexes* J. Phys. Chem. **1986**, *90*, 3868-3871.

(100) Waluk, J.; Komorowski, S. J. *Solvent-dependent photophysics of Indoloquinoxaline* J. Mol. Struct. **1986**, *142*, 159-162.

(101) Waluk, J.; Komorowski, S. J. *Modification of photophysical behaviour by hydrogen bonding: indoloquinoxaline and its methylated derivatives.* Chem. Phys. Lett. **1987**, *133*, 368-372.

(102) Woessner, G.; Goeller, G.; Kollat, P.; Stezowski, J. J.; Hauser, M.; Klein, U. K. A.; Kramer, H. E. A. *Photophysical and photochemical deactivation processes of ultraviolet stabilizers of the (2-hydroxyphenyl)benzotriazole class* J. Phys. Chem. **1984**, *88*, 5544-5550.

(103) McMorrow, D.; Dzugan, T. P.; Aartsma, T. J. *Excited-state dynamics of the intramolecular proton transfer of 3-hydroxyflavone in the absence of external hydrogen-bonding interactions* Chem. Phys. Lett. **1984**, *103*, 492-496.

(104) Herbich, J.; Hung, C. Y.; Thummel, R. P.; Waluk, J. *Solvent-controlled excited state behavior: 2-(2'-pyridyl)indoles in alcohols* J. Am. Chem. Soc. **1996**, *118*, 3508-3518.

(105) Dobkowski, J.; Herbich, J.; Galievsky, V.; Thummel, R. P.; Wu, F. Y.; Waluk, J. *Diversity of excited state deactivation paths in heteroazaaromatics with multiple intermolecular hydrogen bonds* Ber. Bunsen-Ges. Phys. Chem. **1998**, *102*, 469-475.

(106) Herbich, J.; Waluk, J.; Thummel, R. P.; Hung, C.-Y. *Mechanisms of fluorescence quenching by hydrogen bonding in various aza aromatics* J. Photochem. Photobiol., A **1994**, *80*, 157-160.

(107) Sinicropi, A.; Nau, W. M.; Olivucci, M. *Excited state quenching via "unsuccessful" chemical reactions* Photochem. Photobiol. Sci. **2002**, *1*, 537-546.

(108) Kyrychenko, A.; Herbich, J.; Wu, F.; Thummel, R. P.; Waluk, J. *Solvent-induced syn-anti rotamerization of 2-(2'-pyridyl)indole and the structure of its alcohol complexes* J. Am. Chem. Soc. **2000**, *122*, 2818-2827.

(109) Miyasaka, H.; Tabata, A.; Kamada, K.; Mataga, N. *Femtosecond-picosecond laser photolysis studies on the mechanisms of electron transfer induced by hydrogen-bonding interactions in polar solutions: 1-aminopyrene-pyridine systems* J. Am. Chem. Soc. **1993**, *115*, 7335-7342.

(110) Miyasaka, H.; Tabata, A.; Kamada, K.; Mataga, N. *Femtosecond-picosecond laser photolysis studies on the mechanisms of fluorescence quenching induced by hydrogen-bonding interactions-1-pyrenol-pyridine systems* J. Phys. Chem. **1993**, *97*, 8222-8228.

(111) Martin, M.; Ikeda, N.; Okada, T.; Mataga, N. *Picosecond laser photolysis studies of deactivation processes of excited hydrogen-bonding complexes. 2. Dibenzocarbazoie-pyridine systems* J. Phys. Chem. **1982**, *86*, 4148-4156.

(112) Ikeda, N.; Miyasaka, H.; Okada, T.; Mataga, N. *Picosecond laser photolysis studies of deactivation processes of excited hydrogen bonding complexes. 3. Detection of the nonfluorescent charge-transfer state in the excited 1-aminopyrene-pyridine hydrogen bonded pair and related systems* J. Am. Chem. Soc. **1983**, *105*, 5206-5211.

(113) Herbich, J.; Kijak, M.; Zielińska, A.; Thummel, R. P.; Waluk, J. *Fluorescence quenching by pyridine and derivatives induced by intermolecular hydrogen bonding to pyrrole-containing heteroaromatics* J. Phys. Chem. A **2002**, *106*, 2158-2163.

(114) Tanaka, H.; Nishimoto, K. *Ab initio molecular orbital study on the electronlc structure of some excited hydrogen-bonding systems* J. Phys. Chem. **1984**, *88*, 1052-1055.

(115) Perun, S.; Sobolewski, A. L.; Domcke, W. *Role of electron-driven proton-transfer processes in the excited-state deactivation adenine-thymine base pair* J. Phys. Chem. A **2006**, *110*, 9031-9038.

(116) Sobolewski, A. L.; Domcke, W.; Hattig, C. *Tautomeric selectivity of the excited-state lifetime of guanine/cytosine base pairs: The role of electron-driven proton-transfer processes* Proc. Natl. Acad. Sci. U. S. A. **2005**, *102*, 17903-17906.

(117) Taylor, C. A.; El-Bayoumi, M. A.; Kasha, M. *Excited-state two-proton tautomerism in hydrogen-bonded N-heterocyclic base pairs* Proc. Natl. Acad. Sci. U. S. A. **1969**, *63*, 253-260.

(118) Ingham, K. C.; Abu-Elgheit, M.; El-Bayoumi, M. A. *Confirmation of biprotonic phototautomerism in 7-azaindole hydrogen-bonded dimers* J. Am. Chem. Soc. **1971**, *93*, 5023-5025.

(119) Ingham, K.; El-Bayoumi, M. A. *Photoinduced double proton transfer in a model hydrogen bonded base pair. Effects of temperature and deuterium substitution* J. Am. Chem. Soc. **1974**, *96*, 1674-1682.

(120) Hetherington III, W. M.; Micheels, R. H.; B., E. K. *Picosecond dynamics of double proton transfer in 7-azaindole dimers* Chem. Phys. Lett. **1979**, *66*, 230.

(121) Takeuchi, S.; Tahara, T. *Observation of dimer excited-state dynamics in the double proton transfer reaction of 7-azaindole by femtosecond fluorescence up-conversion* Chem. Phys. Lett. **1997**, *277*, 340-346.

(122) Takeuchi, S.; Tahara, T. *Femtosecond ultraviolet-visible fluorescence study of the excited-state proton-transfer reaction of 7-azaindole dimer* J. Phys. Chem. A **1998**, *102*, 7740-7753.

(123) Takeuchi, S.; Tahara, T. *Excitation-wavelength dependence of the femtosecond fluorescence dynamics of 7-azaindole dimer: further evidence for the concerted double proton transfer in solution* Chem. Phys. Lett. **2001**, *347*, 108-114.

(124) Chachisvilis, M.; Fiebig, T.; Douhal, A.; Zewail, A. H. *Femtosecond dynamics of a hydrogen-bonded model base pair in the condensed phase: Double proton transfer in 7-azaindole* J. Phys. Chem. A **1998**, *102*, 669-673.

(125) Fuke, K.; Kaya, K. *Dynamics of double-proton-transfer reaction in the excited-state model hydrogen-bonded base pairs* J. Phys. Chem. **1989**, *93*, 614-621.

(126) Folmer, D. E.; Poth, L.; Wisniewski, E. S.; Castleman, A. W. *Arresting intermediate states in a chemical reaction on a femtosecond time scale: proton transfer in model base pairs* Chem. Phys. Lett. **1998**, *287*, 1-7.

(127) Douhal, A.; Moreno, M.; Lluch, J. M. *On the experimental evidences for 7-azaindole base-pair model ultrafast phototautomerization* Chem. Phys. Lett. **2000**, *324*, 81-87.

(128) Douhal, A.; Moreno, M.; Lluch, J. M. *On the theoretical reports on 7-azaindole base-pair phototautomerization* Chem. Phys. Lett. **2000**, *324*, 75-80.

(129) Moreno, M.; Douhal, A.; Lluch, J. M.; Castano, O.; Frutos, L. M. *Ab initio based exploration of the potential energy surface for the double proton transfer in the first excited singlet electronic state of the 7-azaindole dimer* J. Phys. Chem. A **2001**, *105*, 3887-3893.

(130) Catalán, J.; del Valle, J. C.; Kasha, M. *Resolution of concerted versus sequential mechanisms in photo-induced double-proton transfer reaction in 7-azaindole H-bonded dimer* Proc. Natl. Acad. Sci. U. S. A. **1999**, *96*, 8338-8343.

(131) Catalán, J.; Perez, P.; del Valle, J. C.; de Paz, J. L. G.; Kasha, M. *The concerted mechanism of photo-induced biprotonic transfer in 7-azaindole dimers: A model for the secondary evolution of the classic C_{2h} dimer and comparison of four mechanisms* Proc. Natl. Acad. Sci. U. S. A. **2002**, *99*, 5799-5803.

(132) Sekiya, H.; Sakota, K. *Excited-state double-proton transfer in the 7-azaindole dimer in the gas phase. Resolution of the stepwise versus concerted mechanism controversy and a new paradigm* Bull. Chem. Soc. Jpn. **2006**, *79*, 373-385.

(133) Fuke, K.; Yabe, T.; Chiba, N.; Kohida, T.; Kaya, K. *Double-proton-transfer reaction in the excited state of 1-azacarbazole dimer and 1-azacarbazole-7-azaindole heterodimer studied in a supersonic jet* J. Phys. Chem. **1986**, *90*, 2309-2311.

(134) Fuke, K.; Tsukamoto, K.; Misaizu, F.; Kaya, K. *Picosecond measurements of the vibrationally resolved proton-transfer rate of the jet-cooled 1-azacarbazole dimer* J. Chem. Phys. **1991**, *95*, 4074-4080.

(135) Chen, H. Y.; Chao, I. *Ionization-induced proton transfer in model DNA base pairs: A theoretical study of the radical ions of the 7-azaindole dimer* ChemPhysChem **2004**, *5*, 1855-1863.

(136) Sekiya, H.; Sakota, K. *Excited-state double-proton transfer in the model DNA base pair: Resolution for stepwise and concerted mechanism controversy in the 7-azaindole revealed by frequency-*

and time-resolved spectroscopy Photochem. Photobiol., C: Photochem. Rev. **2008**, *9*, 81-91.

(137) Kown, O.-H.; Zewail, A. H. *Double proton transfer dynamic of model DNA base pairs in the condensed phase* Proc. Natl. Acad. Sci. U. S. A. **2007**, *104*, 8703-8708.

(138) Takeuchi, S.; Tahara, T. *The answer to concerted versus step-wise controversy for the double proton transfer mechanism of 7-azaindole dimer in solution* Proc. Natl. Acad. Sci. U. S. A. **2007**, *104*, 5285-5290.

(139) Serrano-Andres, L.; Merchán, M. *Theoretical CASPT2 study of the excited state double proton transfer reaction in the 7-azaindole dimer* Chem. Phys. Lett. **2006**, *418*, 569-575.

(140) Catalán, J.; De Paz, J. L. G. *The molecular symmetry and electronic spectroscopy of 7-azaindole dimer: Its proton-transfer channels* J. Chem. Phys. **2005**, *123*, 114302-114302-8.

(141) Catalán, J.; Diaz, C.; Paz, J. L. G. *Excited-state proton phototransfer in the (3-methyl-7-azaindole)-(7-azaindole) heterodimer* Chem. Phys. Lett. **2006**, *419*, 164-167.

(142) McMorrow, D.; Aartsma, T. J. *Solvent-mediated proton transfer. The roles of solvent structure and dynamics on the excited-state tautomerization of 7-azaindole/alcohol complexes* Chem. Phys. Lett. **1986**, *125*, 581-585.

(143) Bulska, H.; Grabowska, A.; Pakula, B.; Sepioł, J.; Waluk, J.; Wild, U. P. *Spectroscopy of doubly hydrogen-bonded 7-azaindole. Reinvestigation of the excited state reaction* J. Lumin. **1984**, *29*, 65-81.

(144) Herbich, J.; Sepioł, J.; Waluk, J. *Determination of the energy barrier origin of the excited state double proton transfer in 7-azaindole: alcohol complexes* J. Mol. Struct. **1984**, *114*, 329-332.

(145) Moog, R. S.; Maroncelli, M. *7-Azaindole in alcohols: solvation dynamics and proton transfer* J. Phys. Chem. **1991**, *95*, 10359-10369.

(146) Konijnenberg, J.; Huizer, A. H.; Varma, A. G. O. *Solute–solvent interaction in the photoinduced tautomerization of 7-azaindole in various alcohols and in mixtures of cyclohexane and ethanol* J. Chem. Soc., Faraday Trans. 2 **1988**, *84*, 1163-1175.

(147) Chen, Y.; Gai, F.; Petrich, J. W. *Solvation of 7-azaindole in alcohols and water: evidence for concerted, excited-state, double-proton transfer in alcohols* J. Am. Chem. Soc. **1993**, *115*, 10158-10166.

139

(148) Chen, Y.; Gai, F.; Petrich, J. W. *Solvation and excited-state proton transfer of 7-azaindole in alcohols* Chem. Phys. Lett. **1994**, *222*, 329-334.

(149) Mente, S.; Maroncelli, M. *Solvation and the excited-state tautomerization of 7-azaindole and 1-azacarbazole: Computer simulations in water and alcohol solvents* J. Phys. Chem. A **1998**, *102*, 3860-3876.

(150) Chou, P.-T.; Wei, C.-Y.; Chang, C.-P.; Chiu, C.-H. *7-azaindole-assisted lactam-lactim tautomerization via excited-state double proton transfer* J. Am. Chem. Soc. **1995**, *117*, 7259-7260.

(151) Chapman, C. F.; Maroncelli, M. *Excited-state tautomerization of 7-azaindole in water* J. Phys. Chem. **1992**, *96*, 8430-8441.

(152) Herbich, J.; Dobkowski, J.; Thummel, R. P.; Hegde, V.; Waluk, J. *Intermolecular excited state double proton transfer in dipyridocarbazole:alcohol complexes* J. Phys. Chem. A **1997**, *101*, 5839-5845.

(153) Marks, D.; Zhang, H.; Borowicz, P.; Waluk, J.; Glasbeek, M. *(Sub)picosecond fluorescence upconversion studies of intermolecular proton transfer of dipyrido[2,3-a : 3 ',2 '- i]carbazole and related compounds* J. Phys. Chem. A **2000**, *104*, 7167-7175.

(154) Kyrychenko, A.; Herbich, J.; Izydorzak, M.; Gil, M.; Dobkowski, J.; Wu, F. Y.; Thummel, R. P.; Waluk, J. *Photoinduced double proton transfer: Inter- and intramolecular cases* Isr. J. Chem. **1999**, *39*, 309-318.

(155) Kyrychenko, A.; Herbich, J.; Izydorzak, M.; Wu, F.; Thummel, R. P.; Waluk, J. *Role of ground state structure in photoinduced tautomerization in bifunctional proton donor-acceptor molecules: 1H- pyrrolo[3,2-h]quinoline and related compounds* J. Am. Chem. Soc. **1999**, *121*, 11179-11188.

(156) Kyrychenko, A.; Stepanenko, Y.; Waluk, J. *Molecular dynamics and DFT studies of intermolecular hydrogen bonds between bifunctional heteroazaaromatic molecules and hydroxylic solvents* J. Phys. Chem. A **2000**, *104*, 9542-9555.

(157) Nakajima, A.; Hirano, M.; Hasumi, R.; Kaya, K.; Watanabe, H.; Carter, C. C.; Williamson, J. M.; Miller, T. A. *High-resolution laser-induced fluorescence spectra of 7- azaindole-water complexes and 7-azaindole dimer* J. Phys. Chem. A **1997**, *101*, 392-398.

(158) Huang, Y. H.; Arnold, S.; Sulkes, M. *Spectroscopy and fluorescence lifetimes of jet-cooled 7-azaindole: Electronic states and solvent complex geometry* J. Phys. Chem. **1996**, *100*, 4734-4738.

(159) Kim, S. K.; Bernstein, E. R. *7-Azaindole and its clusters with argon, methane, water, ammonia, and alcohols: molecular geometry, cluster geometry, and nature of the first excited singlet electronic state* J. Phys. Chem. **1990**, *94*, 3531-3539.

(160) Fuke, K.; Yoshiuchi, H.; Kaya, K. *Electronic spectra and tautomerism of hydrogen-bonded complexes of 7-azaindole in a supersonic jet* J. Phys. Chem. **1984**, *88*, 5840-5844.

(161) Bombach, R.; Honegger, E.; Leutwyler, S. *Solut-solvent interactions in microhydrate cluster: carbazole-$(H_2O)n$* Chem. Phys. Lett. **1985**, *118*, 449-454.

(162) Nosenko, Y.; Kunitski, M.; Thummel, R. P.; Kyrychenko, A.; Herbich, J.; Waluk, J.; Riehn, C.; Brutschy, B. *Detection and structural characterization of clusters with ultrashort-lived electronically excited states: IR absorption detected by femtosecond multiphoton ionization* J. Am. Chem. Soc. **2006**, *128*, 10000-10001.

(163) Nosenko, Y.; Kyrychenko, A.; Thummel, R. P.; Waluk, J.; Brutschy, B.; Herbich, J. *Fluorescence quenching in cyclic hydrogen-bonded complexes of 1H-pyrrolo[3,2-h] quinoline with methanol: cluster size effect* Phys. Chem. Chem. Phys. **2007**, *9*, 3276-3285.

(164) Nosenko, Y.; Kunitski, M.; Riehn, C.; Thummel, R. P.; Kyrychenko, A.; Herbich, J.; Waluk, J.; Brutschy, B. *Separation of different hydrogen-bonded clusters by femtosecond UV-ionization-detected infrared spectroscopy: 1H-pyrrolo[3,2-h]quipoline·$(H_2O)_{(n=1,2)}$ complexes* J. Phys. Chem. A **2008**, *112*, 1150-1156.

(165) Hara, A.; Sakota, K.; Nakagaki, M.; Sekiya, H. *Dispersed fluorescence spectra of jet-cooled 7-azaindole- $(H_2O)_{(n)}$ (n=1-3): Does photoinduced excited-state proton transfer occur or not?* Chem. Phys. Lett. **2005**, *407*, 30-34.

(166) Sakota, K.; Komoto, Y.; Nakagaki, M.; Ishikawa, W.; Sekiya, H. *Observation of a catalytic proton/hydrogen atom relay in microsolvated 7-azaindole-methanol cluster enhanced by a cooperative motion of the hydrogen-bonded network* Chem. Phys. Lett. **2007**, *435*, 1-4.

(167) Sakota, K.; Inoue, N.; Komoto, Y.; Sekiya, H. *Cooperative triple-proton/hydrogen atom relay in 7-azaindole$(CH_3OH)_2$ in the gas phase: Remarkable change in the reaction mechanism from vibrational-mode specific to statistical fashion with increasing internal energy* J. Phys. Chem. A **2007**, *111*, 4596-4603.

(168) Douhal, A.; Amat-Guerri, F.; Acuña, A. U. *Probing nanocavities with proton-transfer fluorescence* Angew. Chem. Int. Ed. Engl. **1997**, *36*, 1514-1516.

References

(169) Ghiggino, K. P.; Scully, A. D.; Leaver, I. H. *Effect of solvent on excited-state intramolecular proton transfer in benzotriazole photostabilizers* J. Phys. Chem. **1986**, *90*, 5089-5093.

(170) Huston, A. L.; Scott, G. W.; Gupta, A. *Mechanism and kinetics of excited-state relaxation in internally hydrogen-bonded molecules: 2-(2'-hydroxy-5'-methylphenyl)-benzotriazole in solution* J. Chem. Phys. **1982**, *76*, 4978-4985.

(171) Huston, A. L.; Scott, G. W. *Spectroscopic and kinetic investigations of internally hydrogen-bonded (hydroxyphenyl)benzotriazoles* J. Phys. Chem. **1987**, *91*, 1408-1413.

(172) McMorrow, D.; Kasha, M. *Intramolecular excited-state proton transfer in 3-hydroxyflavone. Hydrogen-bonding solvent perturbations* J. Phys. Chem. **1984**, *88*, 2235-2243.

(173) Douhal, A. *The involvement of rotational processes in the intramolecular proton-transfer cycle* Ber. Bunsen-Ges. Phys. Chem. **1998**, *102*, 448-451.

(174) Barbara, P. F.; Rentzepis, P. M.; Brus, L. E. *Photochemical kinetics of salicylidenaniline* J. Am. Chem. Soc. **1980**, *102*, 2786-2791.

(175) Kijak, M.; Zielińska, A.; Chamchoumis, C.; Herbich, J.; Thummel, R. P.; Waluk, J. *Conformational equilibria and photoinduced tautomerization in 2-(2'-pyridyl)pyrrole* Chem. Phys. Lett. **2004**, *400*, 279-285.

(176) Sobolewski, A. L.; Domcke, W. G. *Computational studies of the photophysics of hydrogen-bonded molecular systems* J. Phys. Chem. A **2007**, *111*, 11725-11735.

(177) Mudadu, M. S.; Singh, A.; Thummel, R. P. *7-pyridylindoles: synthesis, structure, and properties* J. Org. Chem. **2006**, *71*, 7611-7617.

(178) Mudadu, M. S.; Singh, A.; Thummel, R. P. *The preparation and study of 2,9-di(pyrid-2'-yl)carbazoles* J. Org. Chem. **2008**, *73*, 6513-6520.

(179) Gibson, V. C.; Spitzmesser, S. K.; White, A. J. P.; Williams, D. J. *Synthesis and reactivity of 1,8-bis(imino)carbazolide complexes of iron, cobalt and manganese* Dalton Transactions **2003**, 2718-2727.

(180) Jasny, J.; Waluk, J. *Compact multifunctional spectrofluorimeter with a novel design for anisotropy measurements* Rev. Sci. Instrum. **1998**, *69*, 2242-2245.

(181) Velapoldi, R. A. *Considerations on organic compounds in solution and inorganic ions in glasses as fluorescent standard reference materials* in *National Bureau of Standards Special Publication 378,*

References

Accuracy in Spectrophotometry and Luminescence Measurements; Proc. Conf. NBS: Gaithersburg, MD, **1972**.

(182) Johnson, C. W. *Circular dichroism instrumentation* in *Circular dichroism and the conformational analysis of biomolecules*; Fasman, G. D., Ed.; Plenum Press: New York, **1996**.

(183) Jasny, J. *Multifunctional spectrofluorimetic system* J. Lumin. **1978**, *17*, 149-173.

(184) Marquardt, D. W. *An algorithm for least-squares estimation of nonlinear parameters* J. Soc. Indust. Appl. Math. **1963**, *11*, 431-441.

(185) van Dijk, S. I.; Wiering, P. G.; Groen, C. P.; Brouwer, A. M.; Verhoeven, J. W.; Schuddeboom, W.; Warman, J. M. *Solvent-dependent switching between two dipolar excited states in a rigidly extended trichromophoric system* J. Chem. Soc., Faraday Trans. **1995**, *91*, 2107-2114.

(186) Dobkowski, J.; Grabowski, Z. R.; Jasny, J.; Zieliński, Z. *Picosecond trnasient absorption spectra and the twisted intramolecular charge transfer phenomenon* Acta Phys. Pol. A **1995**, *88*, 455-468.

(187) Dobkowski, J.; Galievsky, V.; Jasny, J.; Sazanovich, I. *Time-resolved emission spectroscopy of pyrene derivatives* Pol. J. Chem. **2004**, *78*, 961-972.

(188) Balkowski, G.; Szemik-Hojniak, A.; van Stokkum, I. H. M.; Zhang, H.; Buma, W. J. *Femtosecond excited state studies of the two-center three-electron bond driven twisted internal charge transfer dynamics in 1,8-bis(dimethylamino)naphthalene* J. Phys. Chem. A **2005**, *109*, 3535-3541.

(189) Vergeer, F. W.; Kleverlaan, C. J.; Stufkens, D. J. *The first steps of the light-induced biradical and zwitterion formation from the clusters [Os₃(CO)₁₀(α-diimine)] studied with ultrafast time-resolved absorption spectroscopy* Inorg. Chim. Acta **2002**, *327*, 126-133.

(190) Brutschy, B. *The structure of microsolvated benzene derivatives and the role of aromatic substituents* Chem. Rev. **2000**, *100*, 3891-3920.

(191) Shubert, V. A.; Zwier, T. S. *IR-IR-UV hole-burning: Conformation specific IR spectra in the face of UV spectral overlap* J. Phys. Chem. A **2007**, *111*, 13283-13286.

(192) Vdovin, A.; Sepioł, J.; Jasny, J.; Kauffman, J. M.; Mordziński, A. *Excited state proton transfer in jet-cooled 2,5-di-(2-benzoxazolyl)phenol* Chem. Phys. Lett. **1998**, *296*, 557-565.

(193) Nosenko, Y.; Jasny, J.; Pietraszkiewicz, M.; Mordzinski, A. *Laser spectroscopy of porphycene derivatives: a search for proton tunneling in 2,7,12,17-tetra-tert butylporphycene* Chem. Phys. Lett. **2004**, *399*, 331-336.

143

References

(194) Lommatzsch, U.; Gerlach, A.; Lahmann, C.; Brutschy, B. *Supersonic jet studies on the photophysics of 4-dimethylaminobenzonitrile (DMABN) and related compounds: on the origin of the anomalous fluorescence of DMABN clusters in a supersonic jet* J. Phys. Chem. A **1998**, *102*, 6421-6435.

(195) M. J. Frisch, G. W. T., H. B. Schlegel, G. E. Scuseria, M. A. Robb, J. R.; Cheeseman, J. J. A. M., T. Vreven, K. N. Kudin, J. C. Burant, J. M. Millam,; S. S. Iyengar, J. T., V. Barone, B. Mennucci, M. Cossi, G. Scalmani, N. Rega, G.; A. Petersson, H. N., M. Hada, M. Ehara, K. Toyota, R. Fukada, J. Hasegawa,; M. Ishida, T. N., Y. Honda, O. Kitao, H. Nakai, M. Klene, X. Li, J. E. Knox,; H. P. Hratchian, J. B. C., C. Amado, J. Jaramillo, R. Gomperts, R. E. Stratmann, O.; Yazyev, A. J. A., R. Cammi, C. Pomelli, J. Ochterski, P. Y. Ayala, K. Morokuma,; G. A. Voth, P. S., J. J. Donnenberg, V. G. Zakrzewski, S. Dapprich, A. D.; Daniels, M. C. S., O. Farkas, D. K. Malick, A. D. Rabuck, K. Raghavachari, J. B.; Foresman, J. V. O., Q. Cui, A. G. Baboul, S. Clifford, J. Cioslowski, B. B.; Stefanov, G. L., A. Liashenko, P. Piskorz, I. Komaromi, R. L. Martin, D. J. Fox, T.; Keith, M. A. A.-L., C. Y. Peng, A. Nanayakkara, M. Challacombe, P. M. W. Gill,; B. Johnson, W. C., M. W. Wong, C. Gonzales, J. A. Pople *Gaussian 03, revision C.02, Gaussian*; PA: Pittsburgh, 2003.

(196) Ahlrichs, R.; Bär, M.; Häser, M.; Horn, H.; Kölmel, C. *Electronic structure calculations on workstation computers: the program system Turbomole* Chem. Phys. Lett. **1989**, *162*, 165.

(197) Furche, F.; Ahlrichs, R. *Adiabatic time-dependent density functional methods for excited state properties* J. Chem. Phys. **2002**, *117*, 7433-7447.

(198) Deglmann, P.; May, K.; Furche, F.; Ahlrichs, R. *Nuclear second analytical derivative calculation using auxiliary basis set expansions* Chem. Phys. Lett. **2004**, *384*, 103-107.

(199) Grabowski, Z. R.; Grabowska, A. *The Förster cycle reconsidered* Z. Phys. Chem. **1976**, *101*, 197-208.

(200) Mudadu, M. S. *The synthesis and chemistry of pyridylindole and dipyridylcarbazole derivatives* Ph.D Thesis, University of Houston, **2004**.

(201) Carney, J. R.; Zwier, T. S. *Infrared and ultraviolet spectroscopy of water-containing clusters of indole, 1-methylindole, and 3-methylindole* J. Phys. Chem. A **1999**, *103*, 9943-9957.

(202) Nosenko, Y.; Wiosna-Sałyga, G.; Kunitski, M.; Petkova, I.; Singh, A.; Buma, W. J.; Thummel, R. P.; Brutschy, B.; Waluk, J. *Proton

transfer with a twist? Femtosecond dynamics of 7-(2-pyridyl)-indole in condensed phase and in supersonic jets Angew. Chem. Int. Ed. Engl. **2008**, *47*, 6037-6040.

(203) Sobolewski, A. L.; Domcke, W. *Photophysics of intramolecularly hydrogen-bonded aromatic systems: ab initio exploration of the excited-state deactivation mechanisms of salicylic acid* Phys. Chem. Chem. Phys. **2006**, *8*, 3410-3417.

(204) Coe, J. D.; Levine, B. G.; Martinez, T. J. *Ab initio molecular dynamics of excited-state intramolecular proton transfer using multireference perturbation theory* J. Phys. Chem. A **2007**, *111*, 11302-11310.

(205) Sobolewski, A. L.; Domcke, W.; Hattig, C. *Photophysics of organic photostabilizers. Ab initio study of the excited-state deactivation mechanisms of 2-(2 '-hydroxyphenyl)benzotriazole* J. Phys. Chem. A **2006**, *110*, 6301-6306.

(206) Horng, M. L.; Gardecki, J. A.; Papazyan, A.; Maroncelli, M. *Subpicosecond measurements of polar solvation dynamics: Coumarin 153 revisited* J. Phys. Chem. **1995**, *99*, 17311-17337.

(207) Garg, S. K.; Smyth, C. P. *Microwave absorption and molecular structure in liquids. LXII. The three dielectric dispersion regions of the normal primary alcohols* J. Phys. Chem. **1965**, *69*, 1294-1301.

(208) Riddick, J. A.; Bunger, W. B. *Organic solvents, Vol. 2*; Wiley-Interscience: New York, **1970**.

(209) Maus, M.; Rettig, W. *Comparison of the bandshape and lifetime data analysis of temperature-dependent fluorescence measurements for the investigation of an excited state conformational equilibrium. The case of differently twisted donor-acceptor biphenyls* Phys. Chem. Chem. Phys. **2001**, *3*, 5430-5437.

(210) Ito, A. *Solvent response and dielectric relaxation in supercooled butyronitrile* J. Chem. Phys. **2006**, *125*, 24504.

(211) Phillips, D. *Studies on torsional motion in aromatic amines* J. Photochem. Photobiol., A **1997**, *105*, 307-315.

(212) Sinclair, W. E.; Yu, H. P.; Phillips, D.; Hollas, J. M. *The ground and first excited singlet state torsional potentials of 2-phenylindole from supersonic jet fluorescence spectra* J. Chem. Phys. **1997**, *106*, 5797-5804.

(213) Takei, Y.; Yamaguchi, T.; Osamura, Y.; Fuke, K.; Kaya, K. *Electronic spectra and molecular structure of biphenyl and para-substituted biphenyls in a supersonic jet* J. Phys. Chem. **1988**, *92*, 577-581.

(214) Monte, C. A.; Roggan, A.; Subaric-Leitis, A.; Rettig, W.; Zimmermann, P. *Resonance effects of diabatic crossing within the torsional spectrum of 9-(N-carbazolyl)antracene observed by supersonic jet fluorescence spectroscopy* J. Chem. Phys. **1993**, *98*, 2580-2592.

(215) Takayanagi, M.; Tatsuo, G.; Ichiro, H. *Geometry and torsional potential of 2,2'bithiophene in supersonic jet* J. Phys. Chem. **1994**, *98*, 12893-12898.

(216) Okuyama, U.; Hasegawa, T.; Ito, M.; Mikami, N. *Electronic spectra of tolane in supersonic free jet: Large-amplitude torsional motion* J. Phys. Chem. **1984**, *88*, 1711-1716.

(217) *CCCBDB Computational Chemistry Comparison and Benchmark Database*. http://cccbdb.nist.gov/.

(218) Herzberg, G. *Molecular Spectra and Molecular Structure* Van Nostrand Geinhold: New York, **1945**.

(219) Yokoyama, F.; Watanabe, H.; Omi, T.; Ishiuchi, S.; Fujii, M. *Structure of hydrogen-bonded clusters of 7-azaindole studied by IR dip spectroscopy and ab initio molecular orbital calculation* J. Phys. Chem. A **2001**, *105*, 9366-9374.

(220) Sakai, M.; Daigoku, K.; Ishiuchi, S.; Saeki, M.; Hashimoto, K.; Fujii, M. *Structures of carbazole-$(H_2O)_{(n)}$ (n=1-3) clusters studied by IR dip spectroscopy and a quantum chemical calculation* J. Phys. Chem. A **2001**, *105*, 8651-8657.

(221) Wu, R. H.; Nachtigally, P.; Brutschy, B. *Structure and hydrogen bonding of 2-aminopyridine center dot $(H_2O)_{(n)}$ (n=1, 2) studied by infrared ion depletion spectroscopy* Phys. Chem. Chem. Phys. **2004**, *6*, 515-521.

(222) Matsuda, J.; Ebata, T.; Mikami, N. *Vibrational spectroscopy of 2-pyridone and its clusters in supersonic jets: Structures of the clusters as revealed by characteristic shifts of the NH and C=O bands* J. Chem. Phys. **1999**, *110*.

(223) Matsuda, J.; Ebata, T.; Mikami, N. *IR-UV double-resonance spectroscopic study of 2-hydroxypyridine and its hydrogen-bonded clusters in supersonic jets* J. Phys. Chem. A **2001**, *105*, 3475-3480.

(224) Kaczmarek, L.; Borowicz, P.; Grabowska, A. *Strongly modified [2,2'-bipyridyl]-3,3'-diol (BP(OH)$_2$): a system undergoing excited state intramolecular proton transfer as a photostabilizer of polymers and as a solar energy collector* J. Photochem. Photobiol., A **2001**, *138*, 159-166.

GLOSSARY OF ACRONYMS

1	**7-(2'-pyridyl)indole**
2	**7-(3'-pyridyl)indole**
3	**7-(4'-pyridyl)indole**
4	**2,9-(di-2'-pyridyl)-4,7-di(t-butyl)carbazole**
4H	**2,9-(di-2'-pyridyl)carbazole**
A	absorption
ACN	acetonitrile
1AC	**1-azacarbazole**
7AI	**7-azaindole**
7AI$_2$	**7-azaindole dimer**
AP	**1-aminopyrene**
B3LYP	Becke's three parameter hybrid functional and the correlation functional of Lee, Yang and Parr
BET	back electron transfer
BHT	**2-(2'-hydroxyphenyl)benzothiazole**
BuCN	butyronitrile
BP(OH)$_2$	**[2,2'-bipyridyl]-3,3'-diol**
BSSE	basis set superposition error
CD	circular dichroism
CIS	configuration interaction singles (singly excited configurations)
CT	charge transfer
D-A	donor-acceptor
DF	dispersed fluorescence
DFM	difference-frequency mixing
DFT	density functional theory
DMSO	dimethyl sulfoxide
DPC	**dipyrido[2,3-a:3',2'-i]carbazole**
EADS	evolution-associated difference spectra
ESDPT	excited state double proton transfer
ESIPT	intramolecular excited state proton transfer
ESPT	excited state proton transfer
ET	electron transfer
EtOH	ethanol
fsMPI	femtosecond multiphoton ionization
FTIR	Fourier-transform infrared
FWHM	full width at half-maximum

Glossary of acronyms

HB	hydrogen bonding
HOMO	highest occupied molecular orbital
HPIP	**2-(2'-hydroxyphenyl)imidazol[1,2-a]pyridine**
IC	internal conversion
ICT	intramolecular charge transfer
IRF	instrument response function
IR/fsMPI	double-resonance infrared/fsMPI ion-depletion spectroscopy
IR/R2PI	double-resonance infrared/R2PI ion-depletion spectroscopy
ISC	intersystem crossing
IVR	intramolecular vibrational redistribution
LBHB	low barrier hydrogen bond
LCPL	left circularly polarized
LE	locally excited singlet state
LIF	laser induced fluorescence
LUMO	lowest unoccupied molecular orbital
MCD	magnetic circular dichroism
MCH	methylcyclohexane
MCP	microchannel plate
MeOH	methanol
MMA	methyl methacrylate
3MP	3-methylphentane
MS	mass spectroscopy
MS	**methyl salicylate**
OPA	optical parametric amplifier
OPO	optical parametric oscillator
P	**pyridine**
PBT	proton back transfer
PCM	polarizable continuum model
PEM	photoelastic modulator
PES	potential energy surface
PI	**2-phenylindole**
PMMA	poly (methyl methacrylate)
PMT	photomultiplier
PP	**2-(2'-pyridyl)pyrrole**
PQ	**1H-pyrrolo[3,2-h]quinoline**
S_0	ground singlet state
S_1	lowest excited singlet state
R2PI	resonant two-photon ionization
RCPL	right circularly polarized
REMPI	resonant enhanced multi-photon ionization
SA	**salicylic acid**

Glossary of acronyms

SPC	single-photon counting
SVLF	single vibronic level fluorescence
TDDFT	time-dependent density functional response theory
TICT	twisted intramolecular charge transfer
TIN	**2-(2'-hydroxy-5'-methylpheny1)benzotriazole**
TA	transient absorption
TOF-MS	time-of-flight mass spectrometer
ZPVE	zero-point vibrational energy
β-CD	β-cyclodextrin

PUBLICATIONS

List of publications:

1. G. Wiosna, I. Petkova, M. S. Mudadu, R. P. Thummel, J. Waluk, *Intra- and intermolecular fluorescence quenching in 7-(pyridyl)indoles,* Chem Phys Lett., **2004**, 400, 379-383
2. G. Wiosna-Sałyga, J. Dobkowski, M. S. Mudadu, I. Sazanovich, R. P. Thummel, J. Waluk, *Excited state proton transfer in 2,9-(di-2'-pyridyl)-4,7-di(t-butyl)carbazole,* Chem Phys Lett., **2006**, 423, 288-292
3. M. Kijak, I. Petkova, M. Toczek, G. Wiosna-Sałyga, A. Zielińska, J. Herbich, R.P. Thummel, J. Waluk, *Conformation-dependent photophysics of bifunctional hydrogenb bond donor/acceptor molecules*, Acta. Phys. Pol. A, **2007**, 112, 105-120
4. Y. Nosenko, G. Wiosna-Sałyga, M. Kunitski, I. Petkova, A. Singh, W. J. Buma, R. P. Thummel, B. Brutschy, J. Waluk, *Proton transfer with a twist? Femtosecond dynamics of 7-(2-pyridyl)-indole in condensed phase and in supersonic jets*, Angew. Chem. Int. Ed., **2008**, 47, 6037-6040

CONFERENCES

List of conferences presentations:

1. G. Wiosna, I. Petkova, M. S. Mudadu, R. P. Thummel, J. Waluk, *Quenching of fluorescence by hydrogen bonding in 7-(pyridyl)indoles* Centre for Photoactive Materials (CPM) Workshop on "Photoinduced Charge (Electron and Proton) Migration", Wdzydze, Poland, 30.05-5.06.2004; oral presentation
2. G. Wiosna, I. Petkova, R. P. Thummel, J. Waluk, *Photophysics of 7-(pyridyl)indole,* XXVII European Congress on Molecular Spectroscopy EUCMOS, Kraków, Poland, 5.09–10.09.2004; poster
3. G. Wiosna, I. Petkova, R. P. Thummel, J. Waluk, *Solvent-induced rotamerization and intermolecular fluorescence quenching in 7-(3'-pyridyl)indole*, ChemSession-IInd Warsaw Seminar of PhD Students in Chemistry, Warsaw, Poland, 13.05.2005; poster
4. G. Wiosna, I. Petkova, J. Dokowski, R. P. Thummel, I. Sazanovich, J. Waluk *Ultrafast excited state deactivation processes in 7-(2'-pyridyl)*, Centre for Photoactive Materials (CPM) Workshop on "Novel Experimental Techniques and Instrumentation", Lesko,

Poland, 5.06-11.06.2005; oral presentation

5. G. Wiosna, I. Petkova, J. Dokowski, R. P. Thummel, A. Sobolewski, W. J. Buma, J. Waluk *Ultrafast excited state deactivation processes in hydrogen bonded heteroazaaromatic systems,* XVIth International Conference "Horizons in Hydrogen Bond Research" and Graduate School "Hydrogen Bonding and Hydrogen Transfer", Roskilde, Denmark, 29.08 3.09.2005; oral presentation and poster.

6. G. Wiosna-Sałyga, I. Petkova, R. P. Thummel, A. Sobolewski, W. J. Buma, J. Waluk *Phototautomerization and photophysics of 7-(2'-pyridyl)indole,* ICP2007 - XXIII. International Conference on Photochemistry 2007, Köln, Germany, 29.07 - 03.08.2007; poster

7. G. Wiosna-Sałyga, I. Petkova, R. P. Thummel, A. Sobolewski, W. J. Buma, Y. Nosenko, B. Brutschy, J. Waluk, *Hydrogen-bonding-induced processes in 7-(pyridyl)indole,* XVIIth International Conference "Horizons in Hydrogen Bond Research", St Petersburg, Russia, 1.09–8.09.2007; poster

8. G. Wiosna-Sałyga Y. Nosenko, , M. Kunitski, I. Petkova, W. J. Buma, R. P. Thummel, B. Brutschy, J. Waluk, *Ultrafast excited state deactivaton processes in 7-(2'-pyridyl)indole-proton transfer with a twist?,* XXII IUPAC Symposium on Photochemistry, Gothenburg, Sweden, 28.07-1.08.2008; poster